Effect of Equatorially Trapped Waves on the Tropical Cyclone Drift

by

HYUNGEUN SHIN
M.Sc., Kyungpook National University, 2014
B.Sc., Kumoh National Institute of Technology, 2009

A Thesis Submitted in Partial Fulfillment of the
Requirements for the Degree of

MASTER OF SCIENCE

in the Department of Mathematics and Statistics

Effect of Equatorially Trapped Waves on the Tropical Cyclone Drift

by

HYUNGEUN SHIN
M.Sc., Kyungpook National University, 2014
B.Sc., Kumoh National Institute of Technology, 2009

Supervisory Committee

Dr. Boualem Khouider, Supervisor
(Department of Mathematics and Statistics)

Dr. Slim Ibrahim, Departmental Member
(Department of Mathematics and Statistics)

ABSTRACT

The movement of tropical cyclones (TC) is studied numerically based on a two-dimensional barotropic model, using a previously developed non-oscillatory balanced scheme. The model of TC used here takes an exponential form, and its size and strength are selected to be of a middle scale. Without a background flow, TCs move in the northwest direction due to the beta effect. The amplitudes of high wavenumber modes of the asymmetric flow, that are believed to be responsible for the TC drift, are computed using Fourier analysis. The amplitude of wavenumber one and two modes are dominant, so they are indicators of beta conversion of energy. Also, the effect of the monsoon trough on the TC movement is investigated. The results show a sudden change of the TC propagation path, consistent with earlier work. These two studies correspond to previous works. Here, the effect of equatorially trapped waves such as Kelvin, Rossby, and Mixed Rossby Gravity, on the TC path is newly studied by varying the wavenumber and wave speed of the underlying waves. The effect of the waves is considered because they are believed to contribute to cyclogenesis. For studying the effect, the barotropic flow induced by these waves via momentum transport and its variation were simulated for 50 days, and some patterns are found in the change of maximum wind speed. At a given time during the simulation, a TC is injected and the effect of the background wave is analyzed. Using the wavefield of 11 cases from 10 days to 30 days, the trajectories are calculated, and their patterns appear to be stochastic. So, the patterns are identified by calculating the mean path and its spread. The trajectories of TCs are different for different time of the waves. Kelvin waves make small variations on the length and direction of the trajectory of TCs. On the contrary, Rossby waves cause a dramatic change in the TC path and yield longer trajectories. Meanwhile, TCs in MRG waves keep fairly the same direction and usually have longer traveling distance. These changes vary by wave conditions. Therefore, the three kinds of waves have different effects on the trajectories of the TC. For some peculiar cases, the movements are explained based on wavefields.

Contents

List of Tables

List of Figures

ACKNOWLEDGEMENTS

I wholeheartedly thank Boualem Khouider, my supervisor.
I appreciate his caring, discreet and enthusiastic supports.
Thank to him, I have successfully finished my studies in harsh environments, away from my country.
He gave an opportunity to study mathematics to an mathematically ignorant person.

DEDICATION

I want to dedicate this thesis to my God and my family.
My God always inspire me and encourage me to move forward in my life.
My family have been waiting and providing omnipresent supports.

Chapter 1

Introduction

Tropical cyclones (TC) have been a fascinating topic for decades, so researchers have investigated them by observational and numerical methods. Robert A. Houze Jr. explains the definition, cyclogenesis, development, and structure of tropical cyclones in his review paper, which is very helpful to understand TCs [7]. It has different names depending on the area: hurricane in the Atlantic and eastern North Pacific Oceans, typoon in the western North Pacific Ocean, and cyclone in the South Pacific and Indian Oceans. TC consists of an eye, an eyewall and rainbands. The eye is the center of TC and has no strong flows. The overall picture of TC is that clouds spiral counterclockwise. On a lower altitude near sea surface, there are convergent flows from the rainband area to the center, bringing water vapor. This flow reaches near the center and moves up to provide energy to TC, in which area the eyewall exists. As the water vapor moves up, it becomes clouds in the region of the eyewall. The clouds spread from the eyewall to rainbands. According to the definition, the maximum wind speed of TCs is more than 33 m/s. TCs are the result of tropical stroms and tropical depressions. They usually appear over the ocean areas where sea surface temperature (SST) is more than 26.5 $^{\circ}C$. The region of cyclogenesis is from 5 $^{\circ}$ to 20 $^{\circ}$ on the Northern Hemishphere, but not within $\pm$ 5 $^{\circ}$ in latitude because the Coriolis force is very weak for low-level convergence.

Even though the formation of TCs is not completely understood, there is a theory called marsupial theory that is related to easterly waves [7]. If SST is high enough, cumulonimbus clouds occur. This local phenomenon causes low-level convergence and convective updraft, which is called vortical hot tower (VHT). If many VHTs are combined, then they become a mesoscale convective system (MCS). However, the progress from a MCS to a TC remains unclear. Also, there is a narrow area of maximum wind

with some distance (ranging from 10 km to 100 km) from the eye. Daniel P Stern et al. show the data of wind speed and radius of maximum wind (RMW) of TCs which have been observed from 2004 to 2010 [17].

The movement of TCs has been studied for many reasons, one of which is weather forecasting. The principles of the movement have been analyzed analytically and numerically for decades. One important concept is the beta drift which can be explained based on beta-plane approximation. It enables TCs to move up to the north in the Northern Hemisphere, and to the south in the Southern Hemisphere. In simple analyses of the movement, a nondivergent barotropic model is used without any background flow [4], [13], [16]. Maximum wind speed and RMW are relevant to the direction of TCs, and asymmetric flows take place by energy transfer called beta conversion. The energy conversion occurs through kinetic energy transfer from symmetric flows to asymmetric flows (energy) resulting in anti-cyclonic gyres, known as beta-gyres, on a flank of the TC. Some research reveals the effect of the profiles of vorticity and tangential wind on the movement of TCs [6]. Especially, [13] found an empirical relation between the angular momentum of the TC and the amplitude of the beta-gyres, thus the beta drift speed depends on the angular momentum. The same authors found an empirical relation between the meridional drift speed of TC and its mean relative angular momentum (MRAM) such that the meridional drift speed $= a|MRAM|^{1/2} + b$ where a and b are constants [20].

In addition to the study of these fundamental principles, the interaction between TCs and other disturbances is studied. One simple study of such interaction is with zonal wind of different kinds, and shows that the background zonal shear affects the trajectory of TCs through nonlinear advection [18]. Another example is the interaction of the monsoon with TCs because it contributes to the formation of TCs [19]. The movement of TCs in these simulations is dramatic just as it is in reality [2]. As long as TCs lie close enough to the monsoon trough, TCs suddenly change the track at some time compared with an initial track. Some equatorially trapped waves also contribute to cyclogenesis [15], [21] and [22]. According to previous research, Kelvin, Rossby, Mixed Rossby-Gravity (MRG) waves are associated with cyclogenesis in observations, but the degree of their effect is different from one region to another. Consequently, these waves may influence the trajectory of TCs.

In this research, the movement of TCs is investigated numerically using a non-oscillatory scheme developed by Khouider and Majda (2005) based on a nondivergent barotropic model with a beta-plane approximation. Firstly, the movement is

simulated without any background flow to illustrate the fundamental TC principles. Secondly, the interaction between TCs and the monsoon is discussed using a model of the monsoon in previous research. Lastly, the effect of the three equatorially trapped waves on the TC movement is studied. Particular consideration is devoted to the sensitivity of this effect on the equatorial wave parameters, namely, their wave speed and wavenumber. Moreover, the TC trajectory depends greatly on the phase of the wave during which it is initiated. As the waves develop with time, the trajectories of TCs are different. In order to understand the randomness of the wave phase-TC path relationship, the means of trajectories and standard deviations, for a large range of TC initiation times, are presented. They show a large range of behaviors depending on the type of wave (Kelvin, Rossby, or MRG), the wavenumber, and wave speed.

1.1 A brief introduction to Kelvin, Rossby and MRG waves

This chapter provides the background of Kelvin, Rossby and Mixed Rossby Gravity (MRG) waves in the tropics, some of which is related to the purpose of this research. The information comes from a review paper written by Kiladis et al. [11].

(1) Kelvin wave

Kelvin waves in the tropics are eastward waves and short-period synoptic scale convective cells with a considerable proportion of clouds in the Madden-Julian Oscillation (MJO) because there are divergent and vertical motions for cloudiness in the waves. The relationship between cloudiness and both dynamical and thermodynamical fields of Kelvin waves is different with regions. For wind field, zonal flow has meridional mass outflow away from and toward the equator, causing symmetric ageostrophic circulations. The wavelength is reported to have 10,000 km or much shorter. Kelvin waves propagate with different wave speeds in different areas. According to the observation over the Indian Ocean, the wave speed is from 12 to 15 m/s, but it could be slower through the MJO.

(2) Rossby wave

Rossby waves are westward waves and have symmetric cyclonic circulations on both sides of the equator. The cyclone structures in one case study are propagating at

a speed of around 4.5 m/s. The slow speed and broad spatial scales allow them to be modulated by propagation through varying background wind states. They have barotropic structures which mean that they are weakly coupled to convection, but a more complex vertical structure when deep convection takes place. The structure of Rossby waves varies seasonally and regionally. The variability decreases from west to east across the Pacific.

(3) MRG wave

MRG waves develop hybrid structures with some disturbances, especially over the western Pacific. In the central Pacific, gyres on the equator correspond to MRG waves. They become off-equatorial gyres that propagate northward toward the Philippines region. Relatively fast MRG waves usually exist in the upper troposphere and the lower stratosphere, and show large perturbations in the lower troposphere. Over the western Pacific, it is reported that MRG waves propagate westward at speeds from 15 to 25 m/s. The wavelength is measured to be around 9000 km.

1.2 Models for tropical cyclone and equatorially trapped waves

(1) The barotropic and baroclinic equations for tropical climate dynamics

The derivation of the simple barotropic and baroclinic models for TCs and equatorially trapped waves respectively begins from the primitive equations on a beta plane approximation shown below [8], [9], [5]. The primitive equations on the equatorial beta plane are given by

$$\frac{DV_H}{Dt} + \beta y V_H^{\perp} = -\nabla_H P + S_v \tag{1.1}$$

$$div_H V_H + \partial_z W = 0 \tag{1.2}$$

$$\frac{D\Theta}{Dt} + \frac{N^2\theta_0}{g} W = S_\theta \tag{1.3}$$

$$\frac{\partial P}{\partial z} = g\frac{\Theta}{\theta_0} \tag{1.4}$$

$$W|_{z=0,H_T} = 0 \tag{1.5}$$

In the equations, $V_H = (U, V)$ is the horizontal velocity, and W is the vertical velocity. $V_H^{\perp} = (-V, U)$ is perpendicular to V_H. P is pressure, S_v is the source of momentum and S_θ is the source of heat. Eq. (1.1) is the nonlinear momentum equation with beta approximation, and Eq. (1.2) is the continuity equation for incompressible fluid. $\partial_z W$ is the partial derivative of W with respect to z. β is $\frac{2\Omega}{R}$ where Ω is the angular velocity of the earth and R is the radius of the earth.

$$\frac{D}{Dt} \equiv \frac{\partial}{\partial t} + U\frac{\partial}{\partial x} + V\frac{\partial}{\partial y} + W\frac{\partial}{\partial z}$$
$$\nabla_H \equiv \frac{\partial}{\partial x}\hat{i} + \frac{\partial}{\partial y}\hat{j}$$
$$div_H \equiv \frac{\partial}{\partial x} + \frac{\partial}{\partial y}$$

Eq. (1.3) the energy conservation equation and Eq. (1.4) is the hydrostatic equation, which are based on Boussinesq approximation. So, Θ is the potential temperature, $N = 0.01s^{-1}$ is the Brunt-vaisala buoyancy frequency, $g = 9.8m/s^2$ is the gravitational acceleration, and S_Θ is the source of heat. $\theta_0 = 300K$ is the reference of potential temperature. Eq. (1.5) is the boundary condition for the vertical velocity W, which defines no vertical flow on the boundaries. $H_T \approx 16km$ is the tropospheric height.

The primitive equations are widely used to describe fluid motion in the atmosphere. [14] provides a comprehensive mathematical background of vorticity and incompressible flow, and [3] proves the local existence and uniqueness of smooth solutions of the Boussinesq equatijons. As such, they are the subject of many analytical studies. Awais and Ibrahim, for example, show the wellposedness of the primitive equations without beta approximation and exhibit an instability due to a diabatic forcing in two-dimensional, non-hydrostatic, non-rotating and Boussinesq setting. It also requires continuous dependence upon the initial data. [1].

Next, the equations for barotropic and first baroclinic modes are derived. The equations for barotropic mode are obtained by a vertical averaging over the tropospheric height. The equations for baroclinic mode are derived by the Galerkin projection onto the first baroclinic mode using the inner product

$$< f, g >= \frac{1}{H_T}\int_0^{H_T} f(z)g(z)dz$$

$g = \cos\left(\frac{z\pi}{H_T}\right)$ is used for the horizontal velocity V_H and the pressure P, and $g = \sin\left(\frac{z\pi}{H_T}\right)$ is used for the vertical velocity W and the potential temperature Θ. This results in the approximations

$$\begin{pmatrix} V_H \\ P \end{pmatrix}(x,y,z,t) \approx \begin{pmatrix} \bar{\mathbf{v}} \\ \bar{p} \end{pmatrix}(x,y,t) + \begin{pmatrix} \mathbf{v} \\ p \end{pmatrix}(x,y,t)\cos\left(\frac{z\pi}{H_T}\right)$$
$$\begin{pmatrix} W \\ \Theta \end{pmatrix} \approx \begin{pmatrix} w \\ \theta \end{pmatrix}(x,y,t)\sin\left(\frac{z\pi}{H_T}\right).$$

Here, $\bar{\mathbf{v}}$ and $\bar{p}$ are the barotropic horizontal velocity and the pressure, and $\mathbf{v}$ and θ are the components of baroclinic mode. Therefore, the coupled barotropic-baroclinic equations are obtained below.

$$\frac{\partial \bar{\mathbf{v}}}{\partial t} + \bar{\mathbf{v}} \cdot \nabla \bar{\mathbf{v}} + y\bar{\mathbf{v}}^{\perp} + \nabla \bar{p} = -\frac{1}{2}(\mathbf{v} \cdot \nabla \mathbf{v} + \mathbf{v} div \mathbf{v})$$
$$div \bar{\mathbf{v}} = 0 \tag{1.6}$$

$$\frac{\partial \mathbf{v}}{\partial t} + \bar{\mathbf{v}} \cdot \nabla \mathbf{v} - \nabla\theta + y\mathbf{v}^{\perp} = -\mathbf{v} \cdot \nabla \bar{\mathbf{v}}$$
$$\frac{\partial \theta}{\partial t} + \bar{\mathbf{v}} \cdot \nabla \theta - div \mathbf{v} = S(x,y,t) \tag{1.7}$$

Here, div is 2D divergence. Eq. (1.6) is the barotropic equations, and Eq. (1.7) is the baroclinic equations. $S(x,y,t)$ denotes the projection of S_θ onto the first baroclinic mode. The variables are non-dimensionalized using the following references scales of synoptic tropical dynamics. Gravity speed $c = 50m/s$ associated with the first baroclinic mode is used as a velocity scale, the equatorial Rossby deformation radius $L = 1500km$, the time scale is $T = L/c = 8$ hours, and the temerature scale $\alpha = 15$ K. The barotropic equations do not have vertical velocity and potential temperature whereas the baroclinic equations have their relations given by

$$p = -\frac{gH_T\theta}{\pi\theta_0}$$
$$w = -\frac{H_T}{\pi} div \mathbf{v}$$

In Eq. (1.6), the terms on the right side are forcing terms to solve a background flow, but if there is no background flow, the terms are set to zero. Eq. (1.6) without

the forcing terms can be transformed to the barotropic vorticity equation with non-divergent beta approximation.

[8] developed a nonoscillatory numerical method and simulated dry dynamics of equatorially trapped waves, [9] showed a numerical simulation with moisture effect, and [5] dealt with the interactions between Kelvin wave and barotropic flow.

In this research, three equatorially trapped waves are selected; Kelvin, Rossby and Mixed Rossby Gravity (MRG). The main objective of this work is to study the effects of these waves on the TC dynamics. Consistent with earlier work [e.g, 12], we use the barotropic model in Eq. (1.6) to simulate the TC dynamics under the influence of equatorially trapped waves. For convenience, we use the vorticity-stream function formulation of Eq. (1.6):

$$\frac{\partial \eta}{\partial t} + \bar{u}\frac{\partial \eta}{\partial x} + \bar{v}\frac{\partial \eta}{\partial y} = -\frac{1}{2}\Big[(\frac{\partial^2}{\partial x^2} - \frac{\partial^2}{\partial y^2})(uv) + \frac{\partial^2}{\partial x \partial y}(v^2 - u^2)\Big] \tag{1.8}$$

$$\Delta\psi = \eta - y, \quad \bar{u} = -\partial_y \psi, \quad \bar{v} = \partial_x \psi$$

Here, x and y are respectively the zonal and meridional coordinates with the latter being centered at the equator. Here $\eta = \partial_x \bar{v} - \partial_y \bar{u} + y$ is the potential vorticity of the barotropic flow where $\bar{u}$ and $\bar{v}$ are respectively the zonal and meridional barotropic velocity components. To avoid confusion, we denote the relative vorticity by $\xi = \partial_x \bar{v} - \partial_y \bar{u}$. For simplicity, we will often use the word vorticity to refer to relative vorticity.

The waves provide a dynamical forcing to the barotropic equations (1.6) through the right-hand side term where u and v denote respectively the zonal and meridional velocity components of the first baroclinic mode. For simplicity, here we neglect the effect of the barotropic flow on the first baroclinic equation in (1.7), which renders these equations linear, and allows us to select exact solutions of these equations in the form of equatorially trapped waves to form the forcing in (1.8), because of their physical importance. The numerical treatment of Eq. (1.8) is discussed in Section 2.3.

(2) Equatorially trapped waves

In this section, equations are dimensional. The derivation of the three waves are explained in [10]. Here, it is briefly reviewed. Kelvin, Rossby and MRG waves are linear solutions to Eq. (1.7). For Kelvin wave, firstly barotropic and baroclinic cross-

terms are dropped, the source term $S(x, y, t)$ is ignored (set to zero), and the velocity y-component v is set to zero. Then, an equation $yu = \theta_y$ is obtained. Secondly, the equation is substituted into u and θ equations, then combining the two equations produces the wave equation $u_{tt} - u_{xx} = 0$. The solutions $u(x, y, t) = \phi_{\pm}(x \pm t, y)$ satisfy $y\phi_t - \phi_{yx} = 0$. This has two solutions, one of which is the equation of Kelvin wave after considering physics. Next, the other two waves are explained. Assuming the solution as $(u, v, \theta)^T = (\hat{u}, \hat{v}, \hat{\theta})^T \exp[i(kx - \omega t)]$, and then inserting them into Eq. (1.7) without the barotropic and baroclinic terms lead to

$$\frac{\partial^2 \hat{v}}{\partial y^2} + \Big[\Big(w^2 - k^2 - \frac{k}{\omega}\Big) - y^2\Big]\hat{v} = 0 \tag{1.9}$$

The dispersion relation is

$$\omega^2 - k^2 - \frac{k}{\omega} = 2n + 1, \quad n = 0, 1, 2, \ldots \tag{1.10}$$

n=-1 is for Kelvin wave, and n=0 is for MRG wave. For the rest of n, there are three solutions: two fast waves and one slow wave that is Rossby wave.
Below are the dimensional equations used for these waves where A denotes the magnitude of zonal and meridional wind. The Kelvin wave solution is given by

$$\begin{aligned} u &= A \exp(-y^2/2) \cos(kx - \omega t) \\ v &= 0 \\ \omega &= kc \end{aligned} \tag{1.11}$$

The Kelvin wave in Eq. (1.11) moves eastward along the equator and its meridional structure decays exponentially fast away from the equator. Since the frequency (ω) is a linear function of wavenumber (k), it is non-dispersive. The Rossby wave solution is given by

$$\begin{aligned} u &= A\frac{1}{2} \exp(-y^2/2) \sin(kx - \omega t)\Big(\frac{2y^2 - 1}{k - \omega} - \frac{1}{k + \omega}\Big) \\ v &= Ay \exp(-y^2/2) \cos(kx - \omega t) \\ \omega &= -\frac{\beta k}{k^2 + (2n + 1)\beta/c_e} \end{aligned} \tag{1.12}$$

The velocity components u and v of the Rossby wave (1.12) change their direc-

tion and strength with latitude and depend highly on the wavenumber, and phase speed. Rossby waves are dispersive since the frequency is a nonlinear function of the wavenumber, and they move westward. The MRG wave (also called Yanai wave) solution is given by

$$\begin{aligned} u &= -A\omega y \exp(-y^2/2)\sin(kx-\omega t) \\ v &= A\exp(-y^2/2)\cos(kx-\omega t) \\ \omega &= 0.5kc_e + 0.5\sqrt{k^2c_e^2+4c_e\beta} \end{aligned} \tag{1.13}$$

Equatorially trapped waves play a major role in tropical weather and climate dynamics. They are associated with cloud super-clusters that account for the majority of atmospheric variability on the synoptic scales both in terms of fluid dynamics (wind, temperature) and rainfall. In this research, wavenumber (k) and gravity wave speed $c_e = \sqrt{gh_e}$ are the variables for the waves. Here, g is the gravitational acceleration, and h_e is the depth of the undisturbed layer of fluid. Considering the wave speed $c = \frac{w}{k}$, $c = c_e$ for Kelvin wave.

(3) Tropical cyclone

The structure of TCs has been investigated for a long time, and the general structure consists of an eye, an eyewall, and rainbands. In the eyewall, there is an area having the strongest wind, and the distance from the eye to the area is called radius of maximum wind (RMW). In this research, the following exponential form is adopted for the TC's relative vorticity distribution and is used as the initial TC seeding for all the numerical simulations.

$$\xi(r) = \frac{\alpha}{L_e}\exp(-(r/L_r)^2). \tag{1.14}$$

Here, α is the TC magnitude, L_e is the Rossby deformation radius, and L_r is the synoptic length scale of TC. r is the distance from the center of the TC. In this research, L_e=1500 km, $L_r \approx 40$ km are chosen in consideration of real data to represent a medium-sized tropical cyclone [17]. The profile of vorticity can be changed to the profile of the tangential velocity using the relation

$$\xi(r) = \frac{dV_\theta}{dr} + \frac{V_\theta}{r}.$$

Here, V_θ is the tangential velocity. According to the relation, radial velocity is zero in TC, so the vorticity of the TC is radially symmetric. The associated profiles of vorticity and tangential velocity of the TC are shown in Fig. 1.1 and 1.2, respectively. Accordingly, the radius of maximum wind of the TC is fixed to 45km, and the speed of the maximum wind is set to 50m/s.

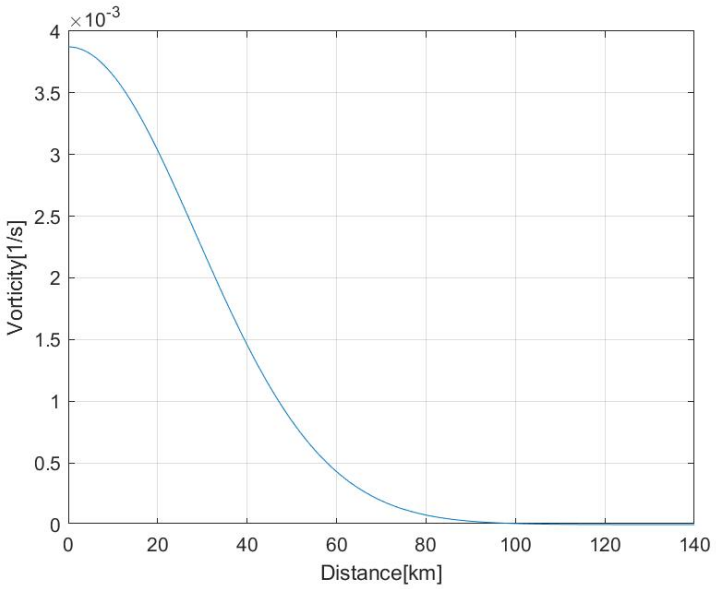

Figure 1.1: The profile of the assumed relative vorticity distribution of the TC at time t=0.

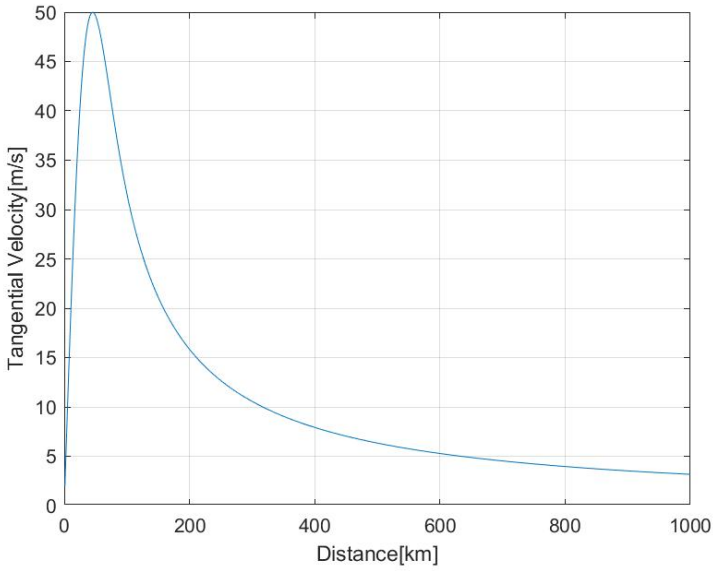

Figure 1.2: Same as Figure 1.1 but for the tangential velocity.

1.3 Numerical method

1.3.1 A non-oscillatory balanced scheme for a barotropic model

(1) Introduction to central schemes

The two dimensional central scheme is used to solve numerically the potential vorticity(η) equation by Khouider and Majda [8] is described here for the sake of completeness. We consider the vorticity equation in conservative form.

$$\eta_t + f_x + g_y = 0 \tag{1.15}$$
$$f = u\eta, g = v\eta$$

Here $\eta = \xi + \beta y$ is the potential vorticity, which is a conserved quantity for 2d flows. u, v are the associated barotropic velocity components that are given by

$$u = -\psi_y, v = \psi_x$$

where ψ is the stream function, which solves the Poisson equation

$$\Delta\psi = \xi.$$

A central scheme is a method to obtain a solution by approximation. Doran levy and Eitan Tadmor suggested using a piecewise-polynomial approximate solution as shown below [12].

$$\eta(x, y, t^n) = \sum_{j,k} p_{j,k}(x, y)\chi_{j,k}(x, y) \tag{1.16}$$

Later, a specfic piecewise-polynomical approximation is selected. In Eq. (1.16), $\chi_{j,k}(x, y) \stackrel{\text{def}}{=} c_{I_{j,k}}$ points a cell (δ - kronecker delta), thus it is zero for other cells except the indicated cell. In other words, each polynomial $p_{j,k}$ is assigned to each cell. In addition, the range of a cell is $I_{j,k} \stackrel{\text{def}}{=} \{(x, y) \mid |x - x_j| \leq \frac{\triangle x}{2}, |y - y_k| \leq \frac{\triangle y}{2}\}$.

In order to calculate the vorticity equation on a computational domain, they used a staggered control volume $I_{j+1/2,k+1/2} \times [t^n, t^{n+1}]$.

$$\overline{\eta}^n_{j+1/2,k+1/2} \stackrel{\text{def}}{=} \frac{1}{\triangle x \triangle y} \iint_{I_{j+1/2,k+1/2}} \eta(x, y, t^n)\mathrm{d}y\mathrm{d}x \tag{1.17}$$

$$= \frac{1}{\triangle x \triangle y}\left[\int_{x_j}^{x_{j+1/2}}\int_{y_k}^{y_{k+1/2}} p_{j,k}(x, y, t)\mathrm{d}y\mathrm{d}x + \int_{x_j}^{x_{j+1/2}}\int_{y_k}^{y_{k+1/2}} p_{j,k}(x, y, t)\mathrm{d}y\mathrm{d}x \right.$$
$$\left. + \int_{x_j}^{x_{j+1/2}}\int_{y_k}^{y_{k+1/2}} p_{j,k}(x, y, t)\mathrm{d}y\mathrm{d}x + \int_{x_j}^{x_{j+1/2}}\int_{y_k}^{y_{k+1/2}} p_{j,k}(x, y, t)\mathrm{d}y\mathrm{d}x\right]$$

Eq. (1.17) is to calculate the average of η at a cell using four neighboring cells at n time. It is used to solve the equation (1.18) where f and g are the functions shown in (1.15). These equations (1.17) and (1.18) are solved by using the second-order central NT scheme

$$\overline{\eta}^{n+1}_{j+1/2,k+1/2} = \frac{1}{\triangle x \triangle y} \iint\limits_{I_{j+1/2,k+1/2}} \eta(x,y,t^n)\mathrm{d}y\mathrm{d}x \tag{1.18}$$
$$-\frac{1}{\triangle x \triangle y}\int_{\tau=t^n}^{t^{n+1}} \left\{ \int_{y=y_k}^{y_{k+1}} [f(\eta(x_{j+1},y,\tau)) - f(\eta(x_j,y,\tau))]\mathrm{d}y \right\}\mathrm{d}\tau$$
$$-\frac{1}{\triangle x \triangle y}\int_{\tau=t^n}^{t^{n+1}} \left\{ \int_{x=x_j}^{x_{j+1}} [g(\eta(x,y_{k+1},\tau)) - g(\eta(x,y_k,\tau))]\mathrm{d}x \right\}\mathrm{d}\tau$$

(2) The second-order central NT scheme

In Eq. (1.16), a specific polynomial is needed for $p_{j,k}(x,y)$. Here, a reconstructed piecewise-linear MUSCL approximation is chosen shown below.

$$p_{j,k}(x,y) = \overline{\eta}^n_{j,k} + \eta^x_{j,k}\left(\frac{x-x_j}{\triangle x}\right) + \eta^y_{j,k}\left(\frac{y-y_k}{\triangle x}\right) \tag{1.19}$$

$\eta^x_{j,k}$ and $\eta^y_{j,k}$ are the derivatives with respect to x and y respectively. So, $p_{j,k}$ are calculated using the given cell averages. Hence, Eq. (1.17) becomes

$$\begin{aligned} \overline{\eta}^n_{j+1/2,k+1/2} &= \frac{1}{4}(\overline{\eta}^n_{j,k} + \overline{\eta}^n_{j,k+1} + \overline{\eta}^n_{j+1,k} + \overline{\eta}^n_{j+1,k+1}) \\ &+ \frac{1}{16}(\eta^x_{j,k} - \eta^x_{j+1,k} + \eta^x_{j,k+1} - \eta^x_{j+1,k+1}) \\ &+ \frac{1}{16}(\eta^y_{j,k} - \eta^y_{j+1,k} + \eta^y_{j,k+1} - \eta^y_{j+1,k+1}) \end{aligned} \tag{1.20}$$

Hence, the mean value in Eq. (1.18) is obtained. The remaining integrals in Eq. (1.18) are approximated by a trapezoidal rule in space and by a mid-point rule in time. The "midpoint" quadrature for the time integral involves half step calculation of $\eta^{n+1/2}_{j,k}$. The values of η at $n+\frac{1}{2}$ are obtained from first order Taylor expansion. f^x is the derivative of f with respect to x, and g^y is the derivative of g with respect to y.

$$\eta^{n+1/2}_{j,k} = \eta^n_{j,k} - \tfrac{\lambda}{2} f^x_{j,k} - \tfrac{\mu}{2} g^y_{j,k}$$

$$\int_{\tau=t^n}^{t^{n+1}} \int_{y=y_k}^{y_{k+1}} f(\eta(x_{j+1},y,\tau))\mathrm{d}y\mathrm{d}\tau \sim \tfrac{\triangle t \triangle y}{2}(f^{n+1/2}_{j+1,k} + f^{n+1/2}_{j+1,k+1})$$

$$\int_{\tau=t^n}^{t^{n+1}} \int_{x=x_k}^{x_{k+1}} g(\eta(x,y_{j+1},\tau))\mathrm{d}y\mathrm{d}\tau \sim \tfrac{\triangle t \triangle x}{2}(g^{n+1/2}_{j,k+1} + g^{n+1/2}_{j+1,k+1})$$

Finally, the equation (1.18) becomes the explicit numerical scheme.

$$\begin{aligned}\overline{\eta}^{n+1}_{j+1/2,k+1/2} &= \frac{1}{4}(\overline{\eta}^{n}_{j,k+1/2}+\overline{\eta}^{n}_{j+1,k+1/2})+\frac{1}{8}(\eta^{x}_{j,k+1/2}-\eta^{x}_{j+1,k+1/2}) \\ &- \lambda(f^{n+1/2}_{j+1,k+1/2}-f^{n+1/2}_{j,k+1/2})+\frac{1}{4}(\overline{\eta}^{n}_{j+1/2,k}+\overline{\eta}^{n}_{j+1/2,k+1}) \\ &+ \frac{1}{8}(\eta^{y}_{j+1/2,k}-\eta^{y}_{j+1/2,k+1})-\mu(g^{n+1/2}_{j+1/2,k+1}-g^{n+1/2}_{j+1/2,k})\end{aligned} \tag{1.21}$$

(3) The central incompressible scheme

The central incompressible scheme is to solve the vorticity equation using the above equations. This scheme consists of three stages: Reconstruction, Prediction, and Correction because it is a second order scheme with half time step.

Reconstruction

This stage is to solve the equation (1.20). In Eq. (1.20), the derivatives use a Min-Mod limiter,

$$\begin{aligned}\eta^{x}_{j,k} &= MM\{\theta(\overline{\eta}^{n}_{j+1,k}-\overline{\eta}^{n}_{j,k}),\frac{1}{2}(\overline{\eta}^{n}_{j+1,k}-\overline{\eta}^{n}_{j-1,k}),\theta(\overline{\eta}^{n}_{j,k}-\overline{\eta}^{n}_{j-1,k})\} \\ \eta^{y}_{j,k} &= MM\{\theta(\overline{\eta}^{n}_{j,k+1}-\overline{\eta}^{n}_{j,k}),\frac{1}{2}(\overline{\eta}^{n}_{j,k+1}-\overline{\eta}^{n}_{j,k-1}),\theta(\overline{\eta}^{n}_{j,k}-\overline{\eta}^{n}_{j,k-1})\}\end{aligned} \tag{1.22}$$

$$MM\{x_1,x_2,\cdots\}=\begin{pmatrix} min_i(x_i) & if x_i>0,\forall i \\ max_i(x_i) & x_i<0,\forall i \\ 0 & otherwise \end{pmatrix}$$

where θ is between 0 and 2. For the first four terms, the given cell averages are used because $\overline{\eta}^{n}_{j,k}=\eta^{n}_{j,k}$.

Prediction

As mentioned above, first order Taylor expansion is used to calculate $\eta^{n+1/2}_{j,k}$.

$$\eta^{n+1/2}_{j,k}=\eta^{n}_{j,k}-\frac{\lambda}{2}f^{x}_{j,k}-\frac{\mu}{2}g^{y}_{j,k} \tag{1.23}$$

In order to evaluate the equation (1.23), horizontal velocities (u,v) are required. There are three ways to do this by the Biot-Savart relation, spectral method and

streamfunction solver. Here, the streamfunction solver is used to obtain the stream function, based on the reconstructed vorticity point-wise values. Now, the equation (1.23) can be evaluated.

Correction

This stage is to solve the equation (1.21). The velocities $(u_{j,k}^{n+1/2}, v_{j,k}^{n+1/2})$ at half time step are required to calculate $f_{j,k}^{n+1/2}$. The velocities are calculated by using streamfunction solver with $\eta_{j,k}^{n+1/2}$ from the Prediction stage.

Poisson solver

A five point-Laplacian stencil is used to solve the Poisson equation for the stream function.

$$\frac{\Psi_{j+1,k} - 2\Psi_{j,k} + \Psi_{j-1,k}}{\triangle x^2} + \frac{\Psi_{j,k+1} - 2\Psi_{j,k} + \Psi_{j,k-1}}{\triangle y^2} = \zeta_{j,k} = \eta_{j,k} - \beta_0 y_k \qquad (1.24)$$
$$1 \leq j \leq N, \quad l \leq k \leq M$$

where ζ is the relative vorticity. The Poisson equation is solved by the FFT method. Now, boundary conditions are necessary to solve the Poisson equation. The west and east side has a periodic condition because a body of fluid flows continuously around the earth. Also, since it is assumed that no flow exists at the north and south boundary, $(\frac{\partial \Psi}{\partial x})_{y=\pm Y} = 0$. For the FFT treatment of no flow condition,

$$\Psi_{j,k} = \sum_{l=1}^{N} \hat{\Psi}_{l,k} exp(I(j-1)(l-1)2\pi\triangle x), \quad I^2 = -1 \qquad (1.25)$$

It is noted that $\hat{\Psi}_{l.0} = \hat{\Psi}_{l,M} = 0$ for mode $2 \leq l \leq N$. However, the mode $l = 1$ needs a special treatment because it becomes trivial.

$$\frac{\partial < \bar{u} >_x}{\partial t} = 0 \ \ at \ \ y = \pm Y \qquad (1.26)$$
$$< \bar{u} >_x (y,t) = \frac{1}{P} \int_0^P u(x,y,t) dx$$

To sum up, the northern and southern boundary conditions for the vertical component of velocity (v) uses Neumann condition. In addition, the stream function by FFT has a problem that the first mode is trivial, so the problem is solved by

zonal averaging of equation $< \bar{u}_x >$ with no flow condition($v = 0$) at $y = \pm Y$. In addition, the vorticity boundary condition is $\zeta = \eta - y = 0$ at $y = \pm Y$. Velocity field is constructed from solving the Poisson equation using second order centered finite difference.

$$u_{j,k} = -\frac{\Psi_{j,k+1} - \Psi_{j,k-1}}{2\triangle y}, \quad v_{j,k} = -\frac{\Psi_{j+1,k} - \Psi_{j-1,k}}{2\triangle x} \tag{1.27}$$

$$\begin{aligned} D_x u_{j,k} + D_y v_{j,k} &\approx \frac{u_{j+1,k} - u_{j-1,k}}{2\triangle x} + \frac{v_{j,k+1} - v_{j,k-1}}{2\triangle y} \\ &= -\frac{\Psi_{j+1,k+1} - \Psi_{j+1,k-1} - \Psi_{j-1,k+1} + \Psi_{j-1,k-1}}{4\triangle y \triangle x} \\ &+ \frac{\Psi_{j+1,k+1} - \Psi_{j-1,k+1} - \Psi_{j+1,k-1} + \Psi_{j-1,k-1}}{4\triangle y \triangle x} = 0 \end{aligned} \tag{1.28}$$

1.3.2 Time splitting method

Here, first order time splitting method is described to solve the source term resulted from the equatorially trapped waves. In the computational procedure, the source term is solved after solving the advection term by using the non-oscillatory balanced scheme. Let S_j be a solution at time t_j. Consider $\frac{d}{dt}S = AS + BS$ where A is the advection operator and B is the source operator. The algorithm is

1. Solve $\frac{d}{dt}S_j^1 = AS_j^1$ on $[t, t + \triangle t]$, with $S_j^1(t) = S_j(t)$
2. Solve $\frac{d}{dt}S_j^2 = BS_j^2$ on $[t, t + \triangle t]$, with $S_j^2(t) = S_j^1(t + \triangle t)$
3. Set $S_j^2(t + \triangle t) = S_j(t + \triangle t) = S_{j+1}(t)$

In one time step, it has two sub time steps for AS_j^1 and BS_j^2. For step 1, $S_j^1(t + \triangle t)$ is calculated from $S_j^1(t) = S_j(t)$. Sequentially, $S_j^2(t + \triangle t)$ is calculated from $S_j^2(t) = S_j^1(t + \triangle t)$. The next step uses $S_j^2(t + \triangle t)$ for step 1.

1.3.3 Computational setting

The computational domain is a channel of 40,000 km (the perimeter of the globe at the equator) in x-direction and 16,000 km in y-direction centered at the equator,

and the grid size is 20 km. After considering CFL condition, the time step use is $\Delta t \approx 3.377 \times 10^{-3}$ (It is non-dimensional as (1.6)). For boundary conditions, we assume periodic symmetry in east-west direction while the meridional wind is set to zero at the north and south walls. The duration of the simulation of a TC is two days, and the data is saved every 6 hours. For the selection of a proper grid spacing, different sizes of grid spacing are tested for the simulation of a TC without a background flow. More precisely, we solve the barotropic equations in Eq. (1.8) with the baroclinic forcing on the right hand side set to zero. The initial condition consists of the TC profile in (1.14).

Fig. 1.3 compares the TC trajectories using 10, 20 and 40 km grid spacing. The trajectories are drawn by tracking the center of the TC. As shown in Fig. 1.1, the vorticity at the center is the highest, which is the same during simulation. While the two cases of 10 and 20 km are similar, the case of 40 km is not. Since the computational cost of using 10 km is higher, 20 km is chosen in this research. Fig. 1.4 shows the convergence of TC drift and vortices as the grid is refined. In the figure, the vorticity contours are relative vorticity field, and the arrows are the directions of wind. These are the same in other figures of the same kind. With a coarser grid, the negative vortex beside the TCs and the size of TC are not properly estimated.

In the simulations with a non-uniform background, the equatorially trapped waves, which are used to force the barotropic flow, are set to move freely. In doing so, the baroclinic forcing in Eq. (1.6) provides an oscillatory barotropic flow response in which TCs evolve. The oscillatory nature of the barotropic response is due to the fact that the free-baroclinic waves that force them continuously circle the periodic domain. We recall that the equatorially trapped waves in (1.11), (1.12) and (1.13) are not exact solutions to Eq. (1.7). They are exact solutions only if $\bar{\mathbf{v}} = 0$ and $S_\theta = 0$, which amounts to neglecting the nonlinear effects in the baroclinic equations and assuming dry dynamics. Such dry equatorially trapped waves are ubiquitous in nature [11]. Except for the TCs that are injected at various specific times, denoted by T_0, initial condition is set to zero so that the barotropic flow background is solely created by the baroclinic waves while the boundary condition is the same as described in this section.

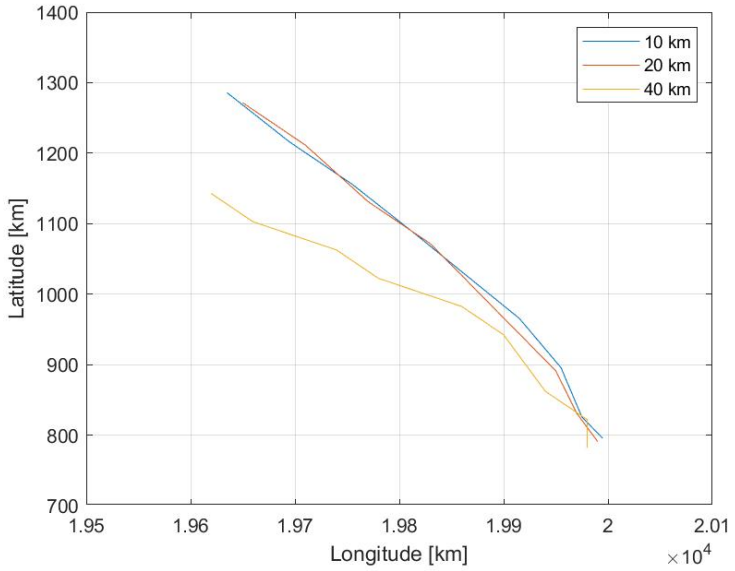

Figure 1.3: Comparison of TC trajectories simulated with the barotropic model in a tropical channel without forcing and with the profile in (1.14) as initial condition using different grid spacing.

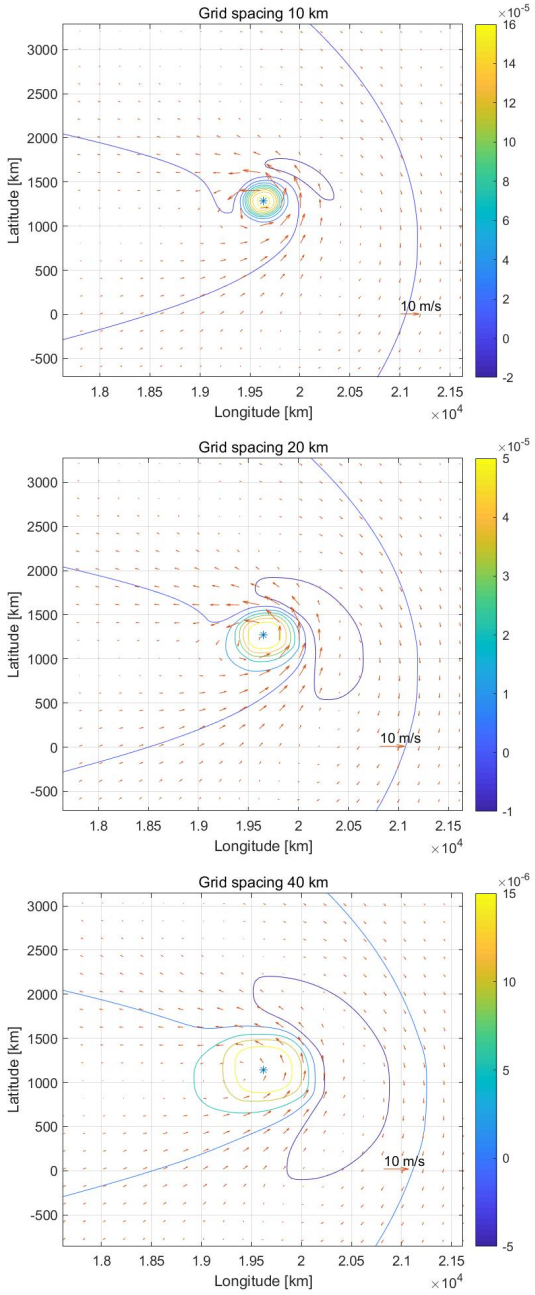

Figure 1.4: Relative vorticity contours and velocity arrows for the solutions in Fig. 1.3 at 48 hours.

Chapter 2

Beta drift

Beta drift causes the tropical cyclone (TC) to move to the north in the northern hemisphere and to the south in the southern hemisphere. It is well represented by the beta-plane approximation while TCs do not move poleward on an f-plane approximation. In a numerical simulation, a TC initially has symmetric rotational flow, but the beta gyre extracts energy from the symmetric flow to asymmetric flow. This chapter shows the behavior of a TC without background flow. In Fig. 5.2, the center of the TC is marked with a "star" marker, and the colorbar indicates the strength of vorticity and compares it with previous studies, and the scale is changing.

In Fig. 5.2, the center of the TC is marked with a "star" marker, and the colorbar indicates the strength of the vorticity. The initial location of the TC is at 20000 km in longitude and 800 km in latitude. As the TC moves northward, the vorticity and wind become weaker because it is a barotropic model. It is seen that there is a huge anticyclonic vortex to the east of the TC at t=36 hours. After 6 hours, another bigger anticyclonic vortex appears adjacent to the TC. Looking at the trajectory in Fig. 2.2, the TC generally moves to the northwest, which is consistent with earlier studies [13]. In detail, the slope of the trajectory slightly changes as it moves. The highest slope occurs around 18 hours, then the slope decreases at 24 hours. The translation speed of the TC gradually increases and then remains nearly the same. In this research, the amplitude of the vorticity of symmetric and asymmetric flows are calculated to understand how the kinetic energy of a TC changes. As mentioned above, the symmetric flow is what a TC initially has, and the asymmetric flow is due to the dynamical interaction of the cyclone and the variation in the Coriolis force, this is known as the beta effect. Here is one way to estimate this asymmetric

flow. Firstly, set a radius to make a circle from the center of a TC. In this research, the radius is 200 km. Secondly, the data of vorticity on the grid of the rectangular coordinate in the circle is transformed to data on the grid of polar coordinate (r,θ). Thirdly, for each θ, calculate the average of data in r direction. Then, use FFT with respect to θ to get the amplitude of the vorticity of symmetric and asymmetric flow. Wavenumber n=0 is from the symmetric flow, and the rest wavenumbers n=1,2,3,... are from the asymmetric flow. Lastly, repeat from the second to the fourth step for each time. According to [13], wavenumber 1 and 2 (w-1 and w-2 in Fig. 2.3) of asymmetric flow are closely related to the beta drift because their amplitudes are much bigger than those of other wavenumbers. Thus, only the graphs of wavenumber 1 and 2 amplitudes are shown in Fig 2.3.

Fig. 2.4 is produced by subtracting 6 hours earlier vorticity from vorticity at the given time. So, it shows the approximate change of vorticity with time. The center of the TC is positioned at the center of each figure. Since the kinetic energy of symmetric flow converts to the kinetic energy of asymmetric flows, the figures show new vortices from the process of kinetic energy conversion. In detail, the figure t=12h is the difference of vorticity between t=12 hours and t=6 hours. At 6 hours, there is no vortex around the TC, but it is seen that new vortices in four locations around the TC are appearing. Then, a vortex occurs on the northwest side of the TC at 18 hours. As time goes by, the creation of a new vortex takes the northeast side. The location of the creation does not change until around 36 hours. After that, the location of the creation rotates to the southeast side. At 48 hours, the creation is happening on both sides. Moreover, the strength of the creation of vortices becomes lower, which corresponds to the result shown in Fig. 2.3.

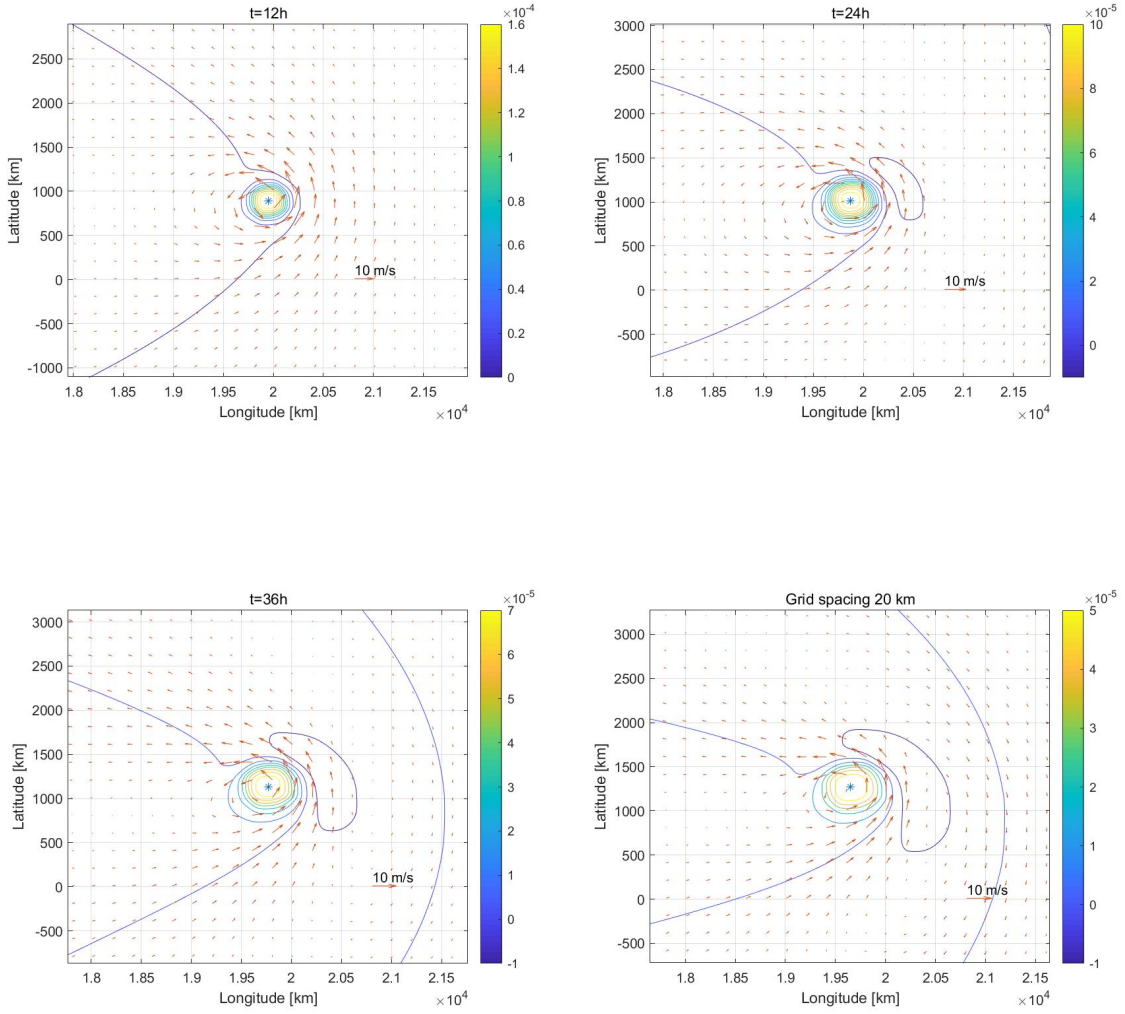

Figure 2.1: Vorticity contours and velocity arrows of a tropical cyclone simulated by the free barotropic equations in Eq. (1.8) with forcing set to zero.

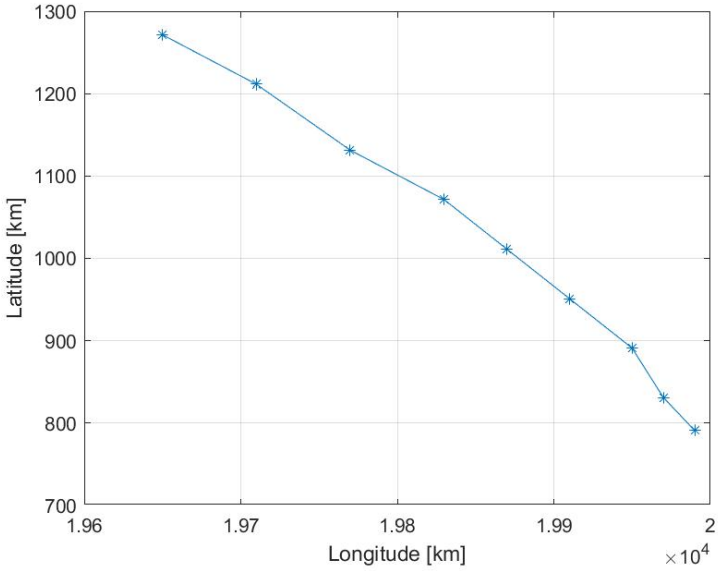

Figure 2.2: Trajectory of the simulated tropical cyclone center in Fig. 2.1.

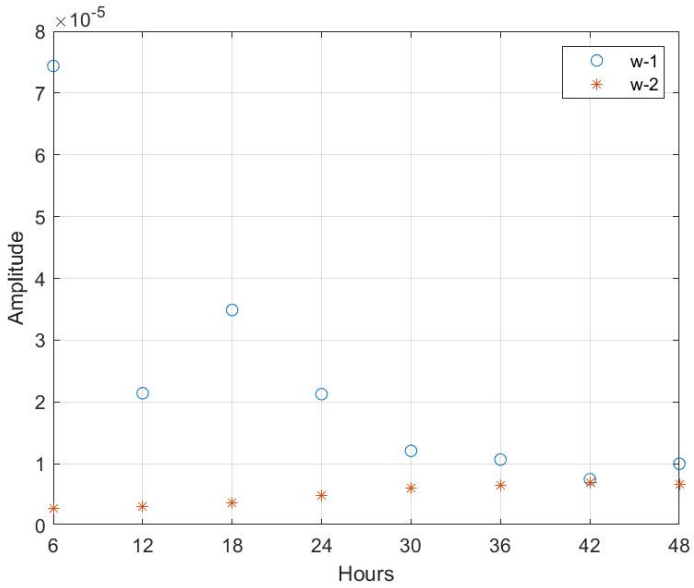

Figure 2.3: Amplitude of wavenumbers one and two of asymmetric flows of the simulated tropical cyclone in Fig. 2.1.

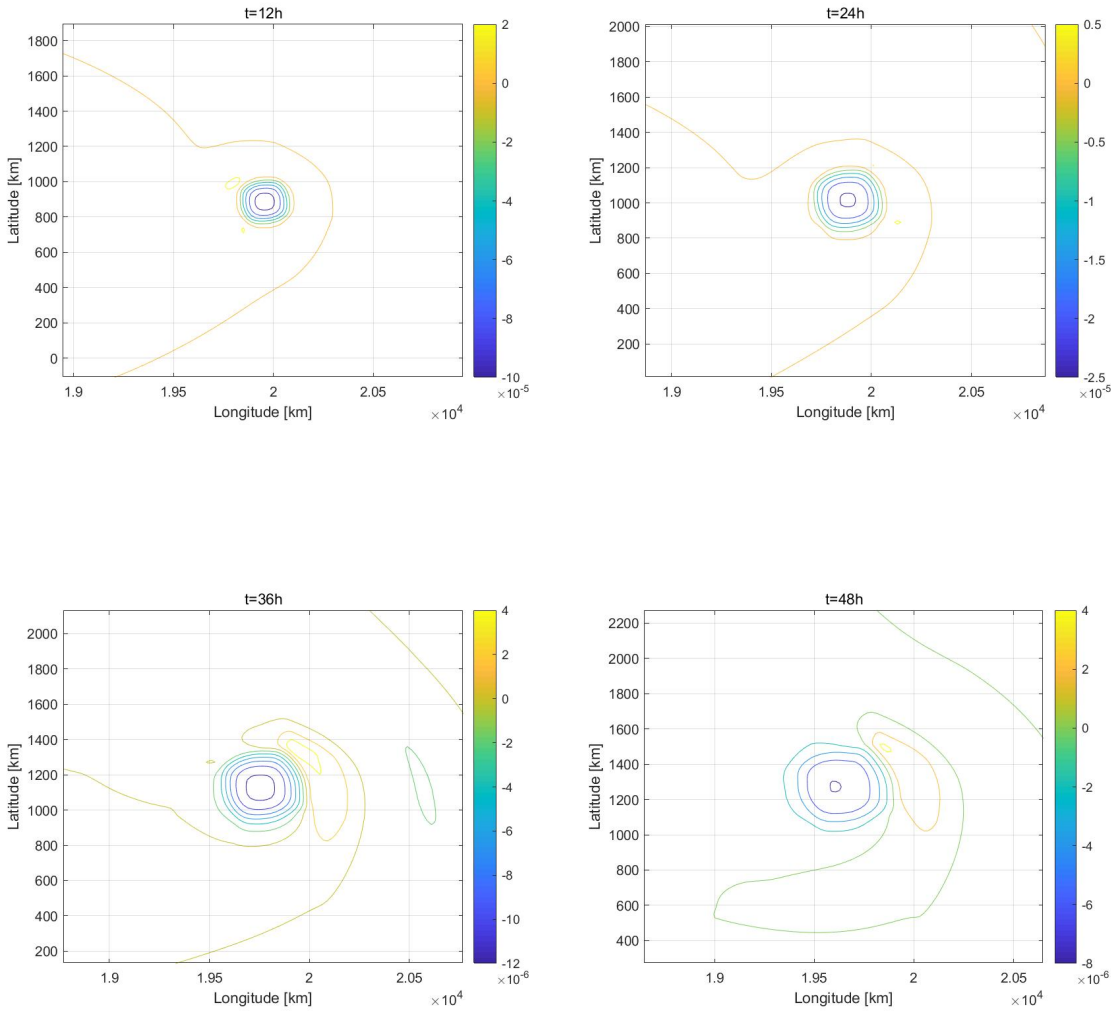

Figure 2.4: Change in vorticity at 6 hours obtained by taking the difference between the TC vorticity at 6 hours and the initial vorticity when this later is artificially made to move with the TC center corresponding to the results in Fig. 2.1 (unit: 1/s).

Chapter 3

Interaction with Monsoon

It is known that a sudden track change occurs when the monsoon and the tropical cyclone (TC) interact [2]. The authors investigated the movement of TCs with different positions and distances from the monsoon in their paper based on a nondivergent barotropic model. Besides, the monsoon contributes to the formation of the TC [19]. The results show that as long as TCs do not lie far from the monsoon, the trajectory changes significantly with several patterns. However, the model of TC used in the paper does not have as strong of a maximum wind that a TC normally has. Thus, it is dubious that such a sudden change may be affected by the amplitude of maximum wind.

$$V_\theta(r) = \frac{V_m}{2}\Big[1 - cos\Big(\frac{\pi r}{R_m}\Big)\Big] \tag{3.1}$$

For verification, the same model of a monsoon is used. (3.1) is the equation of the tangential velocity of a monsoon. Fig. 3.1 and Fig. 3.2 are plots of tangential velocity and vorticity of the monsoon and the TC respectively. The initial location of the TC is at 20400 km in longitude and 800 km in latitude, and the initial location of the monsoon is at 20000 km and 800 km. The maximum wind of the TC in the paper is 20 m/s, which is about twofold less than the proposed TC. The simulation runs for 96 hours (4 days). The monsoon is circular on x,y plane.

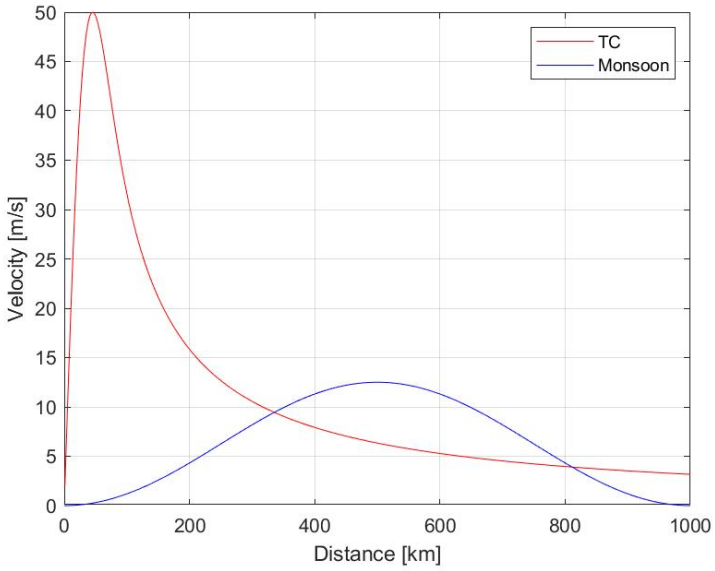

Figure 3.1: Tangential velocity of TC in Fig. (1.2) and Monsoon in (3.1).

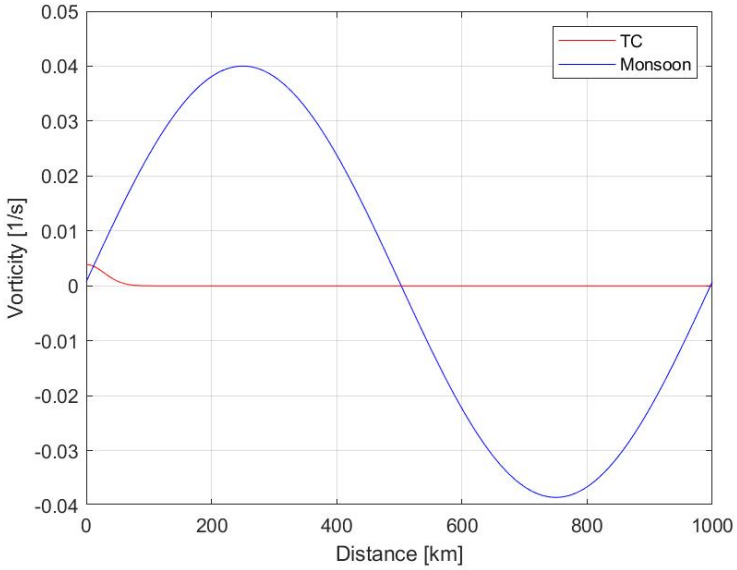

Figure 3.2: Vorticity of TC in Fig. (1.3) and Monsoon in (3.1).

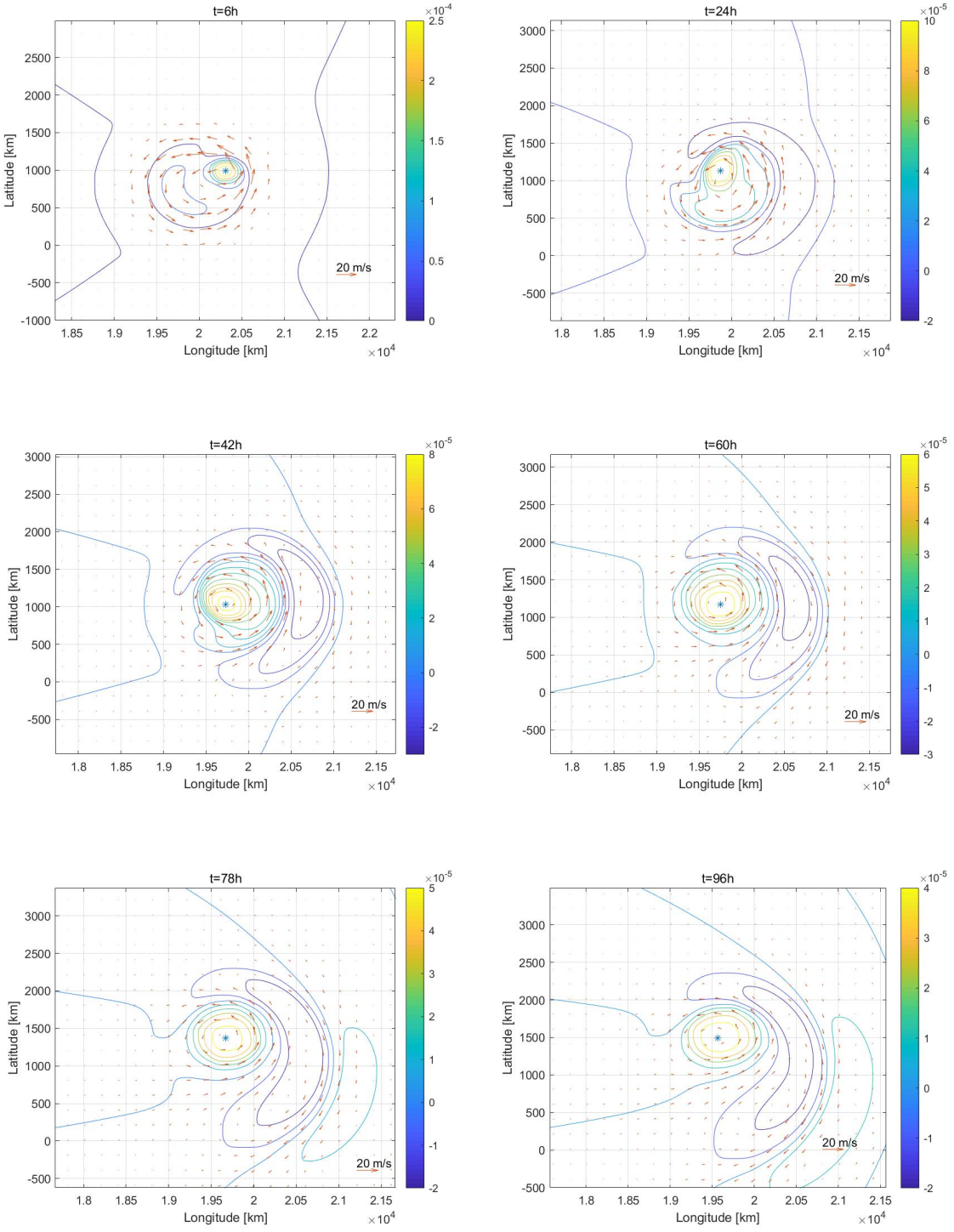

Figure 3.3: Distribution of vorticity and wind for four days for the case of TC evolving inside a monsoon trough.

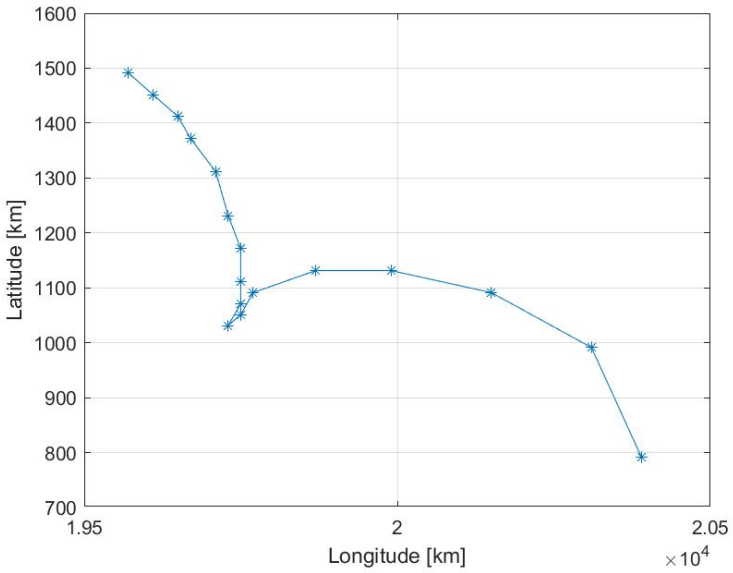

Figure 3.4: Trajectory of tropical cyclone evolving inside a monsoon trough.

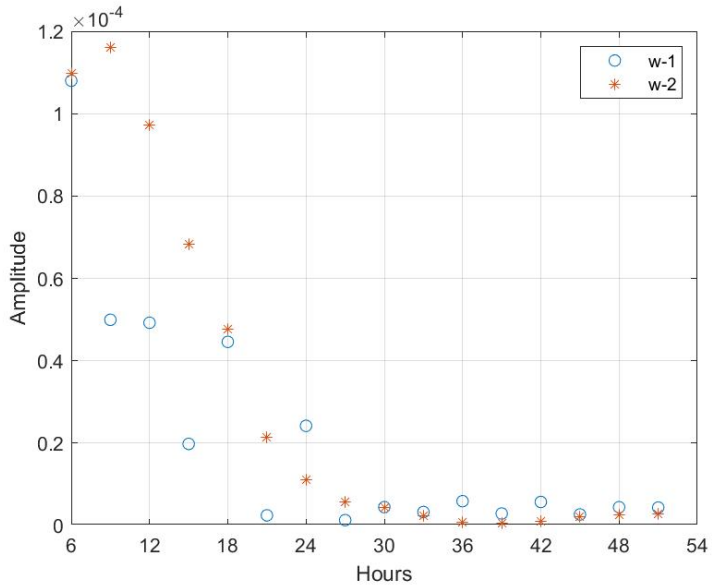

Figure 3.5: Amplitude of wavenumbers one and two of asymmetric flows for the TC in a monsoon trough.

Fig. 3.3 demonstrates the interaction between the TC and the monsoon. At 6 hours, the TC is moving northwestward as described in Chapter 2. One different thing is that a big negative gyre exists adjacent to it. This meets the necessary condition that the beta gyre extracts energy from the symmetric flow to asymmetric flows, and it is favorable for the TC to move northward according to [13]. However, the negative gyre extends and surrounds the TC and the monsoon with time going by, and the TC does not move northward a long distance as shown at 24 hours. In addition, the vorticity inside the monsoon and the negative gyre have more contours. Afterwards, the TC moves in a circle by going south and eastward. For one to two days, the TC and the monsoon combine while the TC barely moves. Afterwards, the slope of the contour of vorticity becomes steeper as it moves to the northwest. Fig. 3.4 shows the trajectory of the TC. Compared with the corresponding result in [2], this result is very similar. The translation speed becomes slower until it goes into the combination process with the monsoon. The direction of translation continuously changes until the step of combination. Since the initial direction is completely different from the last direction, it is hard to estimate the direction of the movement of TCs when they confront the monsoon. Also, when considering how far it goes to the north, it is obvious that the monsoon provides kinetic energy to TCs so that it moves up. Thus, it coincides with the fact that the monsoon plays a role in the formation of TCs. Furthermore, the amplitude of wavenumber one and two (w-1 and w-2 in Fig. 3.5) of asymmetric flows is different from the case without the background shown in Fig. 2.3.

Chapter 4

Tropical cyclone path in presence of equatorial waves

4.1 Experimental setup

In this chapter, the effects of equatorially trapped waves on the movement of tropical cyclone (TC) are discussed based on the simulation of a TC in a wave-active background. As mentioned in the Introduction, Kelvin, Rossby and Mixed Rossby Gravity (MRG) waves are considered. In addition, various phases of the waves are considered as the launching point of the TC. The initial location of the TC is at 20000 km in longitude and 800 km in latitude, independently on the phase of the background wave. Table. 4.1 shows the wave speed (c) of Kelvin, Rossby and MRG waves depending on wavenumber (k) and gravity wave speed (c_e). The definition of wavenumber is

$$wavenumber(k) := \frac{40000km}{Wave\ \ Length} \tag{4.1}$$

Wave speed is calculated using $\frac{\omega}{k}$ and a given frequency. For the simulation of the waves, not only are the wave conditions considered, but the period of development of the waves is also taken into account. Thus, the simulations of the waves are conducted with each wave condition in the table for 50 days. Then, a TC is injected into a certain developed time of each case (in the table) of the waves. So, the injected time $T_o = 0$ means that the simulation of a TC begins without a background flow. In particular, the wave-background development period between 10 and 30 days is chosen to gather statistics about the effect of the waves on the

TCs with various wave parameters. More precisely, for each wave parameter case in Table 4.1, we conduct an ensemble of 11 simulations where the TC injection time T_0 is set to take each one of the values $10, 12, ..., 30$ days.
In all cases, the magnitude of the forcing wave is set to $A = 15$ m/s, where A is the wave amplitude in (1.11), (1.12) and (1.13) in Chapter 1. In this research, numerical simulations are done with the magnitude fixed, but it is an important parameter to be considered in future research. Here, we are interested in the rather subtle effect of the wave speed and wavenumber of the forcing baroclinic waves on the TC speed and path. It is important here to recall that the effect of the baroclinic waves on the TC is indirect. It is indirect in the sense that the baroclinic wave forcing on the right-hand side of Eq. (1.6) induces a barotropic flow background in which TCs evolve and through which they change speed and direction.

4.2 Barotropic flows generated by equatorial waves

Before discussing the TC simulation results in the equatorially trapped waves depending on the injected time T_o of a TC, it is indispensable to study the behavior of the waves with time. Looking at the three waves with a specific condition where the wavenumber is 5 and the maximum wave speed in the wavenumber group, the changes of maximum speed of the waves for 50 days have different patterns in the left figures of 4.1, 4.2 and 4.3. Since the waves are set to move freely, they induce an oscillatory barotropic motion. The panels on the right show the vorticity and wind fields at 10 days. Kelvin and MRG waves have a period of the least fluctuation in between 10 to 30 days while Rossby wave does not fluctuate and has the least change (the slope is lowest) in the period. Furthermore, the maximum speed of Rossby wave is much higher than the two other waves. The vortices generated by the Kelvin wave are equally distributed and have the same shape around the equator. However, some vortices in the Rossby wave case are a bit crushed by adjacent ones. The MRG response has a weak vorticity field around the equator, and there are elliptical vortices farther to the north and south. In the three waves, vortices are meridionally elongated.

Table 4.1: Wave speed of Kelvin, Rossby and MRG waves

case	unit [m/s]	Kelvin	Rossby	MRG
1	$k = 1 \& c_e = 1$	1	-0.332	10.127
2	$k = 1 \& c_e = 5$	5	-1.637	24.142
3	$k = 1 \& c_e = 15$	15	-4.743	45.481
4	$k = 2$ & $c_e = 1$	1	-0.329	5.333
5	$k = 2$ & $c_e = 5$	5	-1.555	13.535
6	$k = 2$ & $c_e = 15$	15	-4.110	27.571
7	$k = 4$ & $c_e = 1$	1	-0.315	2.955
8	$k = 4$ & $c_e = 5$	5	-1.293	8.427
9	$k = 4$ & $c_e = 15$	15	-2.680	19.454
10	$k = 5$ & $c_e = 1$	1	-0.306	2.487
11	$k = 5$ & $c_e = 5$	5	-1.149	7.473
12	$k = 5$ & $c_e = 15$	15	-2.125	18.069
13	$k = 8$ & $c_e = 1$	1	-0.271	1.802
14	$k = 8$ & $c_e = 5$	5	-0.774	6.170
15	$k = 8$ & $c_e = 15$	15	-1.120	16.327
16	$k = 10$ & $c_e = 1$	1	-0.245	1.584
17	$k = 10$ & $c_e = 5$	5	-0.595	5.797
18	$k = 10$ & $c_e = 15$	15	-0.780	15.873

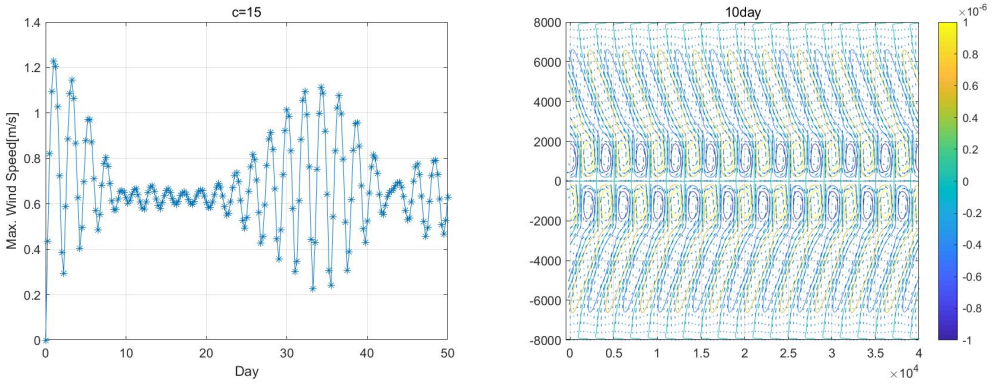

Figure 4.1: Left: Evolution of maximum barotropic speed forced with free moving Kelvin wave with wavenumber k=5, gravity wave speed c_e=15 and magnitude A=15. Right: The vorticity contours of the barotropic response at 10 days.

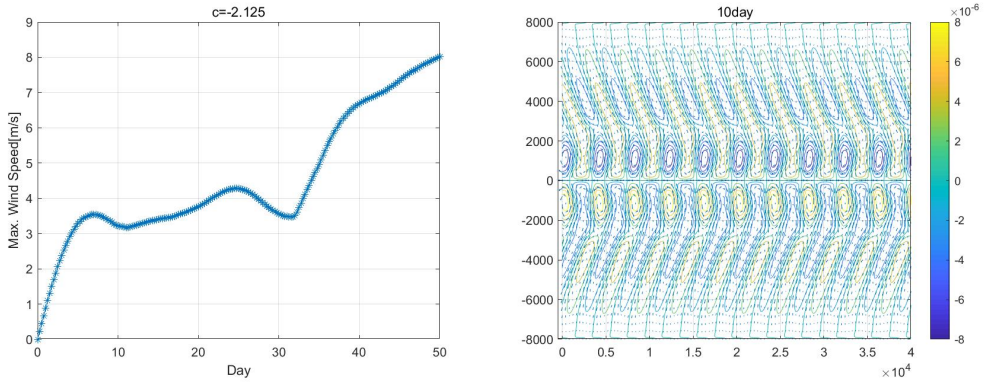

Figure 4.2: Same as Fig. 4.1 but for Rossby wave.

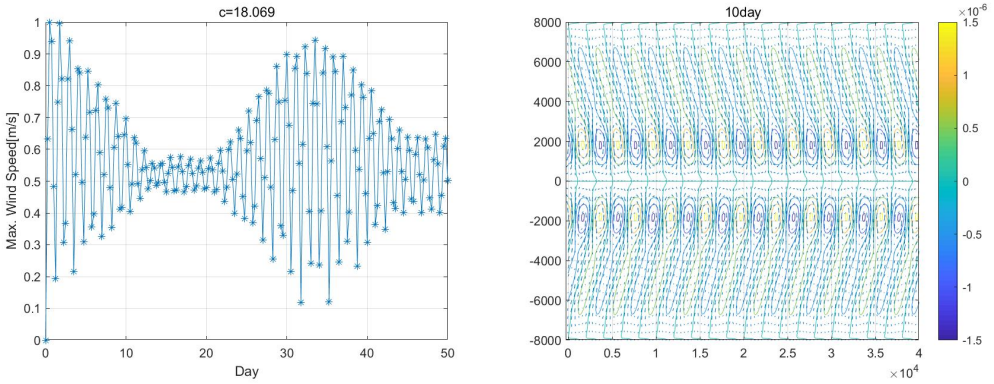

Figure 4.3: Same as Fig. 4.1 but for MRG wave.

4.3 Effects of equatorially trapped waves on the TC path: typical behaviour

Here, the effects of the three equatorially trapped waves on the trajectory of a TC is briefly discussed by comparing some cases. First of all, the effect is investigated during the incipient period of the waves. In simulation, a TC and a wave are simulated simultaneously without any background flow for two days. So, the waves develop for two days. In addition, the trajectory of TC is drawn by tracking the center of the TC where the highest vorticity exists. Fig. 4.4, 4.5 and 4.6 shows the change of TC trajectories due to different wavenumbers ($k = 8, 2$) and different wave speeds of Kelvin, Rossby and MRG waves respectively.
According to Eq. (4.1), 40000 km is the perimeter of the earth at the equator. Wavenumber 8 means that the wavelength is 5000 km. The reference is the trajectory of a TC without a wave background, and it is commonly drawn in Fig. 4.4, 4.5 and 4.6 to compare the effect of the waves on the trajectory of the TC. In Kelvin waves, the smaller the wavenumber and also smaller the wave speed, the shorter the trajectory of TCs is. Besides, the whole trajectory moves to the west and the total distance traveled by the TC to the north becomes shorter. On the other hand, in Rossby waves, the TC moves farther to the north and has the longest traveling distance with wavenumber 2 and wave speed 4.110 m/s among the cases. The rest have little difference in TC trajectory. It may be thought that this is obvious because of the few differences of wave speed, but it is not true. When looking at the corresponding TC trajectories in the developed Rossby wave, the degree of development of Rossby wave is responsible for the little difference in TC trajectory. In MRG waves, TCs usually travel longer than the reference and their trajectories are the closest to each other. They do not show a significant variance of the distance and direction of the movement by the change of wavenumber and wave speed.

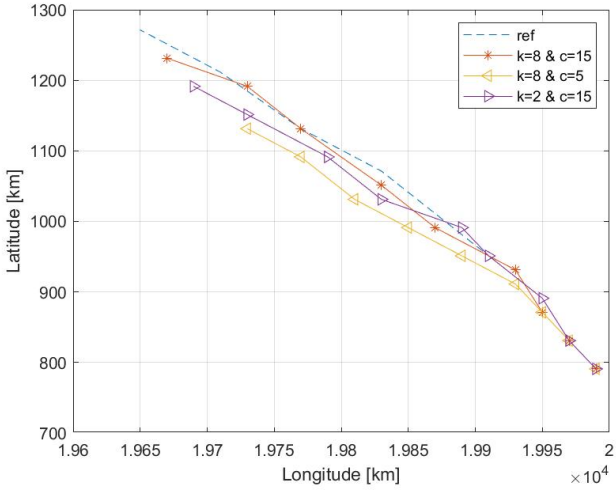

Figure 4.4: TC trajectories in a Kelvin wave generated background with different wave conditions. The dashed line represents the reference case of zero background.

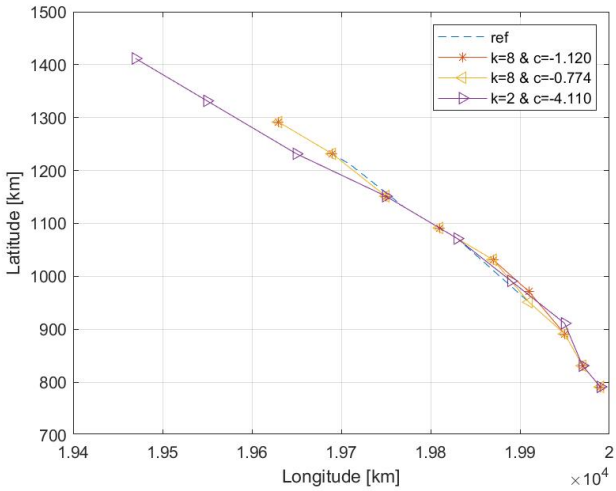

Figure 4.5: Same as Fig. 4.4 but for the case of Rossby waves.

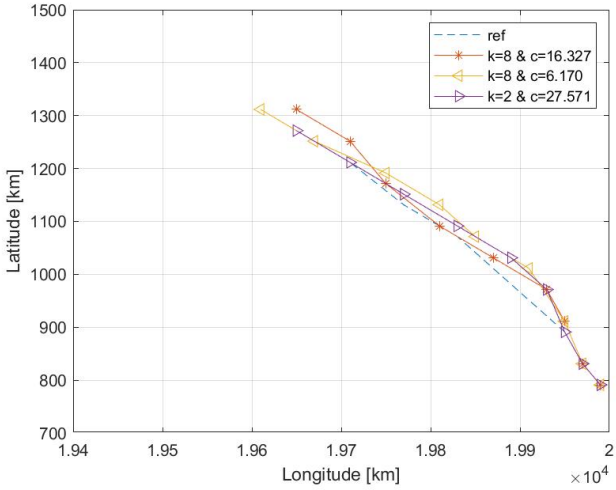

Figure 4.6: Same as Fig. 4.4 but for the case of MRG waves.

Next, TCs are injected into the wave fields at 10 and 30 days with the same wave condition that is $k = 5$ and $c_e = 15$ m/s, and TCs are simulated for two days. The trajectories of TCs are shown in Fig. 4.7, 4.8 and 4.9. For the reminder, the reference is the trajectory of the TC without background flow. The trajectories of TCs in Kelvin and MRG waves move close to the reference whereas the trajectories of TCs in Rossby wave are divergent from the reference. Meanwhile, considering wave fields with all the conditions, the patterns of trajectories are different.
All the cases for the change of maximum speed of wind is shown in Appendix A. For all the waves, the patterns of the change of maximum speed are different depending on wavenumbers and type of waves. For Kelvin wave, slower wave speed causes higher maximum speed in each group of wavenumber. Also, the number of fluctuations becomes fewer. On the other hand, Rossby wave has the opposite patterns that maximum speed increases and the number of fluctuations decreases as wave speed becomes slower. However, it is hard to find a pattern for graph shape in MRG wave cases, but the lower wave speed and higher wavenumber cause higher maximum speed. Appendix B shows the different wind and vorticity fields at 10 and 30 days.

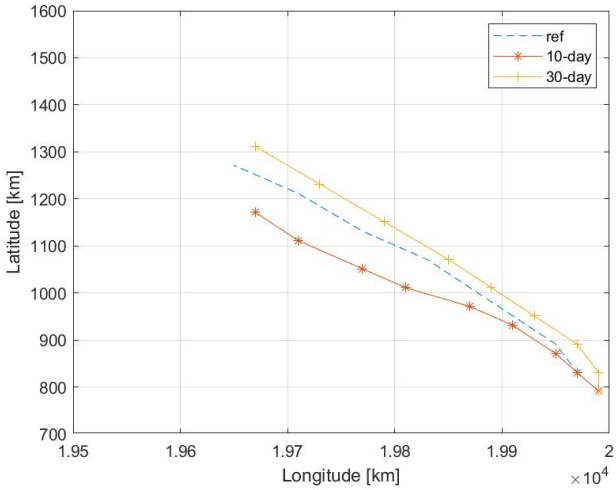

Figure 4.7: Paths of tropical cyclone in different injected times in a Kelvin generated background with wavenumber k=5, gravity wave speed c_e=15 and magnitude A=15.

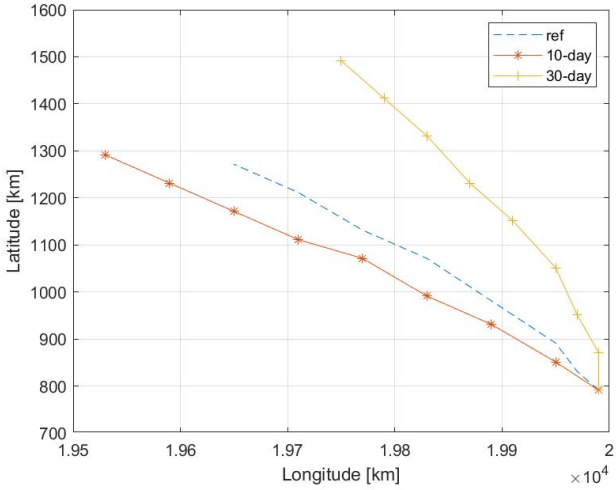

Figure 4.8: Same as Fig. 4.7 but for a Rossby generated background with wavenumber k=5, gravity wave speed c_e=15 and magnitude A=15.

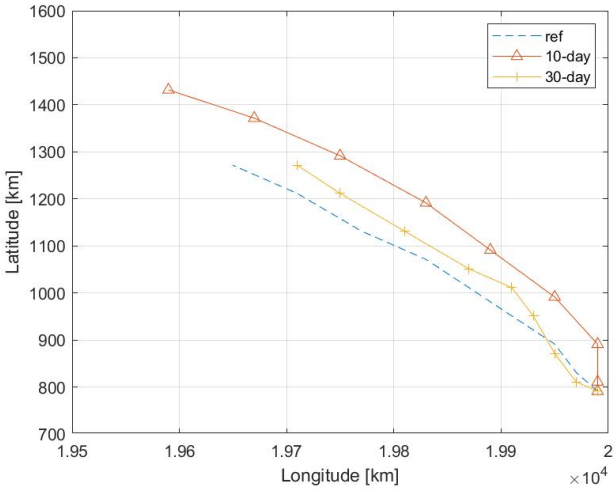

Figure 4.9: Same as Fig. 4.7 but for a MRG generated background with wavenumber k=5, gravity wave speed c_e=15 and magnitude A=15.

4.4 Effects of equatorially trapped waves on the TC path: statistical analysis

As described above, the trajectory of the TC varies on the type of wave, wavenumber and wave speed. Also, wavefields are changing with time. Thus, it is hard to estimate the trajectory of the TC with certainty independently on the phase of the background wave. For this reason, it would be better to represent trajectories of TCs with days under fixed type of wave, wavenumber and wave speed. For 11 different cases, the mean path (Avg) and the standard deviation (s) are calculated. The calculation of the mean is done by summing up the eleven TC positions at each time and dividing the sum by eleven. The standard deviation is calculated at each time as well. For the remainder, ref is for a TC without background flow. All the figures have the same range for consistency.

(1) Kelvin wave cases
First of all, the reference in all the figures is always in the range of the bounds. In general, the relative position of the reference to mean path shows the same pattern in wavenumber 1 and 2, wavenumber 4 and 5, and wavenumber 8 and 10 respectively. For example, in the case with k=1 and c=1 m/s, ref is between Avg and Avg+s. The same position of the reference is found in the case with k=2 and c=1 m/s. In addition, as the TC moves, the bound becomes gradually wider. The bound also becomes wider as wave speed is slower and wavenumber increases. For instance, the case with k=10 and c=1 m/s has more than 200 km deviation. Compared with other cases, the range of bounds of the case is noticeable. Besides, the length of the TC trajectories is affected by wavenumber and wave speed. In each group of wavenumbers, slower wave speed causes shorter trajectories. Especially, the cases with wavenumber 4 and 5 have much shorter than the other cases with other wavenumbers. Overall, significant changes in trajectory occur with wavenumber 4, 5, 8 and 10. The wavenumber 4 and 5 affect the direction of the movement of the TC so that the bounds are the widest. The wavenumber 8 and 10 influence the distance. However, as wave speed increases, such effects disappear.

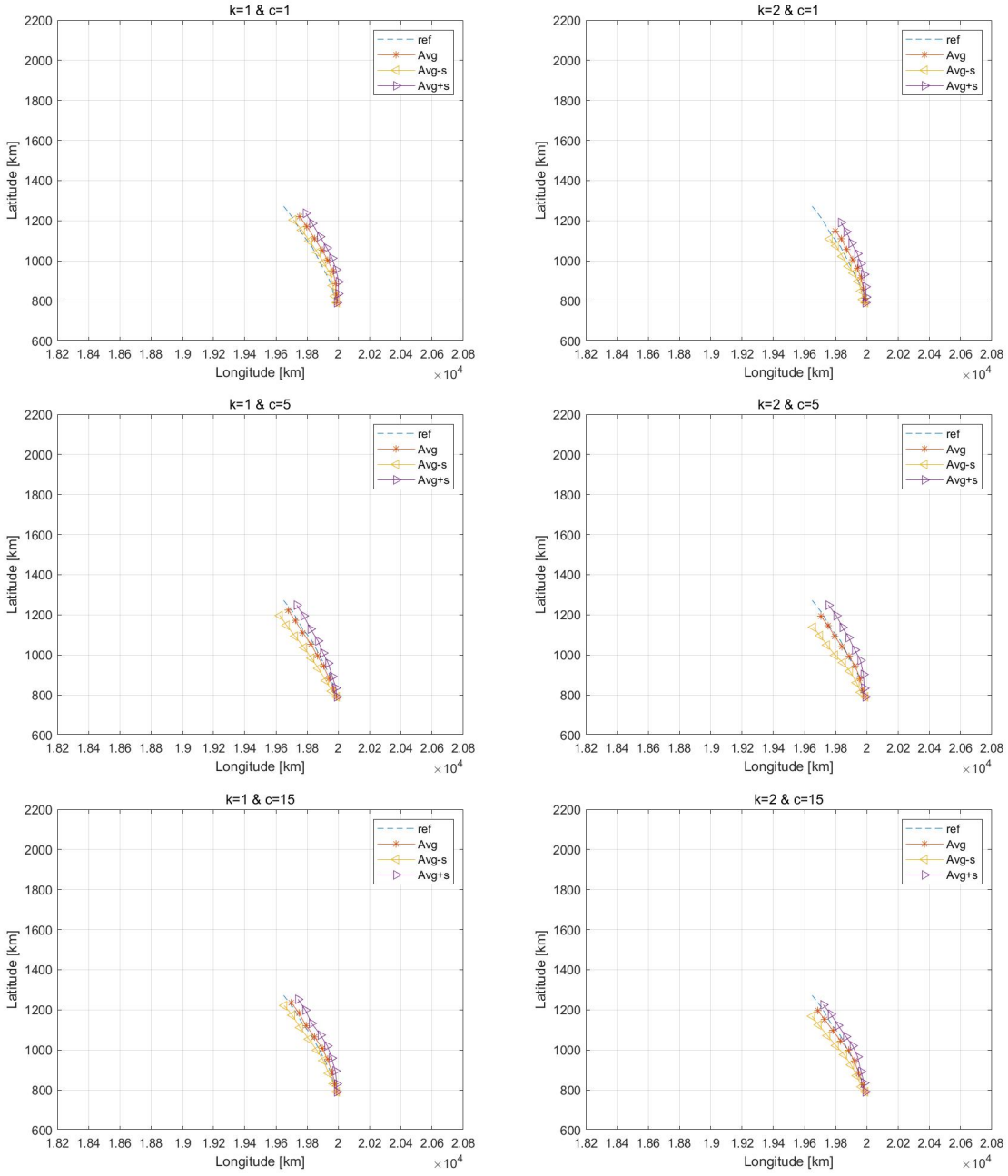

Figure 4.10: Mean path and deviations in Kelvin wave generated background with wavenumbers 1 and 2, and gravity phase speeds 1 m/s, 5 m/s and 15 m/s.

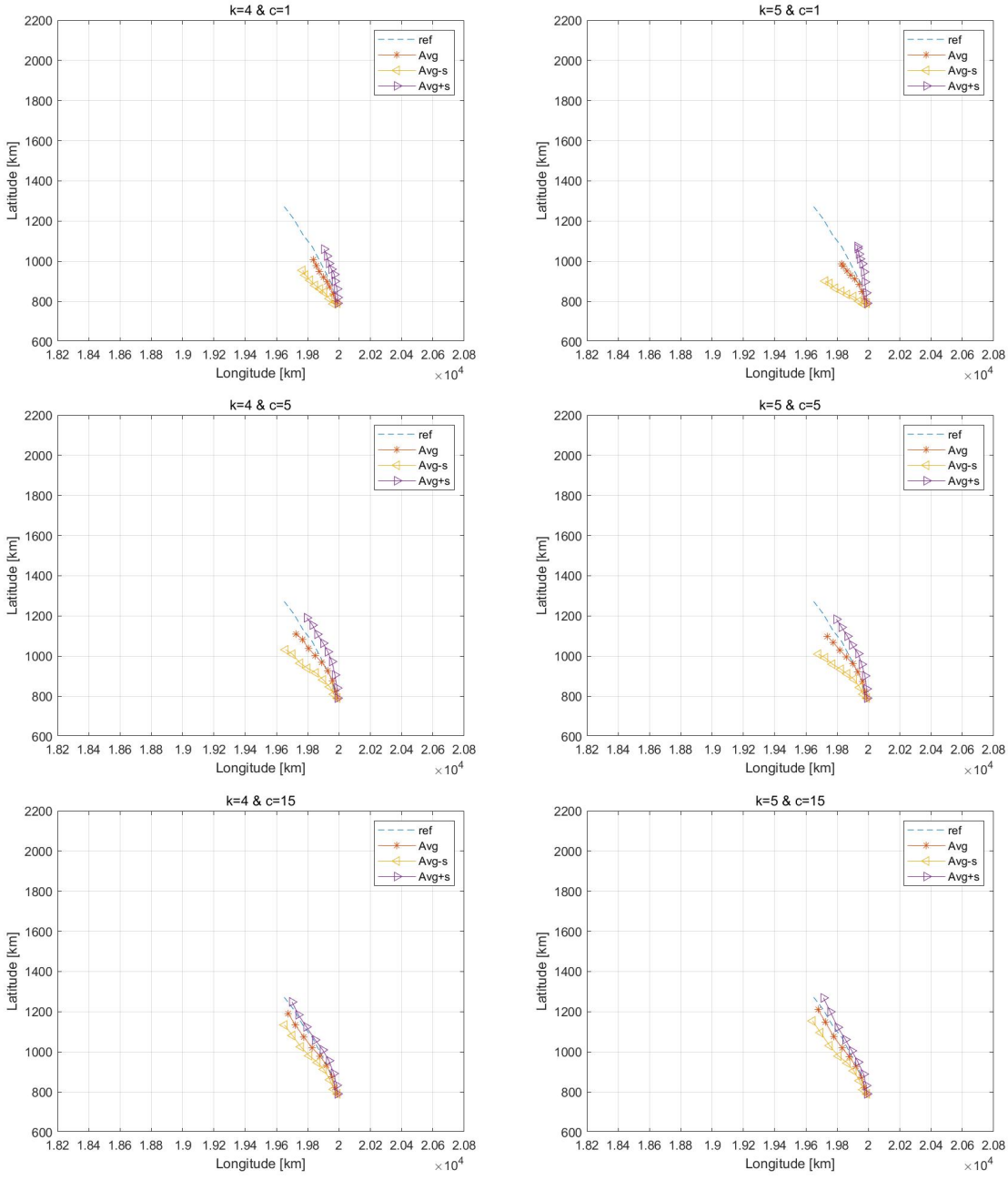

Figure 4.11: Same as Fig. 4.10 but with wavenumber 4 and 5.

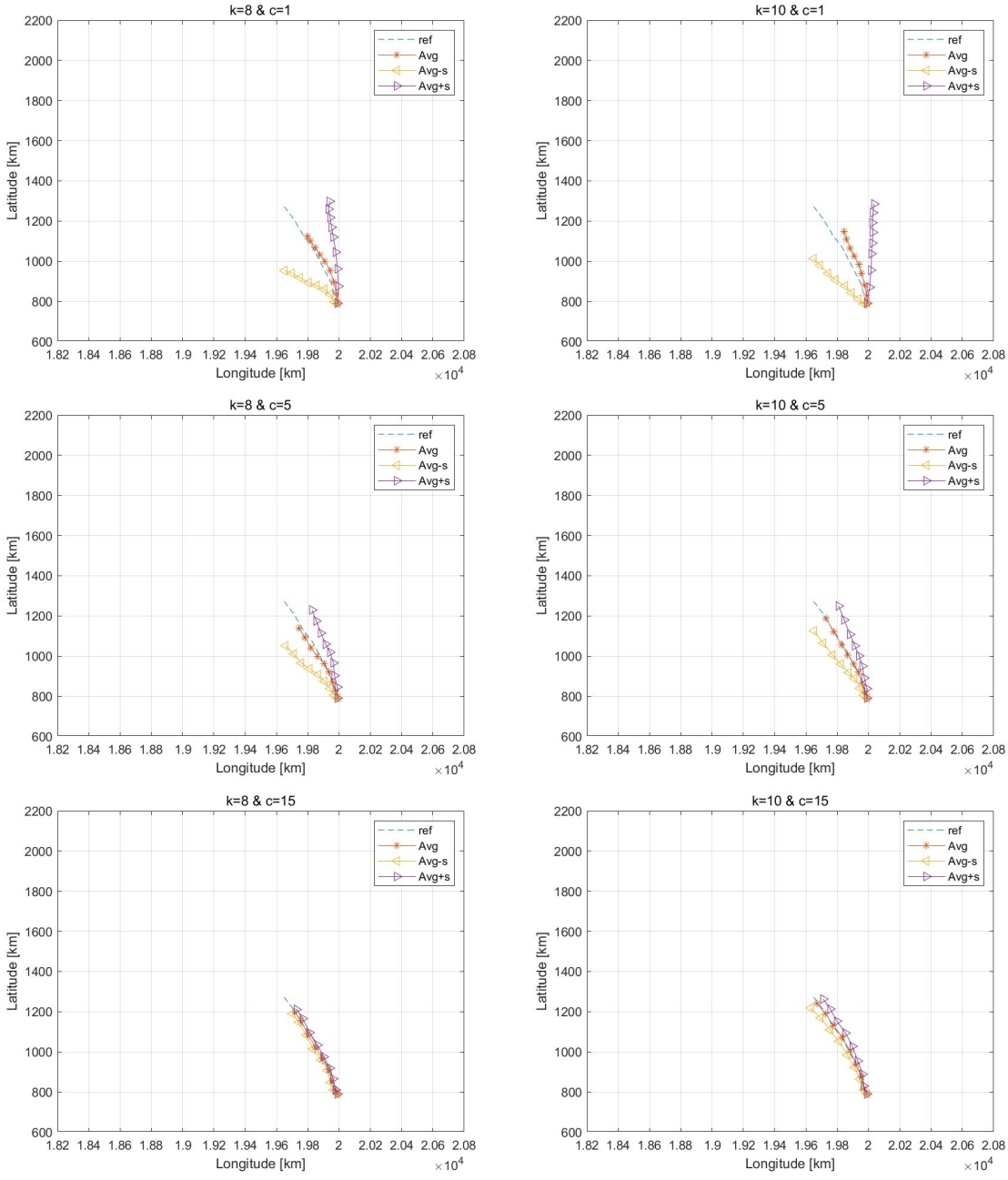

Figure 4.12: Same as Fig. 4.10 but with wavenumber 8 and 10.

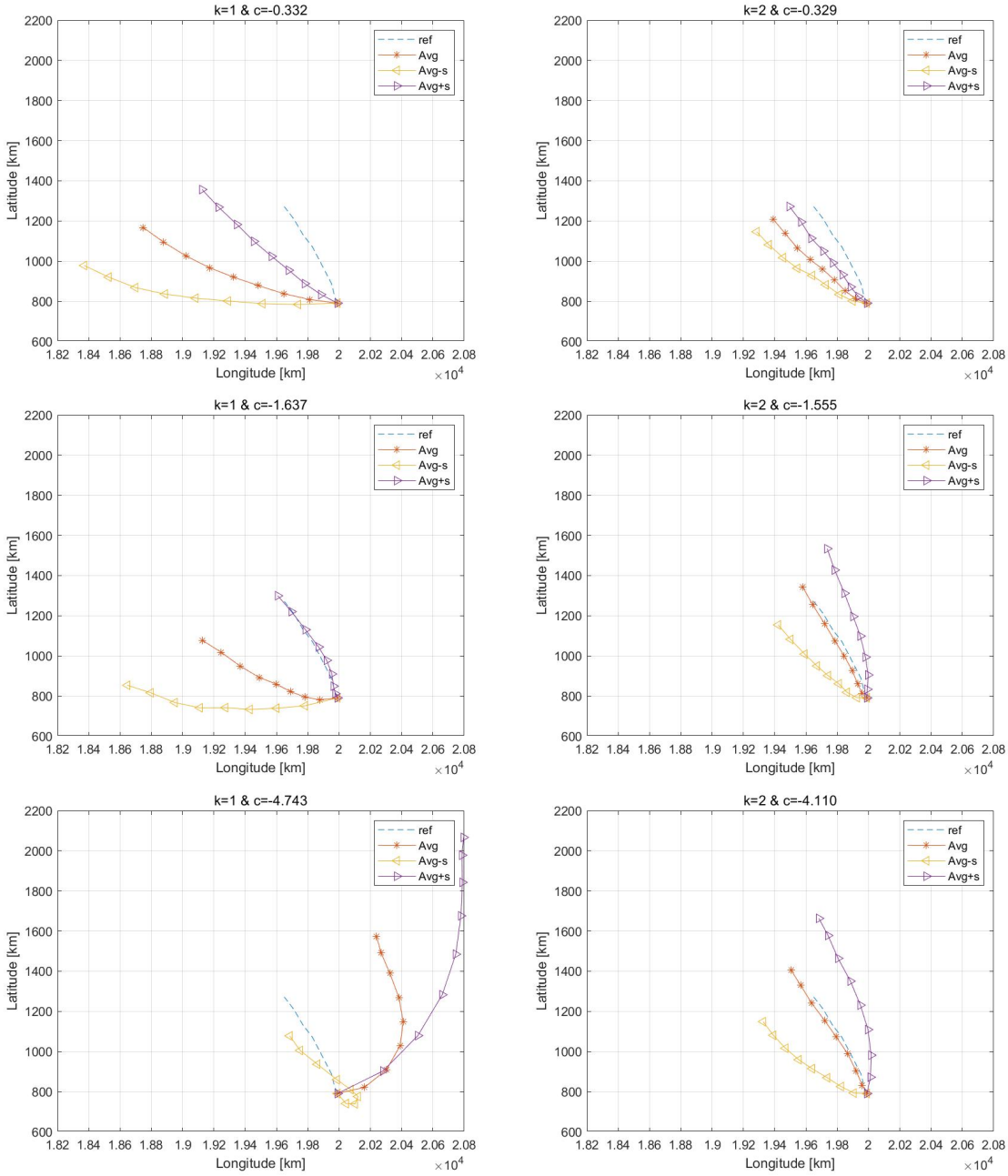

Figure 4.13: Same as Fig. 4.10 but for Rossby wave with wavenumber 1 and 2, and gravity phase speeds 1 m/s, 5 m/s and 15 m/s.

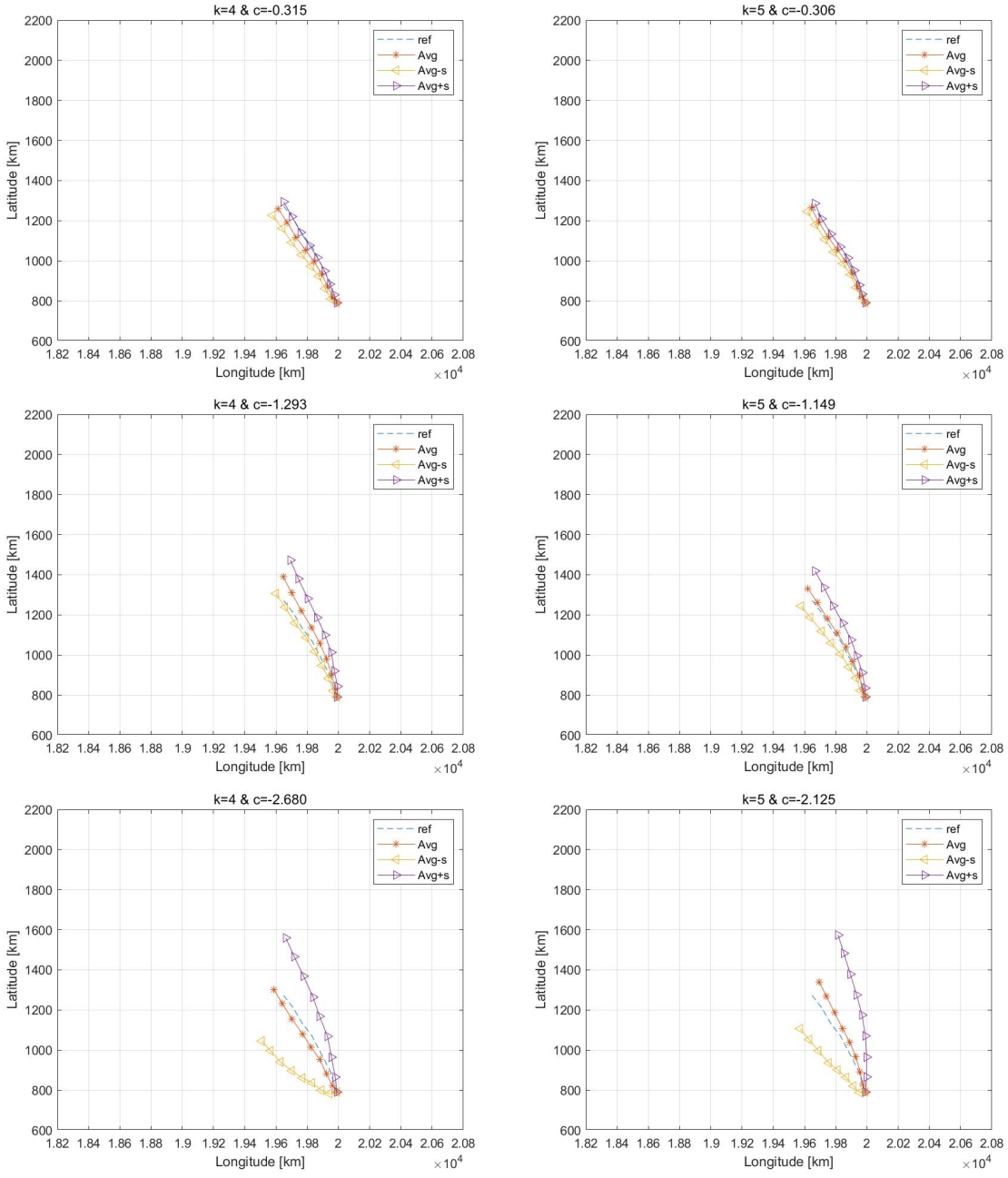

Figure 4.14: Same as Fig. 4.13 but with wavenumber 4 and 5.

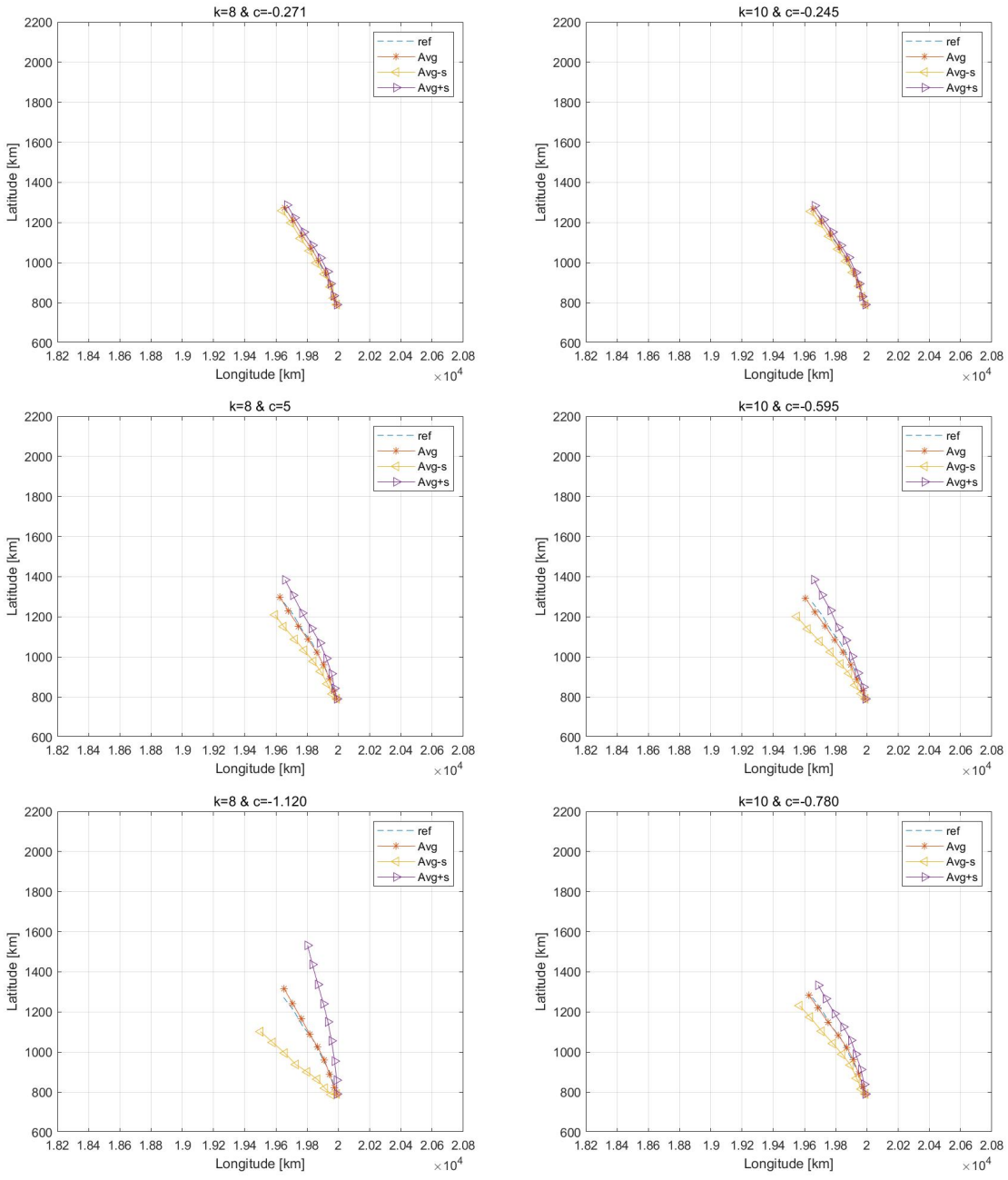

Figure 4.15: Same as Fig. 4.13 but with wavenumber 8 and 10.

(2) Rossby wave cases

In general, the TC trajectories tend to have a similar trajectory as the wave speed decreases. With wavenumber 1, the pattern is not seen, but the trajectories are hard to expect because the deviations are the widest. In addtion, the mean path and deviations with different wave speeds are not similar. Most of trajectories with wavenumber 1 do not follow the direction of reference. With $k = 1$ and $c = -4.743$ m/s, the TC moves to the east and north. In other cases with other wavenumbers, the direction of TCs is northwestward with different angles. All cases normally have longer lengths of trajectory than that of the reference, and a TC could move around 800 km farther to the north as shown in the case with $k = 1$ and $c = -4.743$ m/s. However, some cases also show that it could have shorter latitudinal distances than the reference. Only the two cases ($k = 8\&c = -0.271$ m/s, $k = 10\&c = -0.245$ m/s) are nearly the same as the reference in terms of direction and length of trajectory. These results demonstrate the randomness of movement of TCs in Rossby wave.

(3) MRG wave cases

Overall, the trajectories of TCs in MRG waves are relatively close to the reference, and they tend to move northward. With wavenumber 1 and 2, the traveling lengths and directions of the TCs are very similar. After that, as wavenumber increases, the length is longer, and TCs move more northward until wavenumber 8. In each wavenumber, slower wave speed makes the length longer. Furthermore, slower wave speed makes the trajectories divergent except the cases with wavenumber 5.

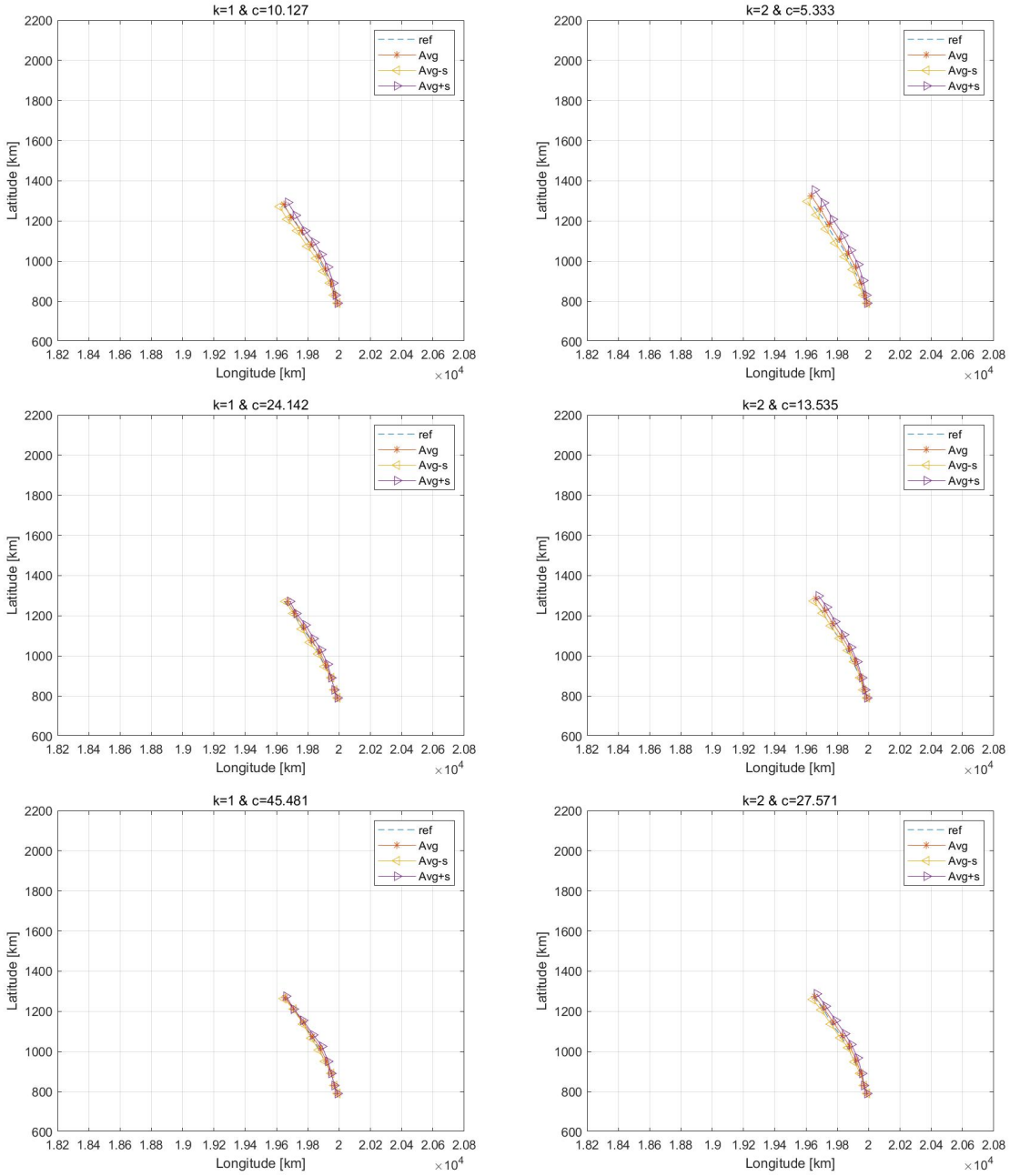

Figure 4.16: Same as Fig. 4.10 but for MRG wave with wavenumber 1 and 2, and gravity phase speeds 1 m/s, 5 m/s and 15 m/s.

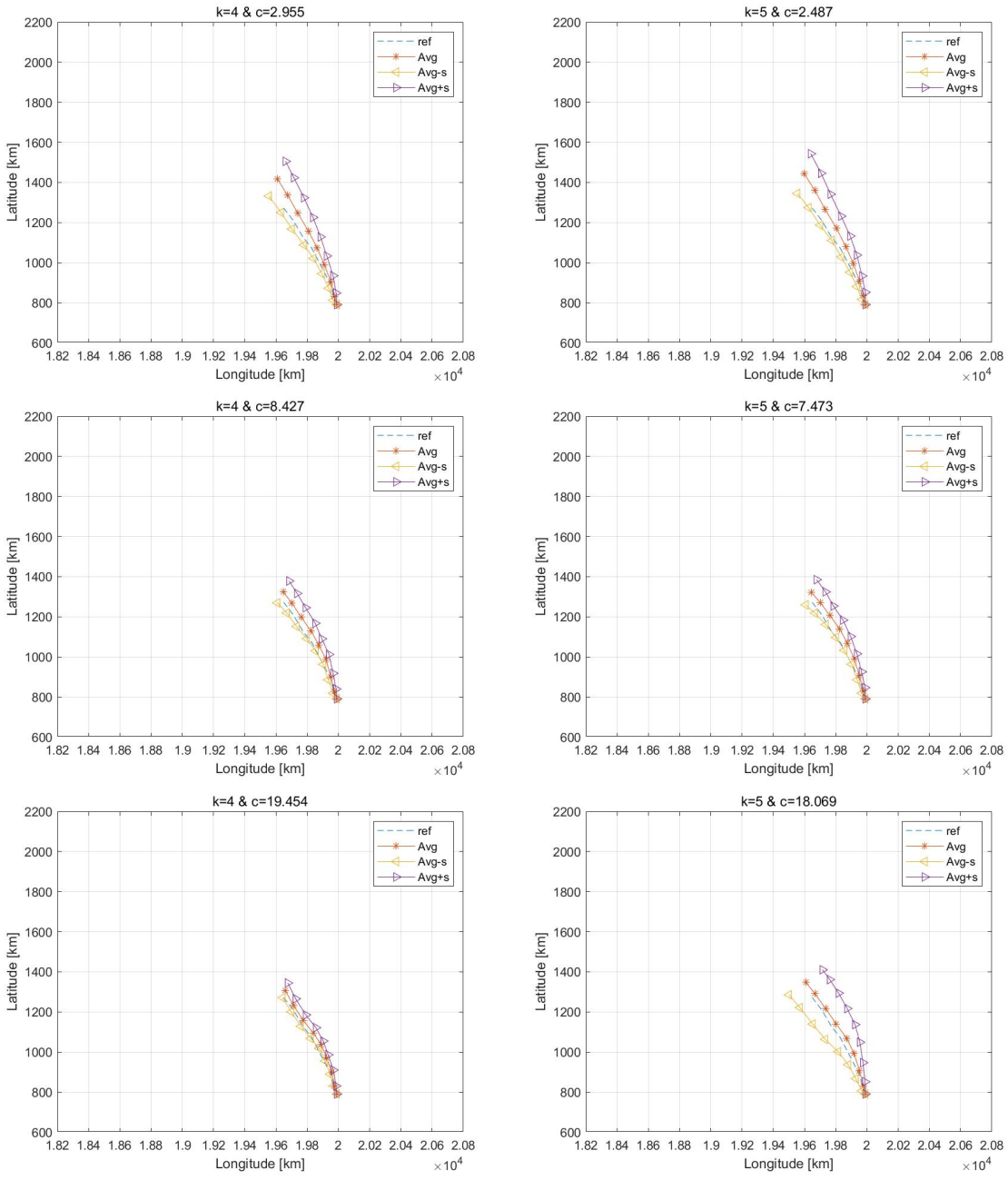

Figure 4.17: Same as Fig. 4.16 but with wavenumber 4 and 5.

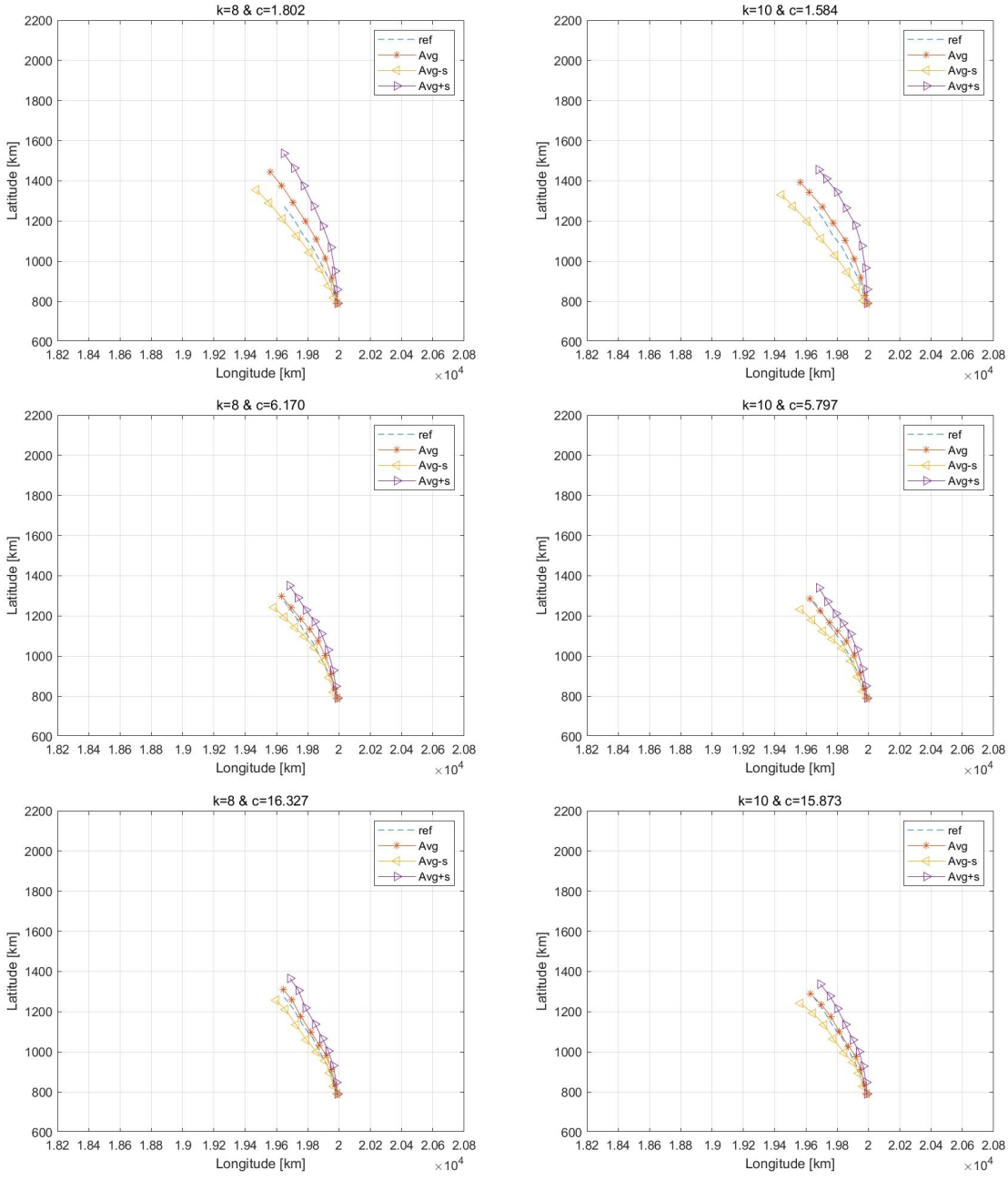

Figure 4.18: Same as Fig. 4.16 but for with wavenumber 8 and 10.

Chapter 5

An analysis of the relation between TC trajectories and the equatorially trapped waves

5.1 An analysis of the effect of the equatorially trapped waves on the traveling distance of TC

In the previous chapter, the effect of the equatorially trapped waves on the movement of TCs has been discussed. The equatorially trapped waves provide background flows for TCs. In this chapter, how the background flows affect the traveling distance of TCs will be discussed.

Fig. 5.1 is the scatterplot of the relation between maximum vorticity and traveling distance of TCs at 48 hours. The maximum vorticity exists at the center of the TC, and it implies the kinetic energy of the TC. The plot does not show that there is some relation between maximum vorticity and traveling distance. In order to investigate this further, we introduce the correlation coefficient

$$C_{\xi,d} = \frac{\sum_{j=1}^{n} \Delta\xi_j \cdot \Delta d_j}{(\sum_{j=1}^{n} \Delta\xi_j^2)^{1/2} (\sum_{j=1}^{n} \Delta d_j^2)^{1/2}} \tag{5.1}$$

Here, d_j is the straight distance of each case, d_{ref} is the straight distance of the reference and $\Delta d = d_j - d_{ref}$. ξ_j is the maximum vorticity of each case, ξ_{ref} is the

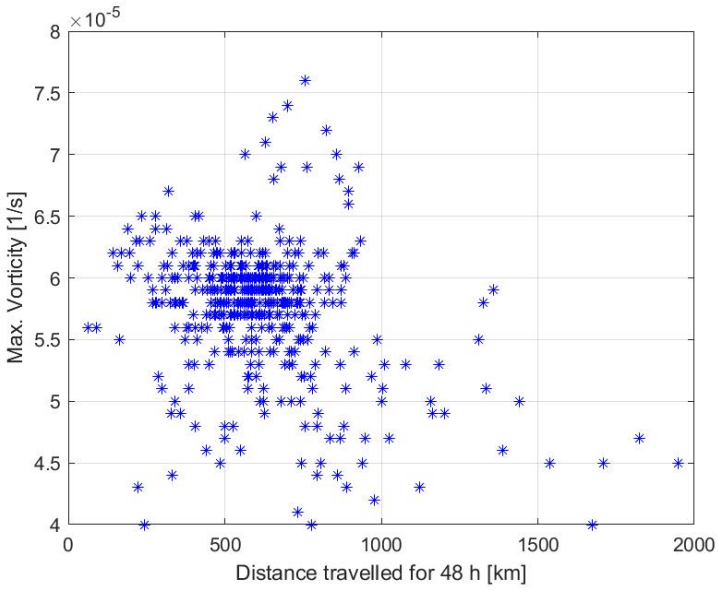

Figure 5.1: Scatterplot of traveling distance and maximum relative vorticity at 48 hours.

maximum vorticity of reference and $\Delta\xi_j = \xi_j - \xi_{ref}$. In the scatterplot, distance traveled for 48h is d_j, and maximum vorticity is ξ_j. They are all evaluated at 48 hours. The calculated $C_{\xi,d}$ is about -0.3585.

Thus, the change in vorticity is not the primary parameter that affects the change in the traveling distance of TCs by the equatorially trapped waves. Therefore, we are bound to conjecture here that the advection by the oscillatory background flow, induced by the waves, is the primary driver for the change in the traveling distance of TCs.

The length of the mean paths of TCs are summarized in Fig. 5.2. The length is measured from the initial to final positions following a straight line, but it is not the length of the trajectory of the TC. In the figure, the vertical axis is the deviation with respect to the reference distance corresponding to the uniform background case, and the horizontal axis is the case number in Table. 4.1. The deviation is the distance between Avg and Avg+s (or Avg-s) at 48 hours in Figs. 16, 17, and 18. Overall, the distance of TCs in Kelvin wave is shorter than that of the reference while TCs in Rossby and MRG waves move longer, which is consistent with the results in Chapter 4. As the wavenumber increases, the variation of the deviation of Kelvin and MRG wave cases becomes wider. However, Rossby cases have the opposite pattern.

In detail, Kelvin waves with $c = 1$ m/s are more influential among cases with the same wavenumbers. Especially, $c = 1$ m/s and $k = 4, 5$ have nearly the same effect. Also, the case $c = 1$ m/s has the largest fluctuation. As the wavenumber increases, so does the fluctuation. Considering that Cases 13 and 16 have very similar deviations and the deviation of Case 15 is less than that of Case 18, the fluctuation may decrease with higher wavenumbers. Rossby wave cases do not exhibit a pattern until Case 6, and wavenumber 1 and 2 are dominant over the change of wave speed for the Rossby wave forcing.

Faster wave speeds produce higher deviations, but the wavenumber seems to have a weaker effect. On the other hand, among MRG wave cases, cases with $c_e = 15m/s$ make the mean and deviation higher than cases with the same wavenumbers and lower gravity wave speeds. An increase of wavenumber has little effect on the means and deviations compared with the other two waves.

In addition, the results in Fig. 5.2 can be used to infer the TC average speed from the mean path, since all cases are run for two days. In Kelvin wave cases, faster wave speed makes TC speed faster. On the contrary, Rossby wave cases 7 to 18 demonstrate that TC speed is partially germane to wavenumber. Larger wavenumber is responsible for slower TC speed. Similarly, among MRG wave cases, larger wavenumber causes faster TC speed. However, the physics to determine TC speed should be further studied.

5.2 Discussion on trajectories of tropical cyclone and wave fields

In this chapter, how wavefields or advection affect the trajectories of tropical cyclone (TC) is described for some significant cases. Other cases have a similar direction and distance to the reference without background flow. In general, a weak wind and vorticity field does not quite influence the movement of a TC. In the figures of wave fields, arrows indicate the direction of wind, and the length means the strength of wind. In addition, the red point is the center of the TC and the black circle is where wind speed is 5 m/s. Recall that the Kelvin and the MRG waves move to the east while the Rossby wave moves to the west according to the simulation setting.

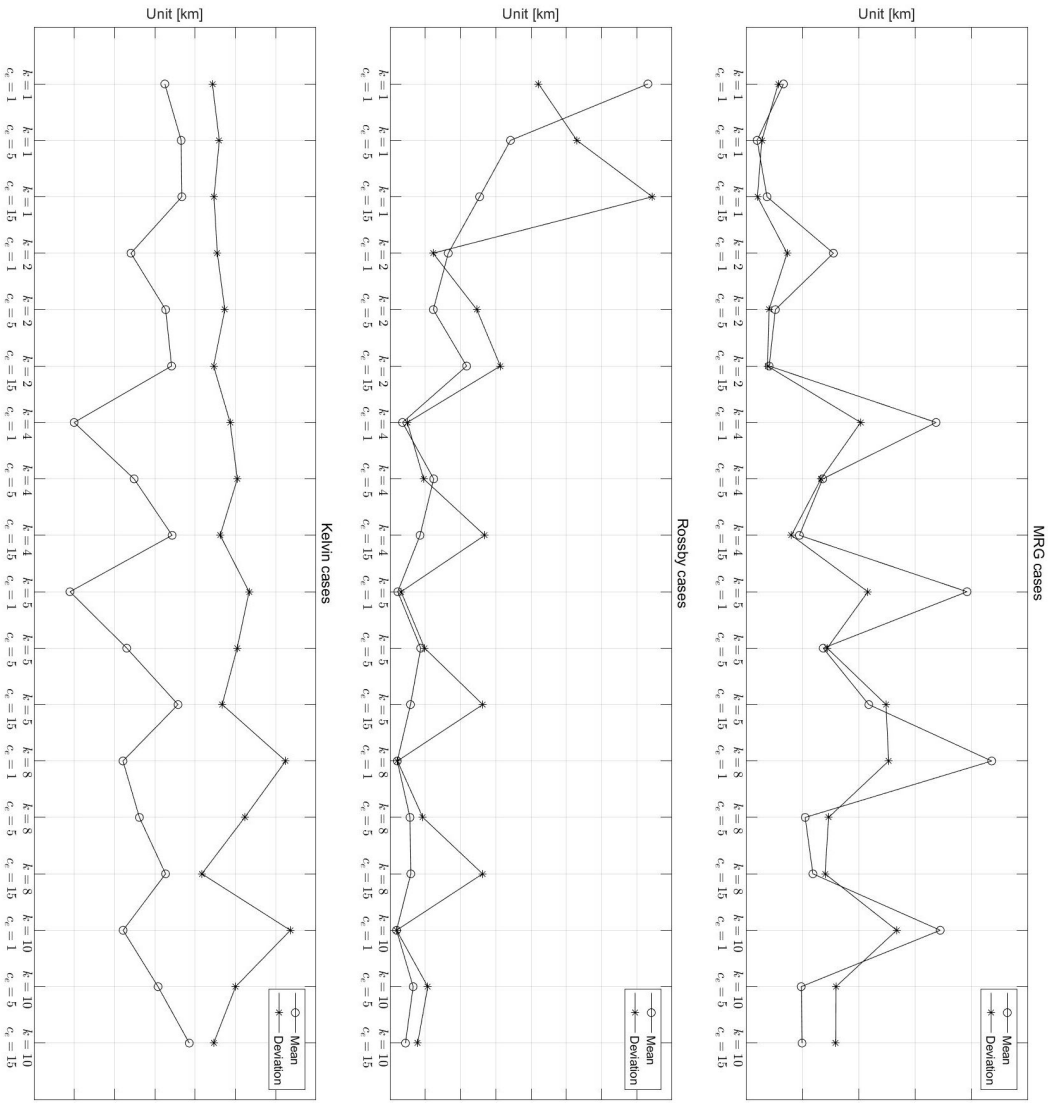

Figure 5.2: Distance of mean paths and deviations at 48 hours in terms of the simulation cases in Table 4.1.

5.2.1 Kelvin wave cases

Fig. 5.3 shows the trajectories of the selected cases and wave fields before putting a TC. The responses of wave fields of Kelvin wave to TCs are not crucial to the movement of the TC, so it is enough to look at the initial wave fields in order to explain how trajectory is determined.
First of all, the case with $k = 8\&c = 15$ m/s is a typical case that is similar to the reference. Since a negative vortex has clockwise wind, it restricts the wind of the TC which rotates counterclockwise. The vortex consumes the kinetic energy of the TC, which is for moving to the north. However, the case with $k = 8\&c = 15$ m/s is not affected as much as the other two cases. The first reason is that the size of the negative vortex is the smallest. The second is that the strength of the vortex is weakest. Lastly, the wave speed is 15 m/s, the wave passes the TC so quickly that the wave does not influence it. These can also explain the differences between cases with $k = 4\&c = 1$ m/s, $k = 4\&c = 5$ m/s and $k = 5\&c = 5$ m/s. In the wave field of $k = 5\&c = 5$ m/s, there is a wind in the center of the TC which forces the TC to the south, but the trajectory does not show the impact. However, in the case with $k = 10\&c = 1$ m/s, the TC moves to the south in accordance with the wind in the center until it develops enough negative vortex for moving northward. The position of the vortex is on the southwest side, so the tropical cyclone moves to the northeast. These interpretations are possible because the interaction between Kelvin wave field and TCs is not strong. If the interaction is strong, the movement of TCs cannot be explained by the wave field at an injection time because the wavefield is very different from the initial wave field. On the contrary, it does not work for cases with Rossby and MRG waves.

5.2.2 Rossby wave cases

The trajectories of TC become convergent to the reference as wavenumber and wave speed increase. Two cases with $k = 1\&c = -1.637$ m/s and $k = 1\&c = -4.743$ m/s are greatly affected, so these are considered. Unlike Kelvin wave, higher wave speed of Rossby wave can change the movement of the TC. The response of Kelvin wave is a simple distribution of alternative positive and negative vortices, but there are big rotating wind fields and negative vortices in Rossby wave. In Fig. 5.5 and 5.6, the left figures are the initial wave field, and the right figures are the wavefield at 24 hours. For the case with $k = 1\&c = -1.637$ m/s, the TC is initially positioned in

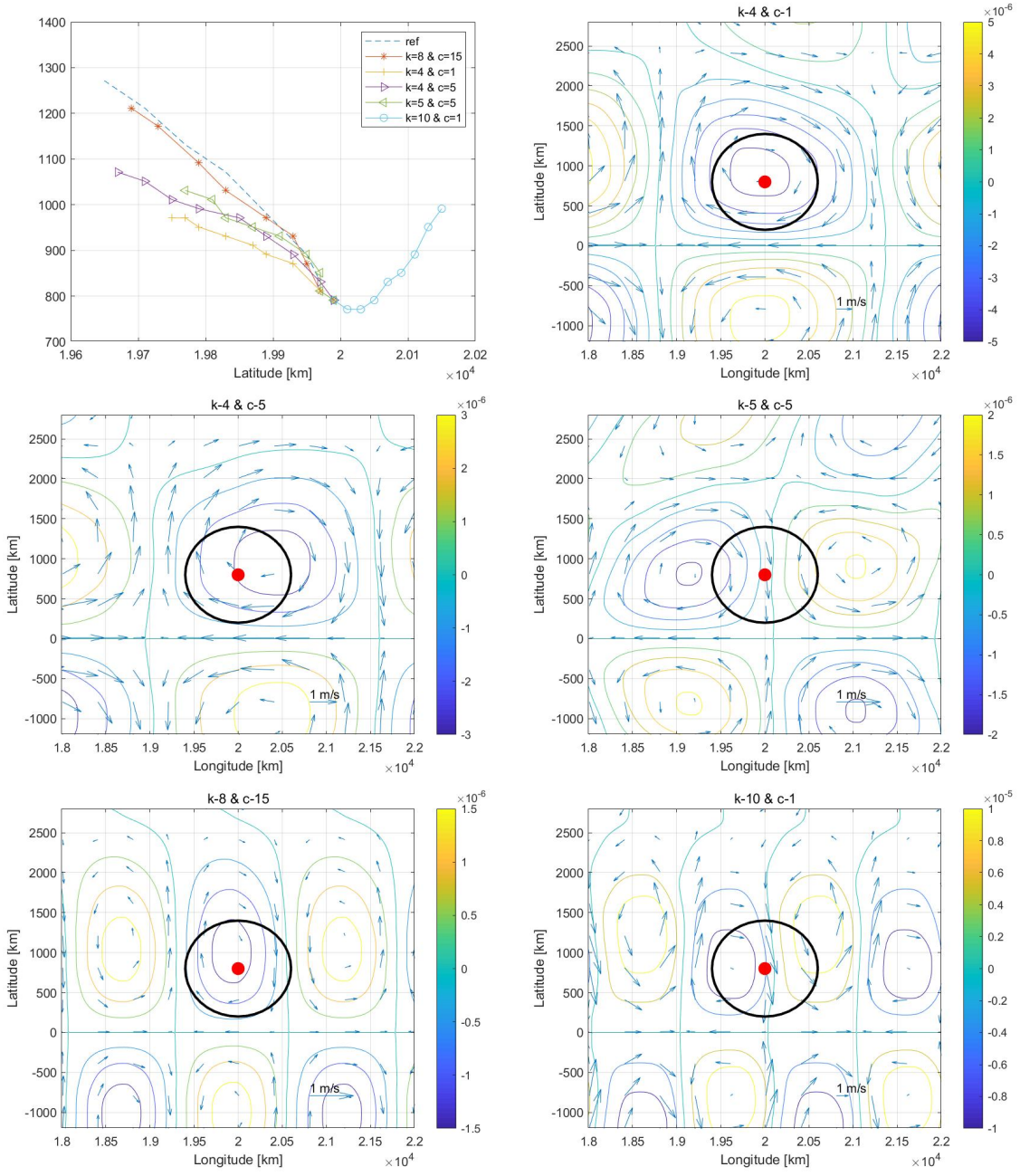

Figure 5.3: Trajectories of tropical cyclone and corresponding pre-existing Kelvin wave generated backgrounds.

the middle of a big negative vortex. In the lower half part of the TC, there is a strong wind field going to the west, but the upper part is very calm. It can be guessed that a TC moves to the west by the force of the wind field for some time. Finally, it moves less than 200 km to the north, and it does not have a surrounding negative vortex that the reference has. Thus, the occurrence of a negative vortex is suppressed by the wind field and the big negative vortex. Also, the shape of the TC at 24 hours is somewhat crushed, which shows the impact of the wind field. Besides, the wind field pushes the TC to the west so that the trajectory is very long toward the west.

For the case with $k = 1\&c = -4.743$ m/s, the TC is initially placed on a wind field going northeastward. Then, it moves in the same direction as the wind field. From around 12 hours, it develops an adjacent negative vortex on the right side. As time goes by, the negative vortex is growing and surrounding the northeast side of the tropical cyclone. Hence, the trajectory becomes northwestward from 18 hours to 36 hours. Around 36h, the TC meets a strong wind field flowing to the southeast, and then the negative vortex rotates and surrounds the tropical cyclone on the southeast side. With the position of the negative vortex, it is hard for the TC to move northward.

5.2.3 MRG wave cases

In general, TCs in MRG waves travel longer than and similar distances to the reference. Among TCs with longer distances, two cases with different wavenumbers are chosen to study the factors that make TCs move longer. In view of Fig. 5.7, the slopes of the two TC trajectories after 6 hours are different. The wavefield with $k = 8\&c = 1.802$ m/s has stronger positive vorticity, and the TC is initially located on it. This environment is helpful for the TC to move to the north. Looking at the figures at 30 hours, the TC in wave with $k = 8\&c = 2.955$ m/s has a bigger negative vortex beside it than the TC in wave with $k = 8\&c = 1.802$ m/s. However, the TC in wave with $k = 8\&c = 1.802$ m/s has a stronger negative vortex. These reasons could determine their difference in length of trajectory. Moreover, the TCs have to pass the region in which there is a wind field moving to the south. The wave with $k = 4\&c = 2.955$ m/s has such a wider region, so the TC may get affected longer. Now, two cases with the same wavenumber and wave speed are compared. In Fig. 5.10, the TC is simulated from 10 day developed wave. In Fig. 5.11, the TC is

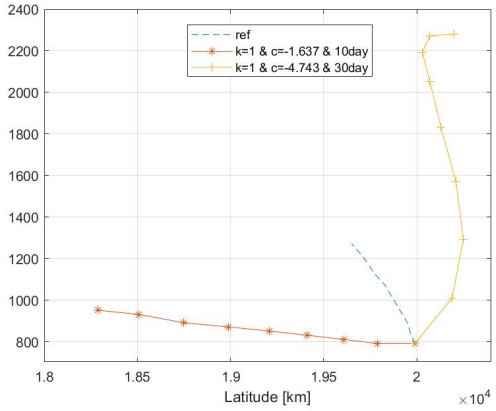

Figure 5.4: Trajectories of tropical cyclone in Rossby wave generated background.

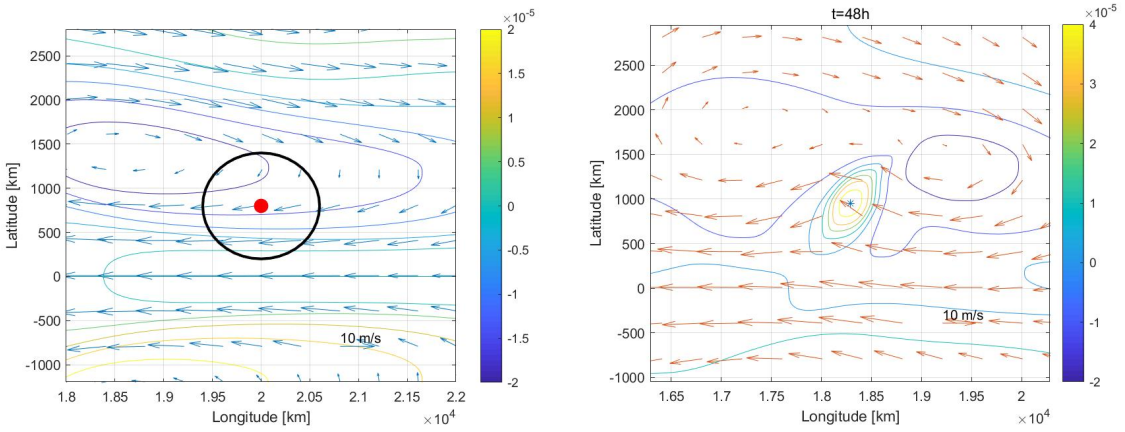

Figure 5.5: Rossby wave generated background of k=1 & c=-1.637 at 0h and 48h.

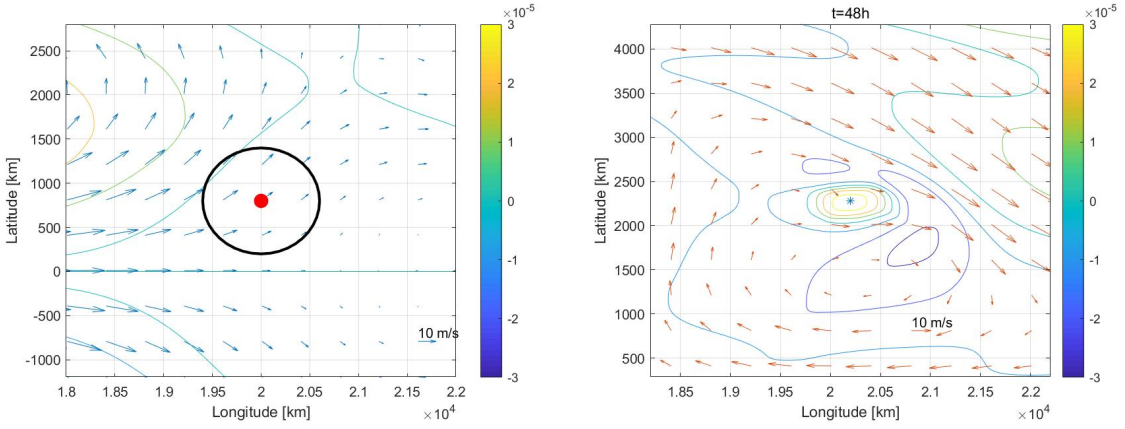

Figure 5.6: Rossby wave generated background of k=1 & c=-4.743 at 0h and 48h.

simulated from 30 day developed wave. Looking at the figure at 0 hours, the TC of 10 day is located below a big negative vortex. It surely passes the vortex and confronts a wind field moving to the north. On the contrary, the TC of 30 day is initially located on a wind field moving to the south, so it does not move to the north during the first 6 hours. Afterwards, it passes a big negative vortex that consumes the kinetic energy of TC. In view of the figures at 30 hours, the TC of 10 day has a stronger negative vortex.

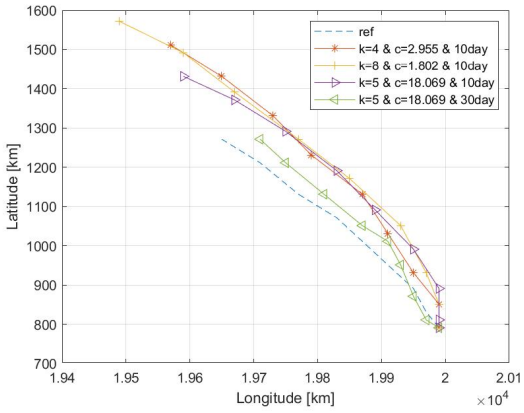

Figure 5.7: Trajectories of tropical cyclone in MRG wave generated background.

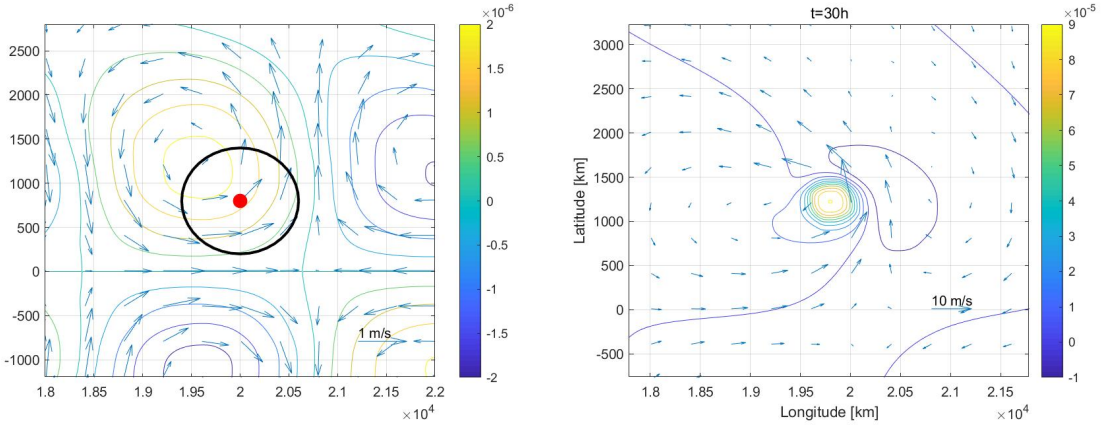

Figure 5.8: MRG wave generated background of $k = 4 \& c = 2.955$ at 0h and 30h.

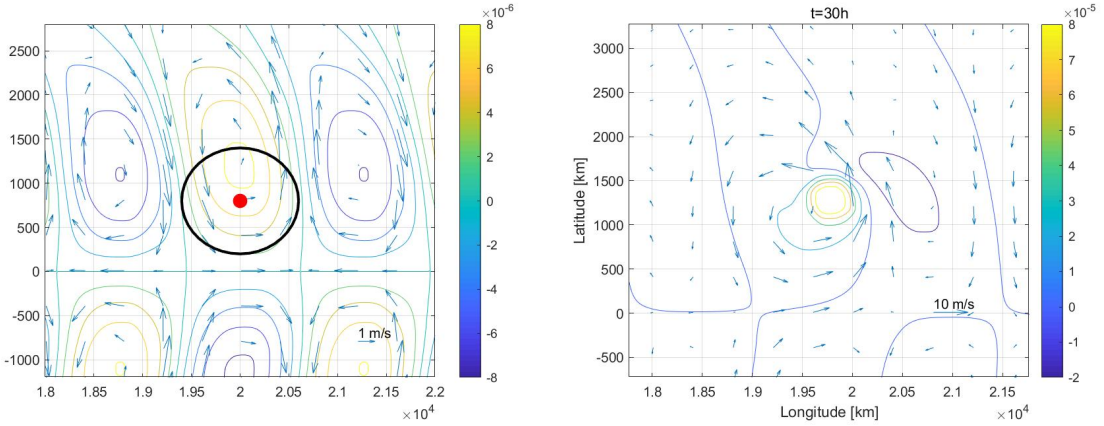

Figure 5.9: MRG wave generated background of $k = 8 \& c = 1.802$ at 0h and 30h.

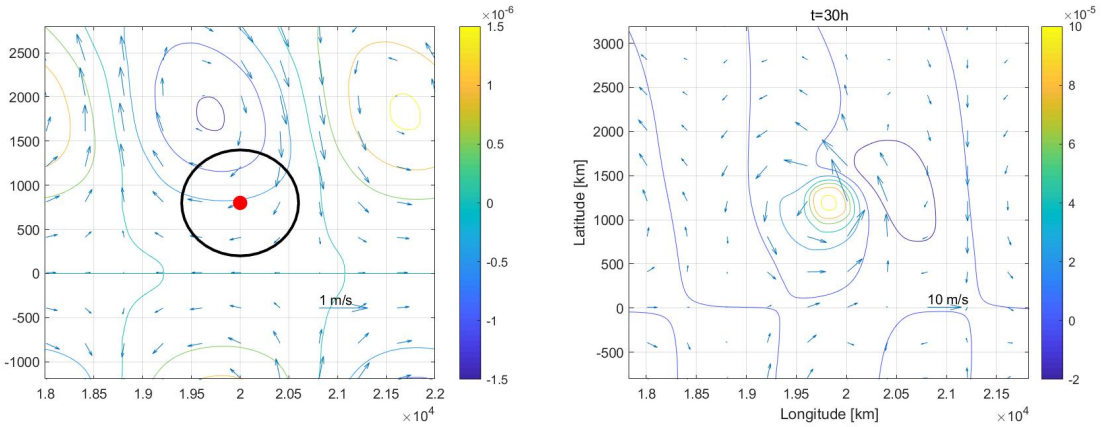

Figure 5.10: MRG wave generated background of $k = 5\&c = 18.069\&10day$ at 0h and 30h.

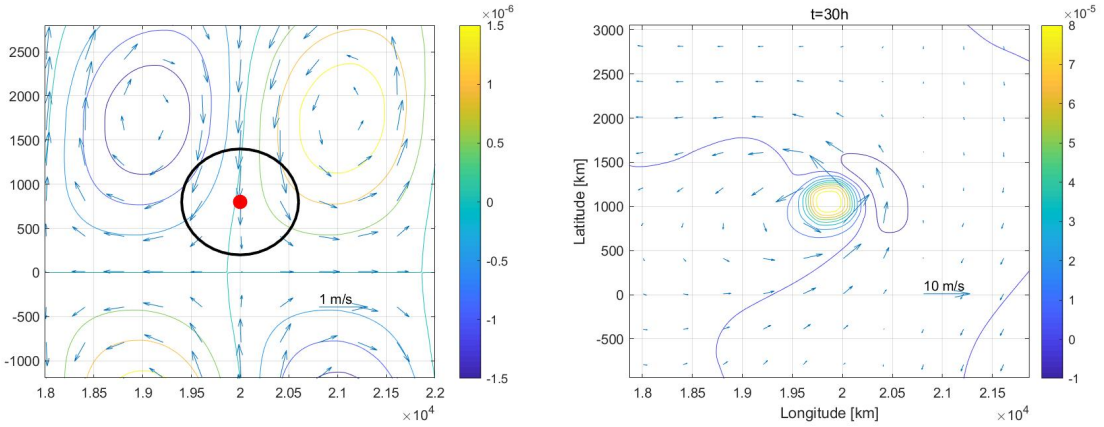

Figure 5.11: MRG wave generated background of $k = 5\&c = 18.069\&30day$ at 0h and 30h.

Chapter 6

Conclusions

The movement of tropical cyclones (TC) has been an interesting topic for decades, and the physics have been investigated based on a barotropic model. In addition, the interaction of a TC with other tropical flow dynamics such as equatorial waves and monsoon troughs, has been studied in some simple model setting. In this research, the non-divergent barotropic equations were numerically solved using a non-oscillatory balanced scheme. Then, the interaction between TC and monsoon is simulated using the same conditions of a case of a previous research [2]. Lastly, the effects of equatorially trapped waves are studied, which is a novel result.

Without background flow, it is found that a TC moves to the northwest. Due to advection nonlinearities, the TC develops asymmetric flows to its sides with negative vorticity to the east due to the beta-effect, which helps advect the TC in the north-west direction. This process is called the beta drift. The development of asymmetric flows is studied using Fast Fourier Transform after some data arrangement. As a result, the amplitudes of wavenumber 1 and 2 are dominant, which is consistent with previous research [16]. Moreover. the amplitude varies with time, but the amplitude of wavenumber 1 is always bigger than that of wavenumber 2. Furthermore, the negative vortex appears on the east of the TC and extends to the north, which determines the direction of the movement of the TC.

It is known that the TC suddenly changes the direction of movement if it meets the monsoon trough [2]. The previous work shows the sudden change of direction depending on the position of the TC and the distance from the monsoon trough. For a demonstration, one case is simulated, but the numerical settings of the work are different from the settings in this research. This simulation runs for 4 days. After 1 day, the TC is combined with the monsoon trough, and then it rarely moves

for some time. Afterwards, it moves to the north from the west. During the movement, there is a huge negative vortex surrounding ranging from the northeast to the southeast side of the TC. Besides, the amplitudes of asymmetric wavenumber 1 and 2 have a different pattern from those of the TC without a background flow. Sometimes, the amplitude of wavenumber 2 is bigger than that of wavenumber 1. The effects of equatorially trapped waves on the movement of the TC are investigated using different wavenumbers and wave speeds. The equatorially trapped waves considered are Kelvin, Rossby and MRG waves. Using barotropic response from 10 days to 30 days, the TC is simulated. After simulating waves and TCs at the same time, the means and deviations of trajectory are calculated to deal with the random behavior of TC trajectories. As a result, some patterns of change of TC trajectory are identified depending on the type of waves. The cases with Kelvin waves have several types of patterns. Firstly, higher wave speed makes the trajectory of the TC convergent to that of the reference. Secondly, the trajectory does not change a lot for wavenumber 1 and 2. However, with wavenumber 4 and 5, it becomes much shorter. Lastly, it becomes divergent with wavenumber 8 and 10. Then, the cases with Rossby waves show that the trajectory is longer and divergent with lower wave speed. Next, the cases with MRG waves show that MRG waves provide favorable environments for TCs to move longer and to the north. The TCs are relatively close to the reference and usually travel longer distances.

An analysis is performed to comprehend how the waves affect the TC trajectory. There are two speculations: one is that the waves influence the kinetic energy of TCs which determines TC trajectories; another is that the fluid flow induced by the waves affects TC trajectories. The kinetic energy of TCs is related to the maximum vorticity which is measured at the center of TCs. Since there is a weak relation between maximum vorticity and TC trajectory, the fluid flow is a more dominant factor.

Appendix A

Time evolution of maximum velocity of barotropic flow generated by free moving equatorial wave forcing for 50 days

Different wavenumbers and phase speed of the forcing waves are used as indicated. The wave magnitude is fixed to $A = 15m/s$.

Kelvin, wavenumber-1

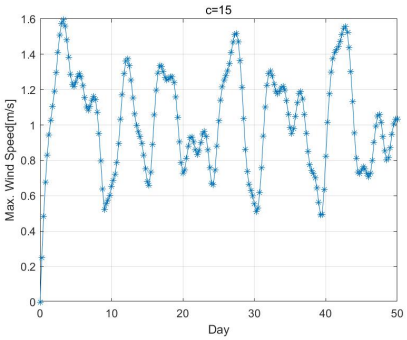

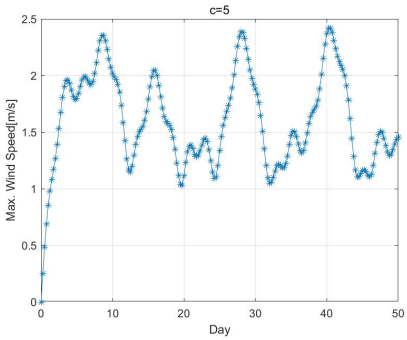

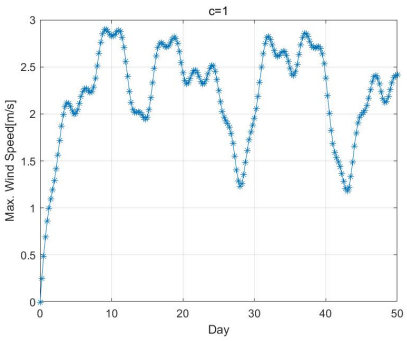

Kelvin, wavenumber-2

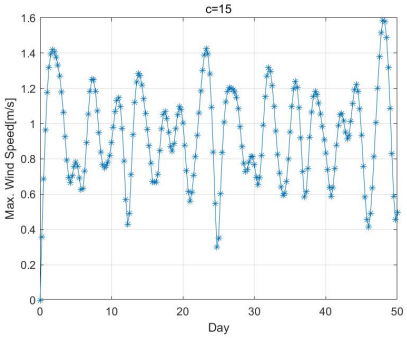

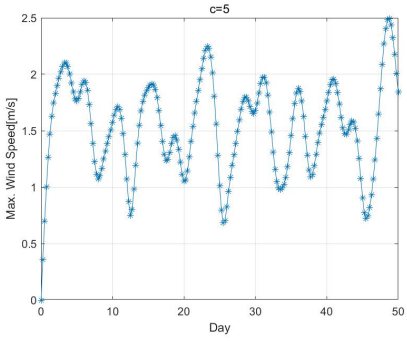

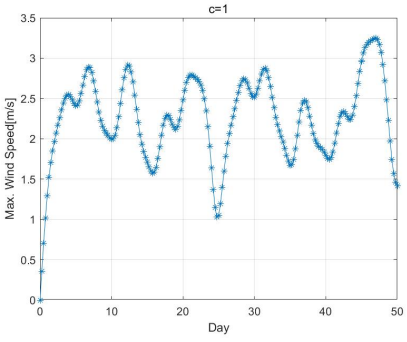

Kelvin, wavenumber-4

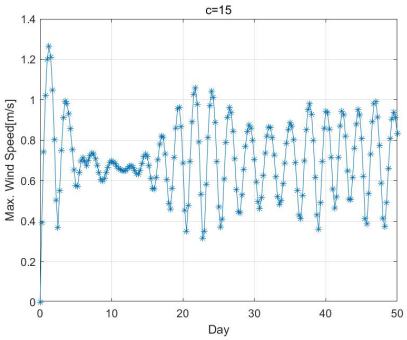

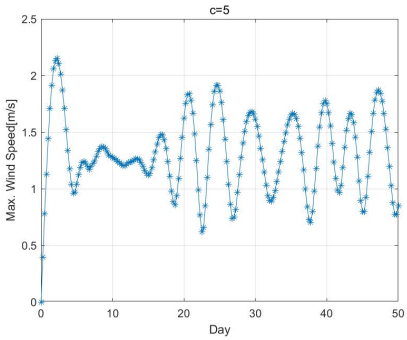

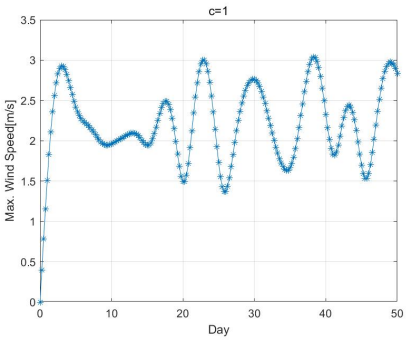

Kelvin, wavenumber-5

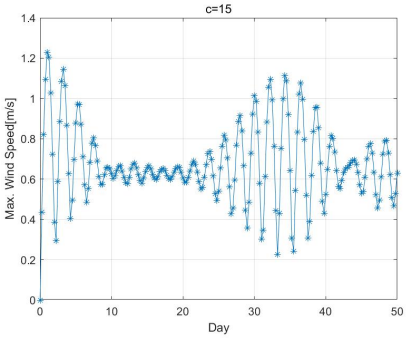

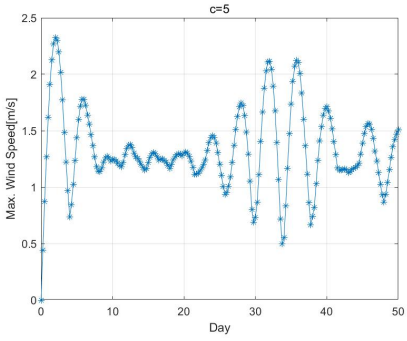

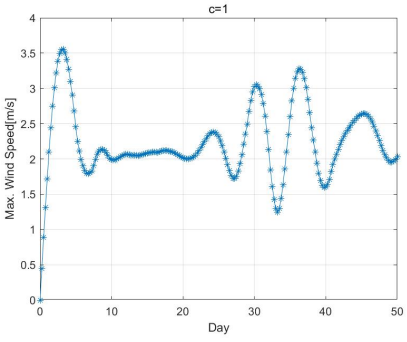

Kelvin, wavenumber-8

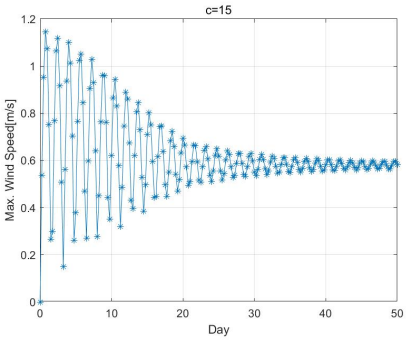

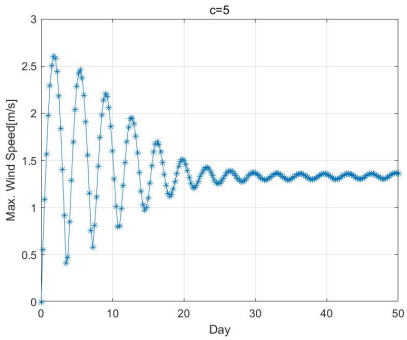

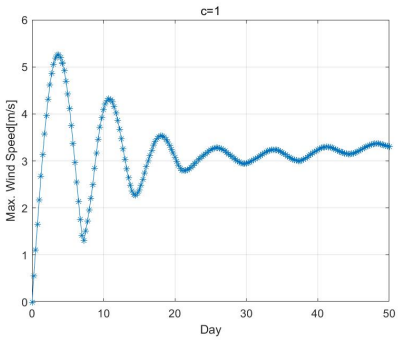

Kelvin, wavenumber-10

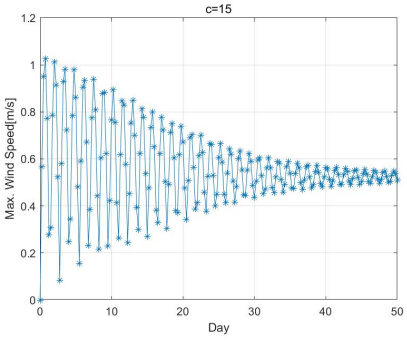

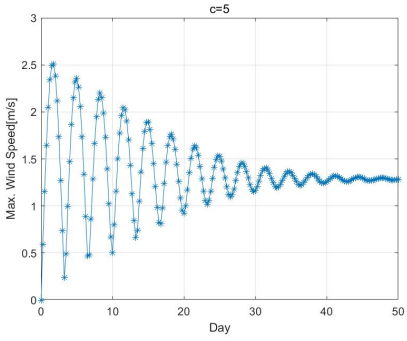

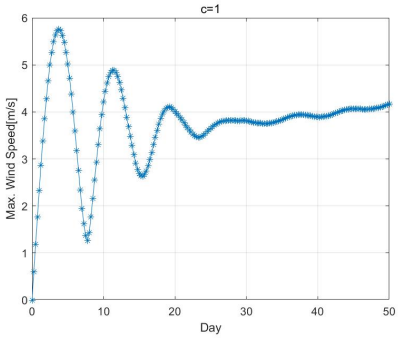

Rossby, wavenumber-1

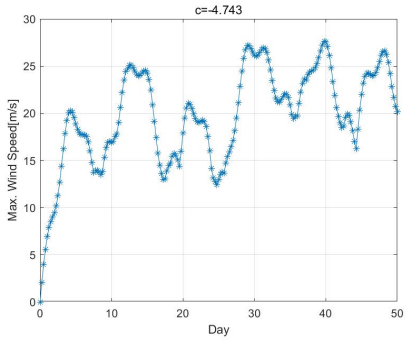

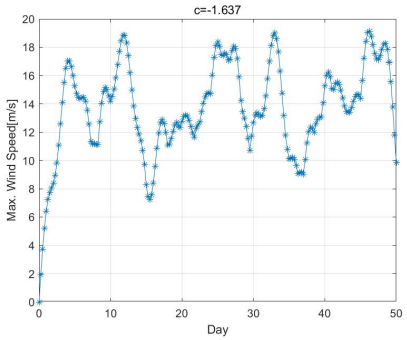

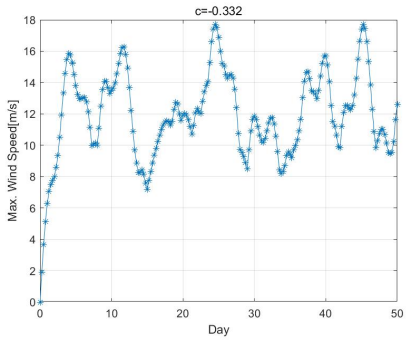

Rossby, wavenumber-2

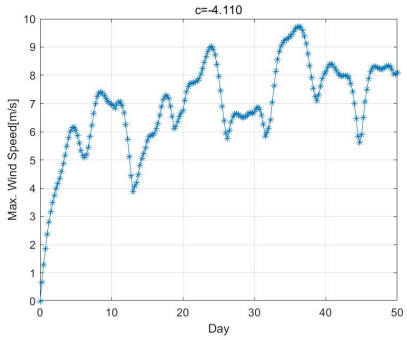

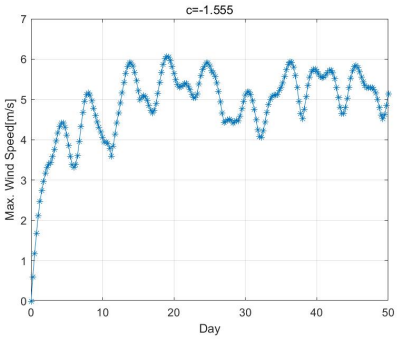

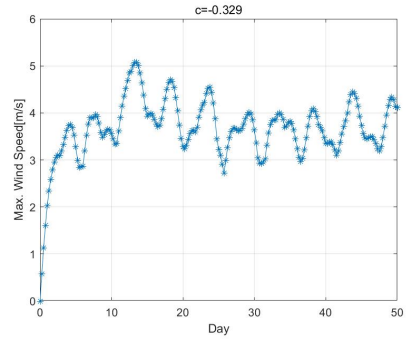

Rossby, wavenumber-4

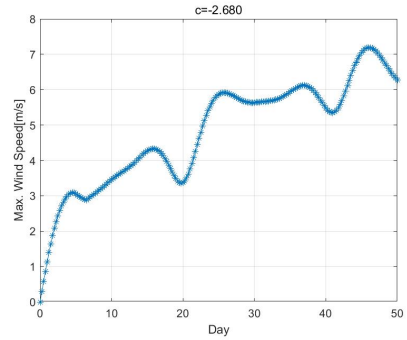

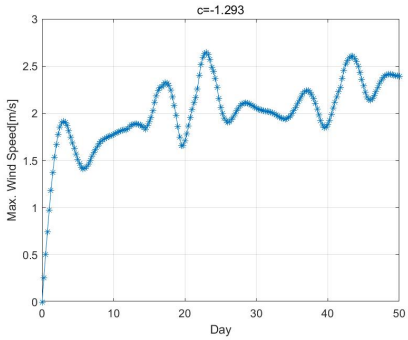

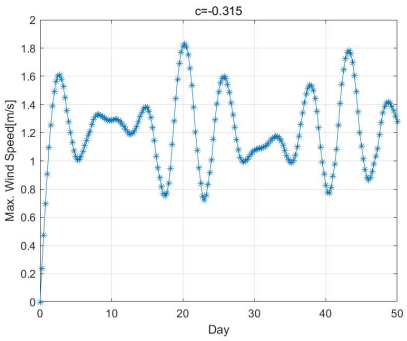

Rossby, wavenumber-5

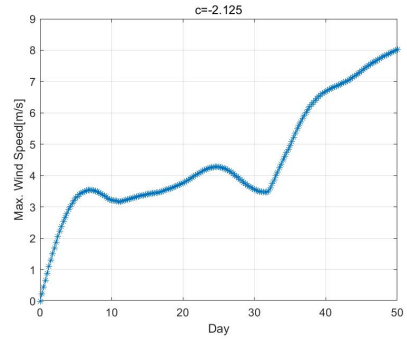

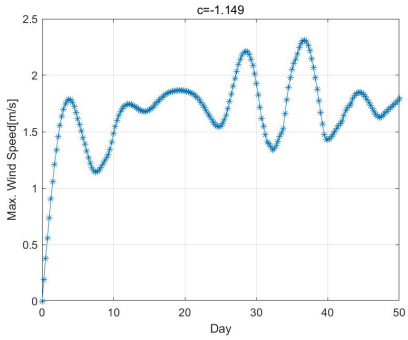

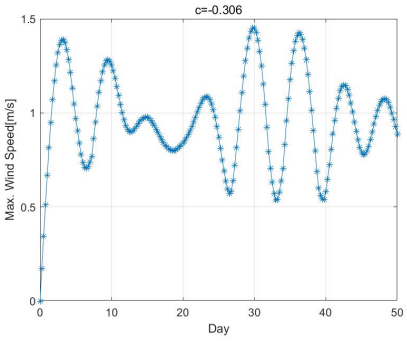

Rossby, wavenumber-8

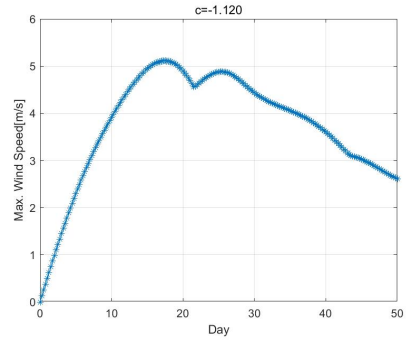

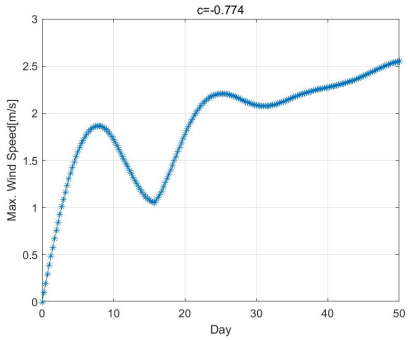

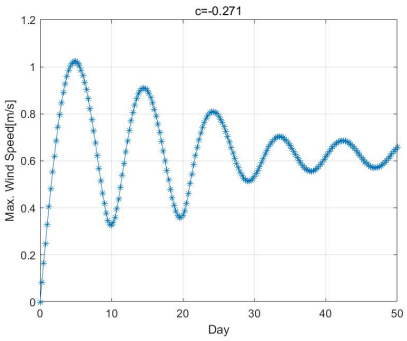

Rossby, wavenumber-10

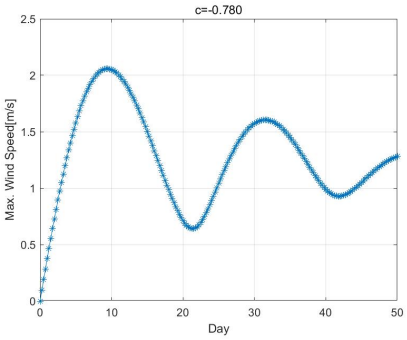

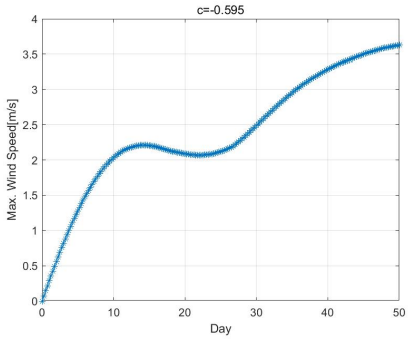

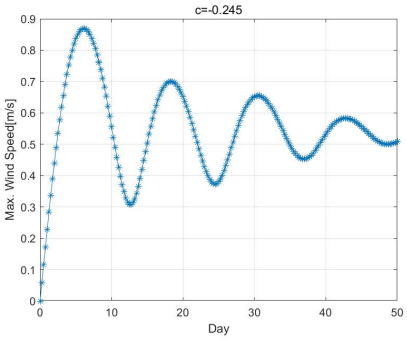

MRG, wavenumber-1

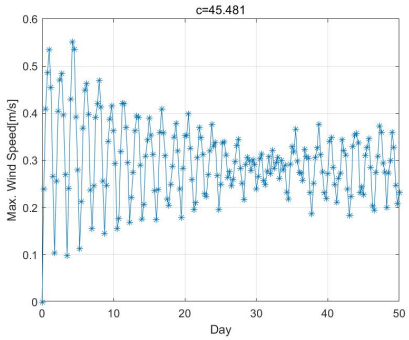

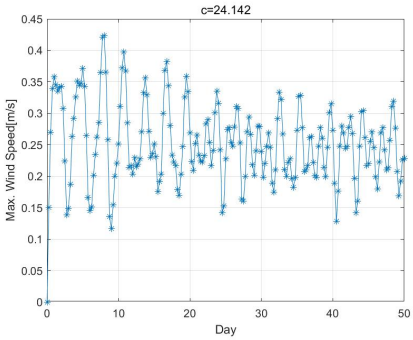

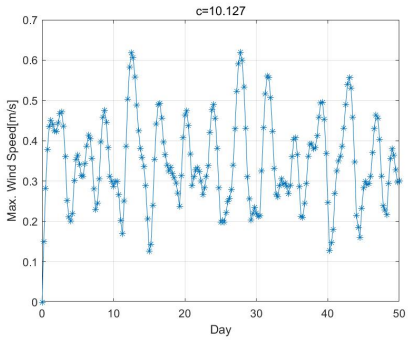

MRG, wavenumber-2

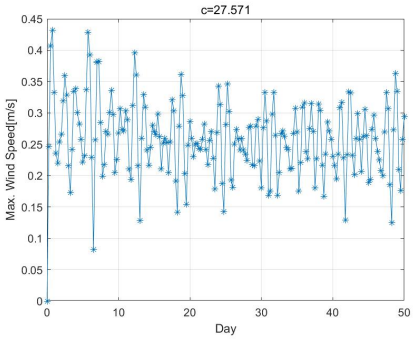

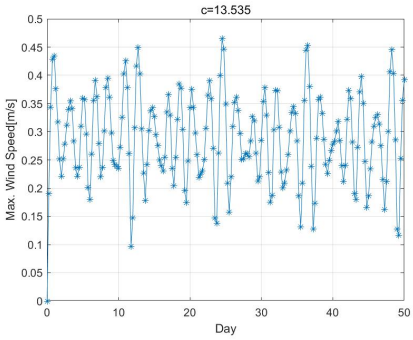

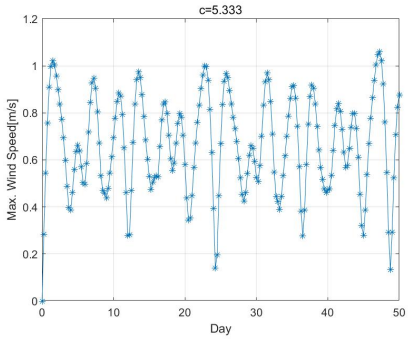

MRG, wavenumber-4

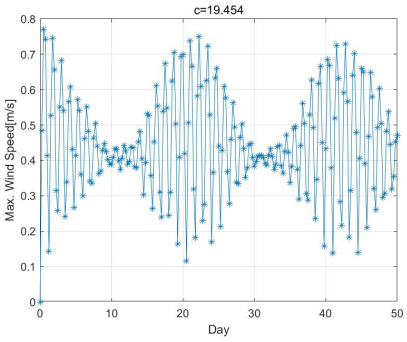

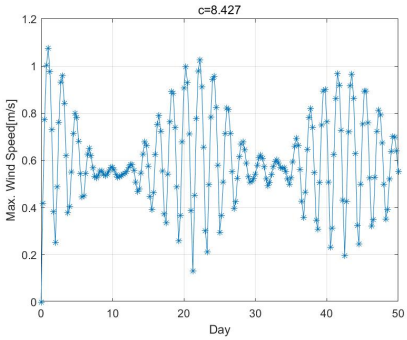

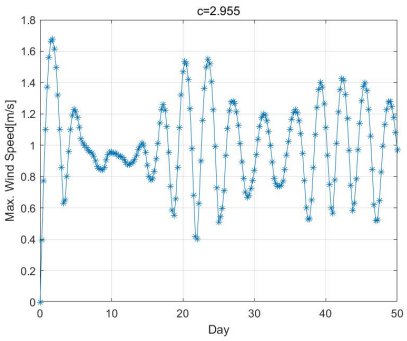

MRG, wavenumber-5

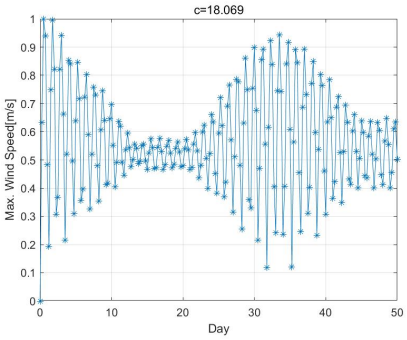

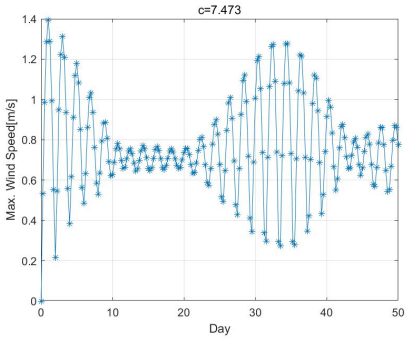

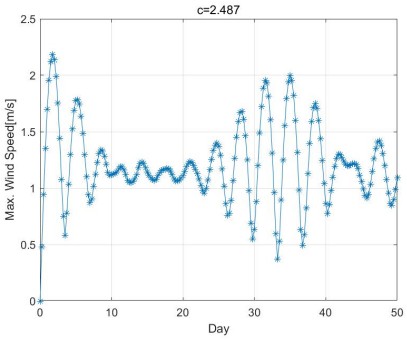

MRG, wavenumber-8

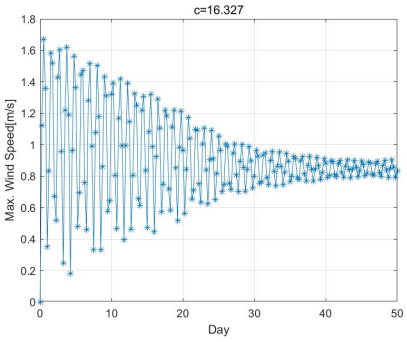

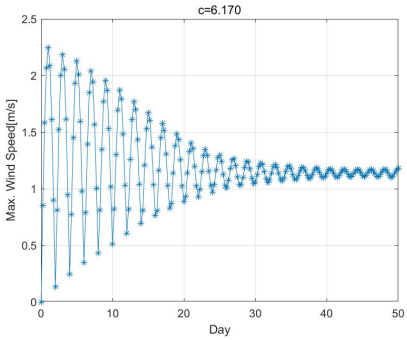

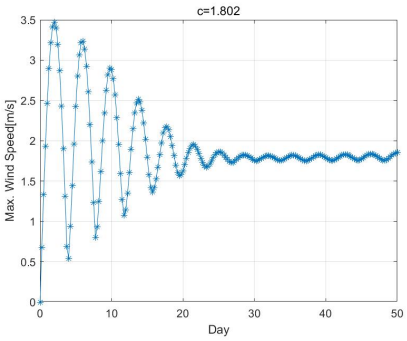

MRG, wavenumber-10

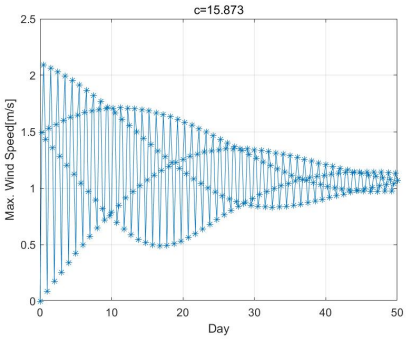

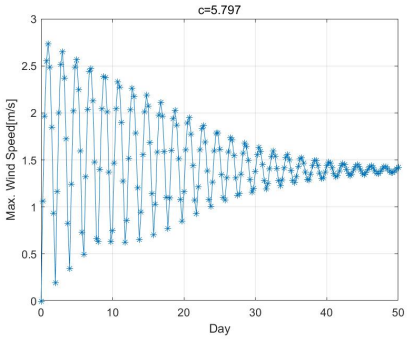

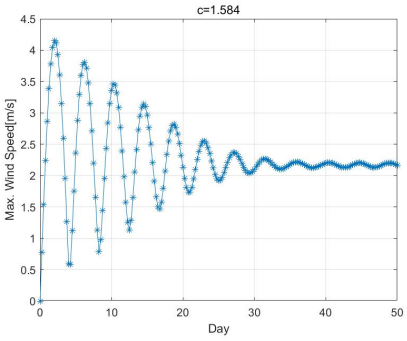

Appendix B

Barotropic flow field backgrounds generated by equatorially trapped waves at 10 and 30 days

The parameters are the same as in Appendix A.

Kelvin, wavenumber 1, wavespeed $15m/s$

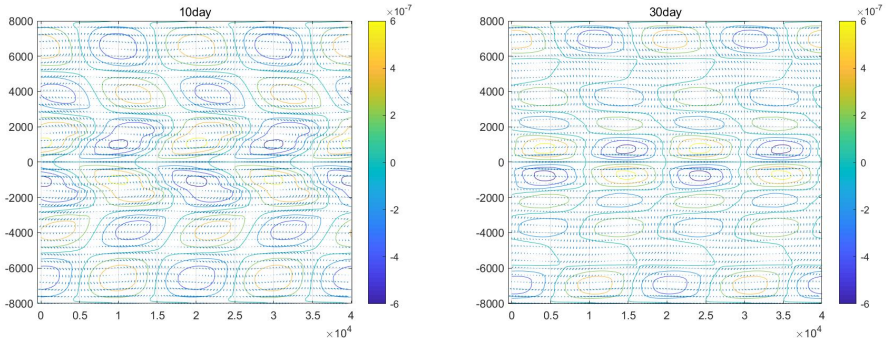

Kelvin, wavenumber 1, wavespeed $5m/s$

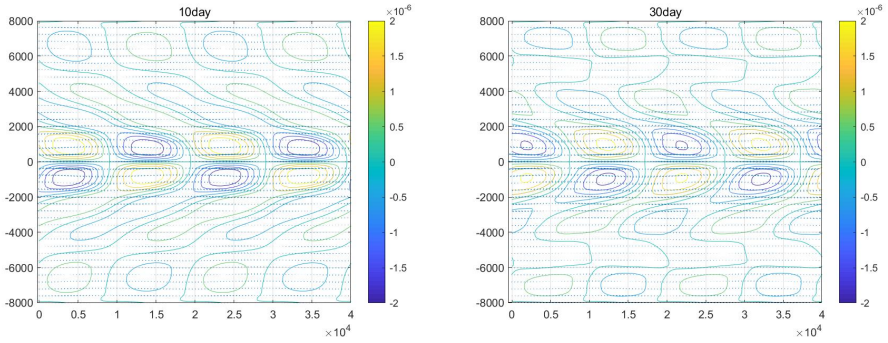

Kelvin, wavenumber 1, wavespeed $1m/s$

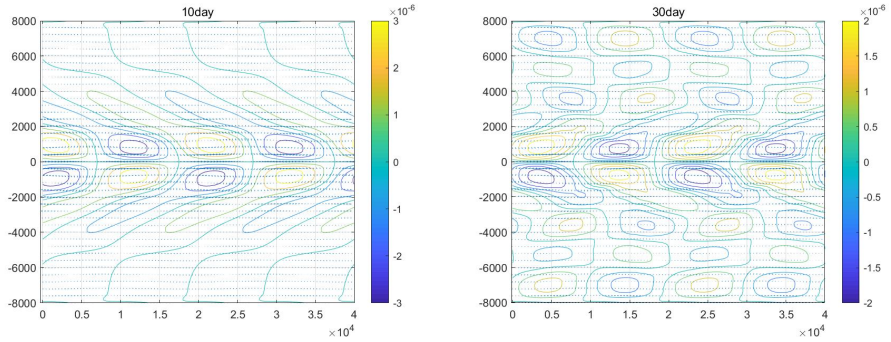

Kelvin, wavenumber 2, wavespeed $15m/s$

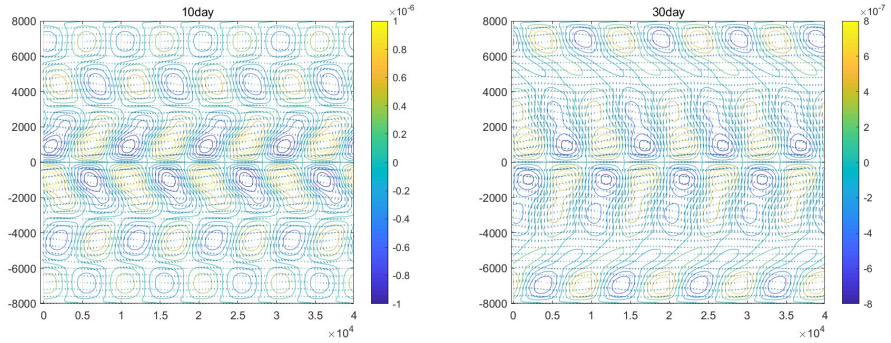

Kelvin, wavenumber 2, wavespeed $5m/s$

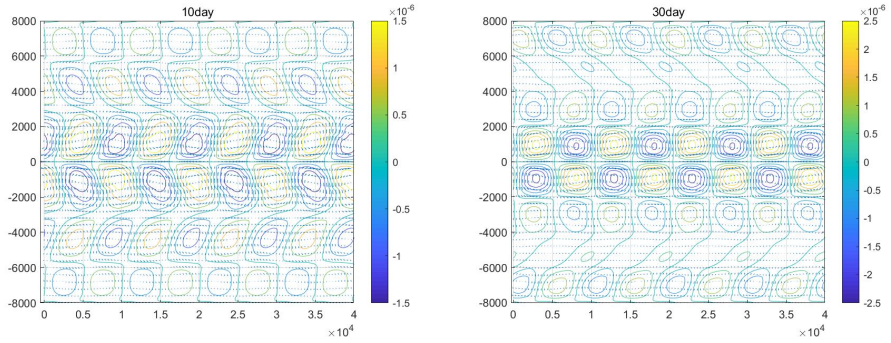

Kelvin, wavenumber 2, wavespeed $1m/s$

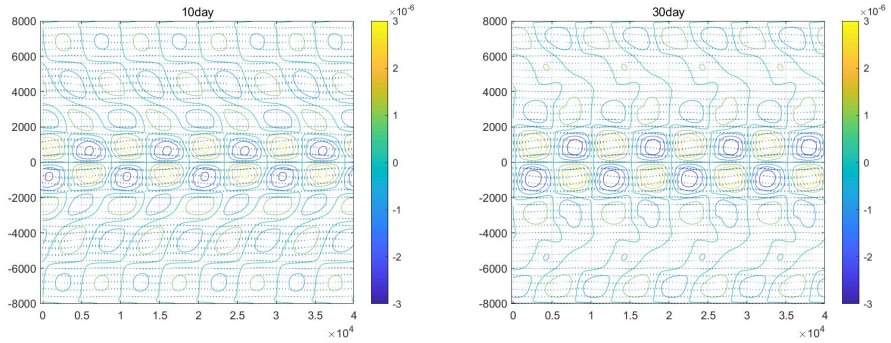

Kelvin, wavenumber 4, wavespeed $15m/s$

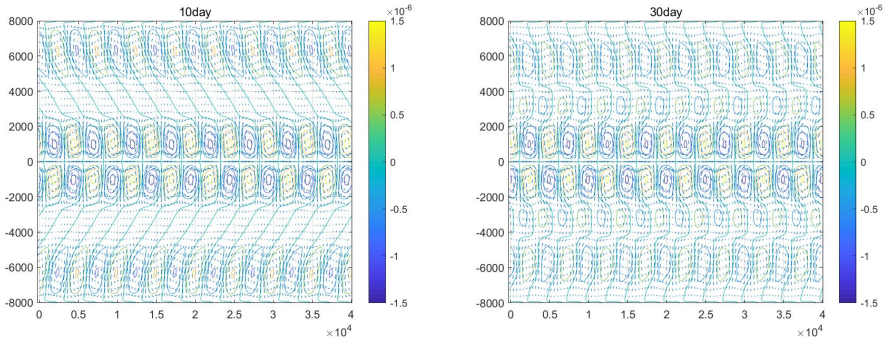

Kelvin, wavenumber 4, wavespeed $5m/s$

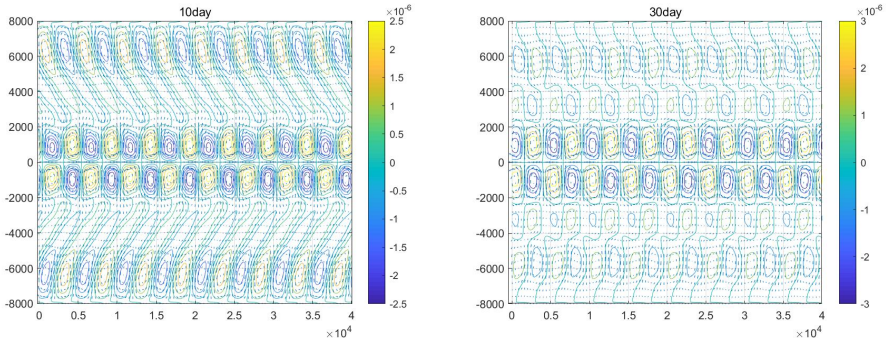

Kelvin, wavenumber 4, wavespeed $1m/s$

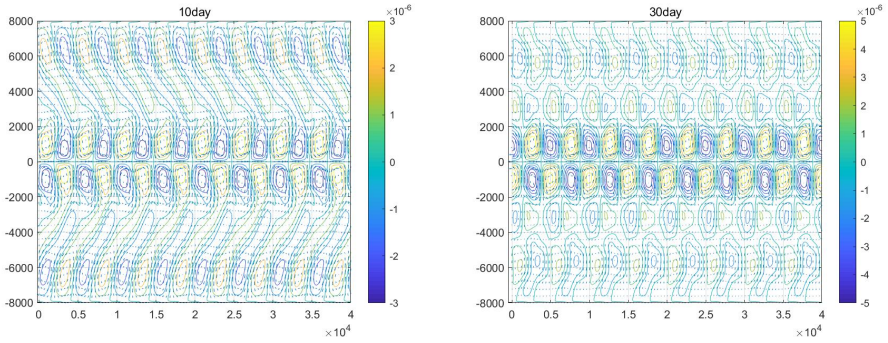

Kelvin, wavenumber 5, wavespeed $15m/s$

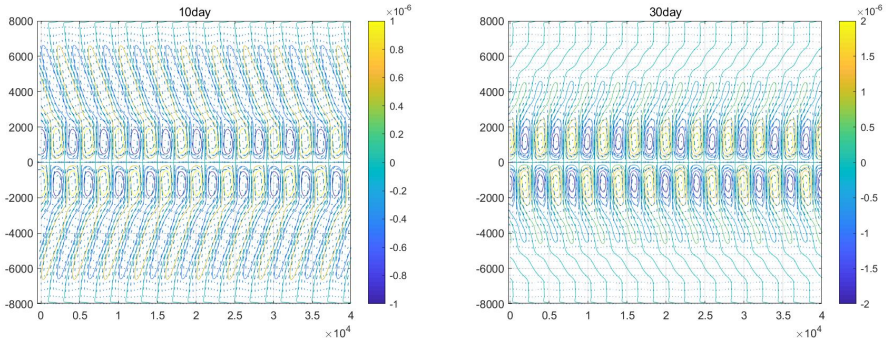

Kelvin, wavenumber 5, wavespeed $5m/s$

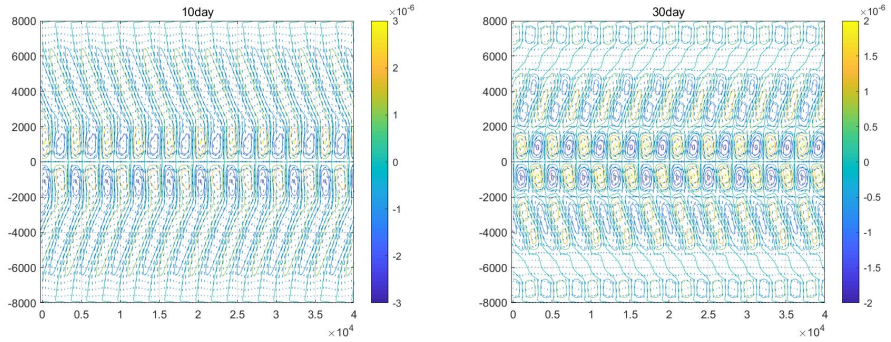

Kelvin, wavenumber 5, wavespeed $1m/s$

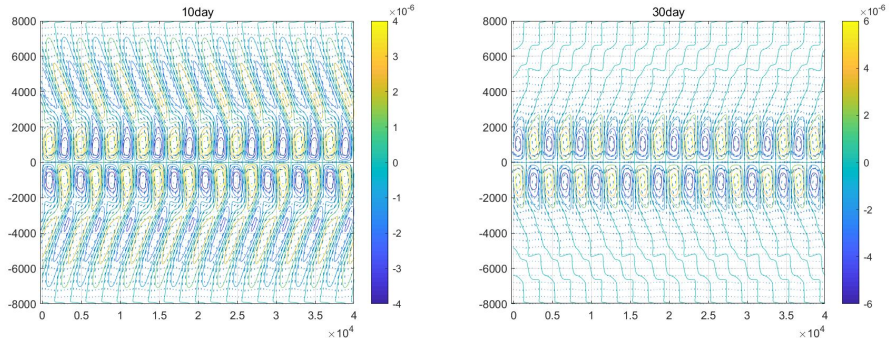

Kelvin, wavenumber 8, wavespeed $15m/s$

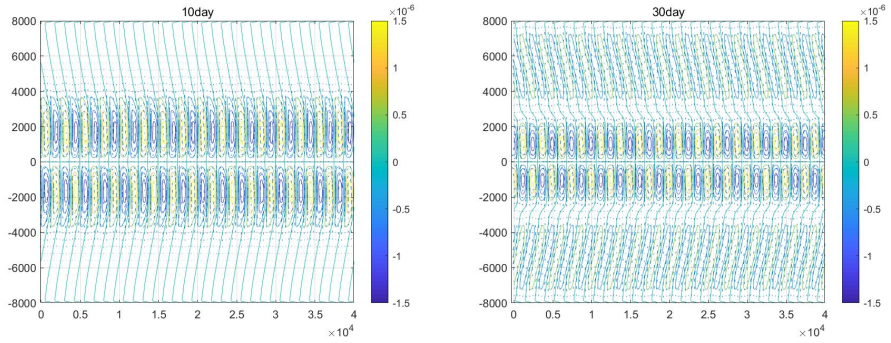

Kelvin, wavenumber 8, wavespeed $5m/s$

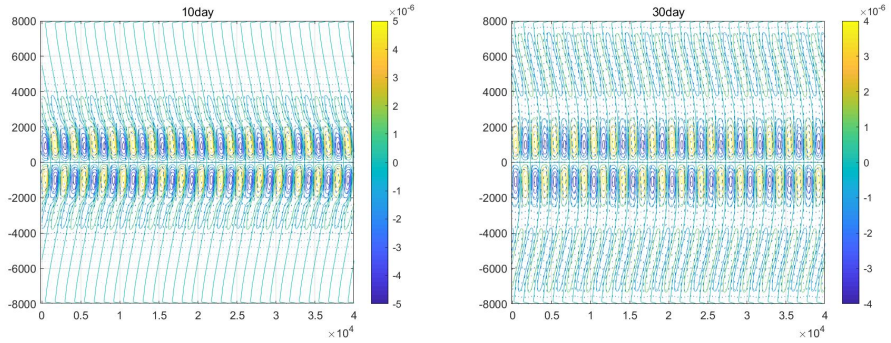

Kelvin, wavenumber 8, wavespeed $1m/s$

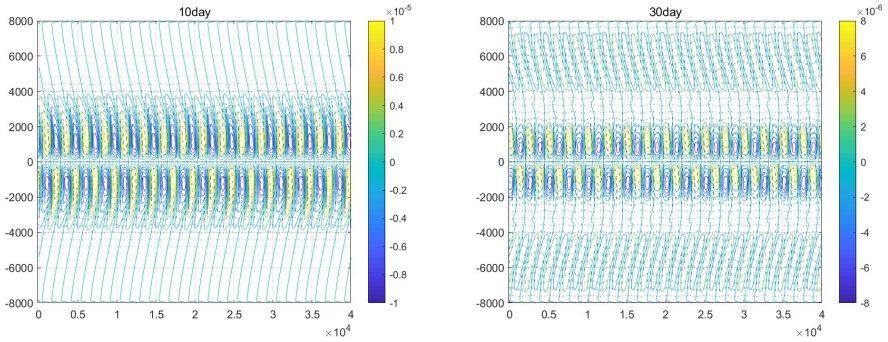

Kelvin, wavenumber 10, wavespeed $15m/s$

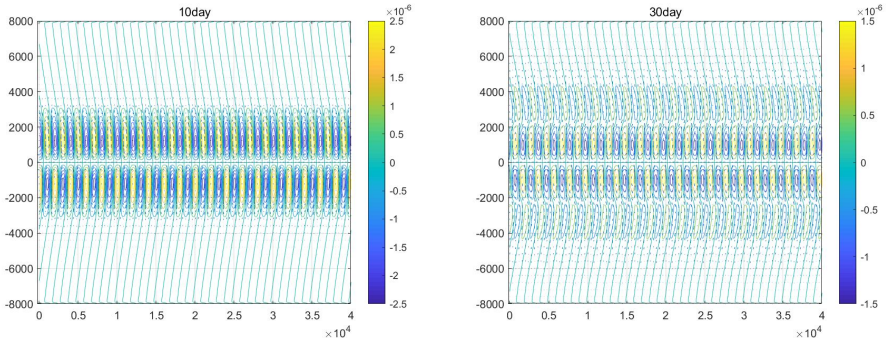

Kelvin, wavenumber 10, wavespeed $5m/s$

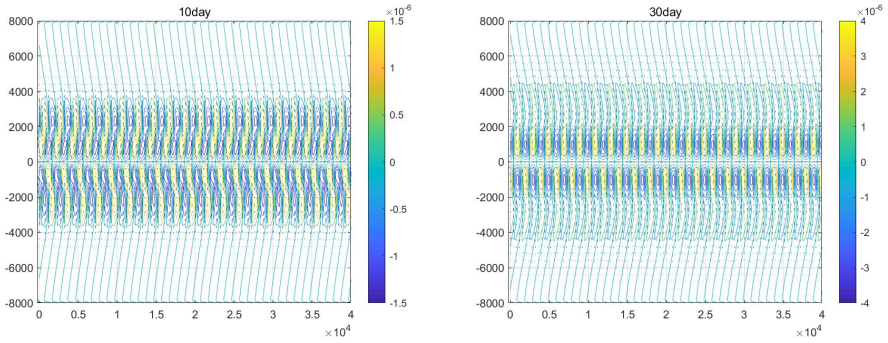

Kelvin, wavenumber 10, wavespeed $1m/s$

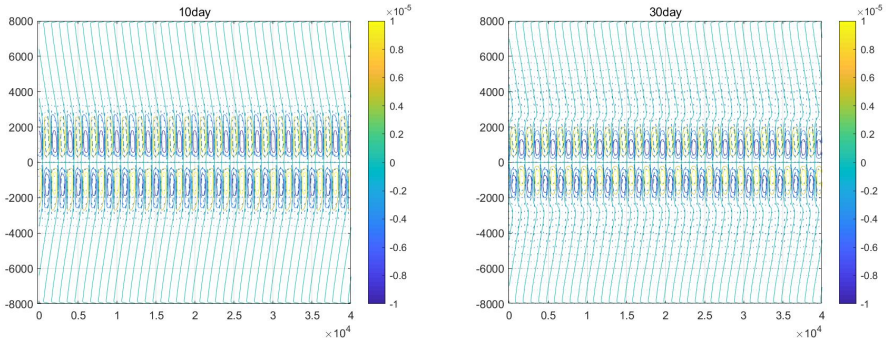

Rossby, wavenumber 1, wavespeed -4.743 m/s

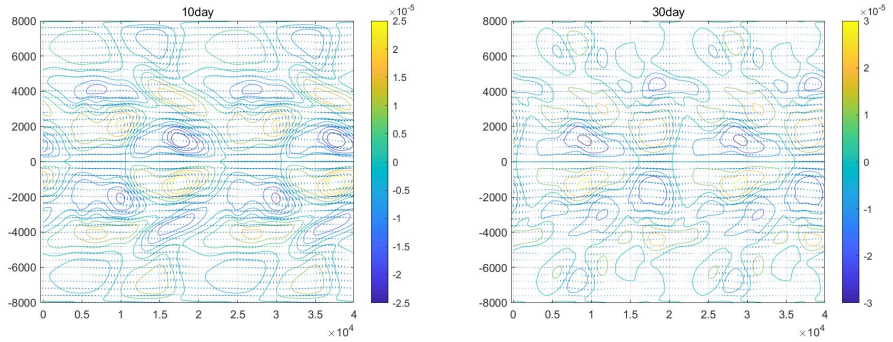

Rossby, wavenumber 1, wavespeed -1.637 m/s

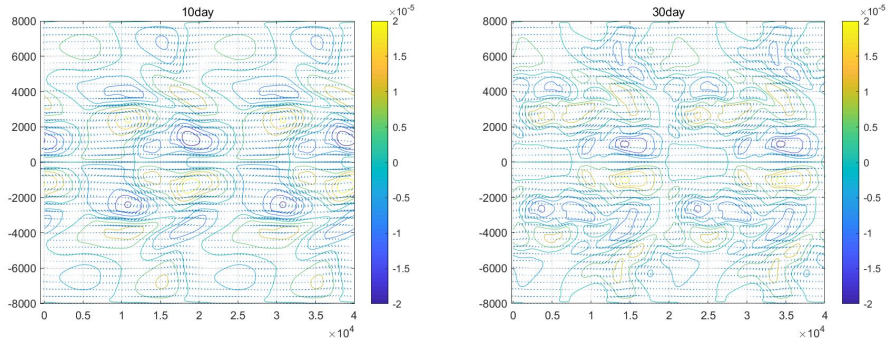

Rossby, wavenumber 1, wavespeed -0.332 m/s

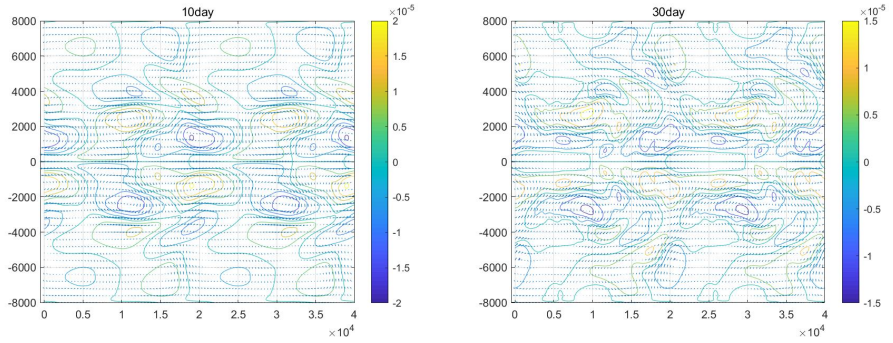

Rossby, wavenumber 2, wavespeed -4.110 m/s

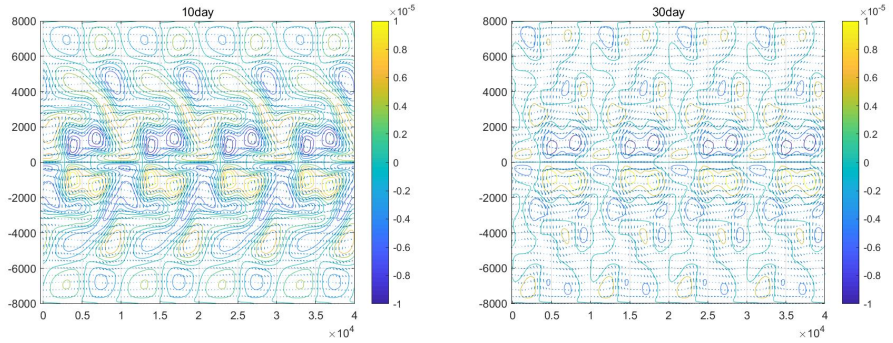

Rossby, wavenumber 2, wavespeed -1.555 m/s

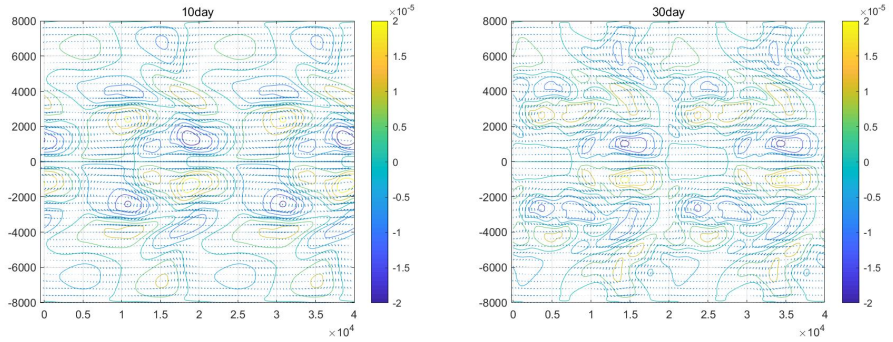

Rossby, wavenumber 2, wavespeed -0.329 m/s

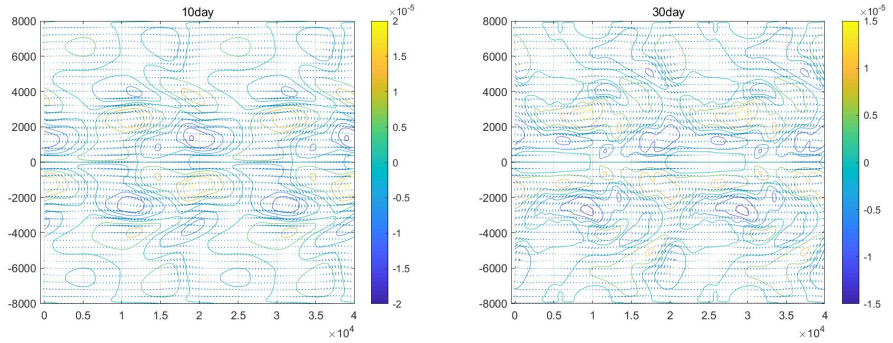

Rossby, wavenumber 4, wavespeed -2.680 m/s

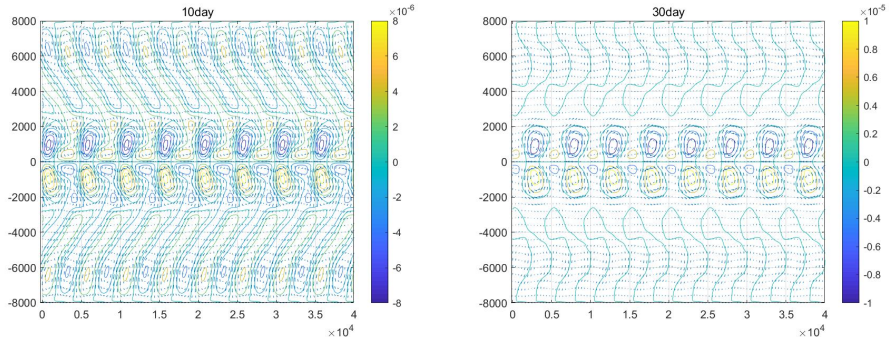

Rossby, wavenumber 4, wavespeed -1.293 m/s

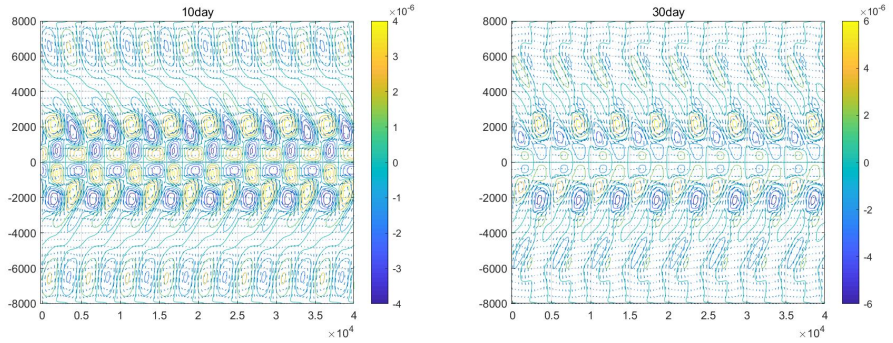

Rossby, wavenumber 4, wavespeed -0.315 m/s

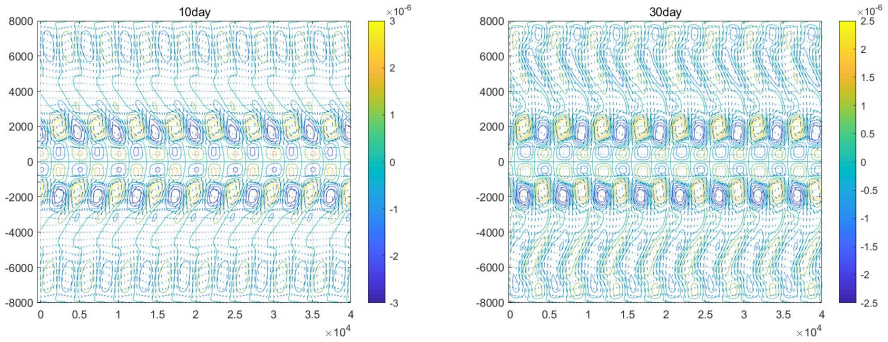

Rossby, wavenumber 5, wavespeed -2.125 m/s

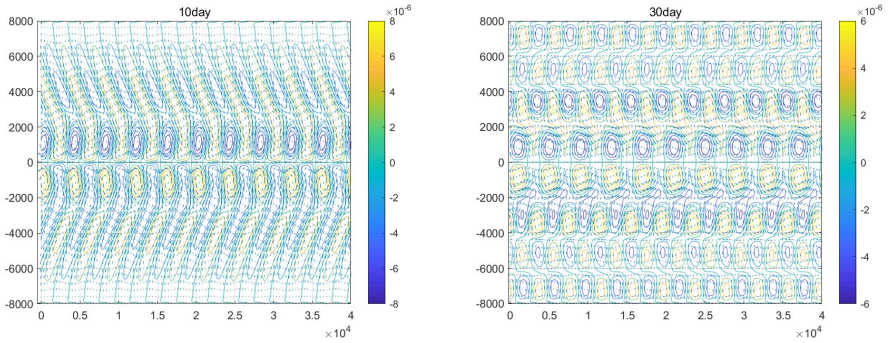

Rossby, wavenumber 5, wavespeed -1.149 m/s

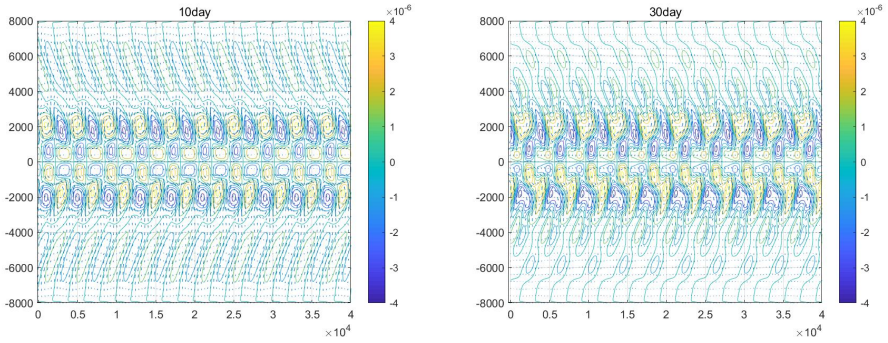

Rossby, wavenumber 5, wavespeed -0.306 m/s

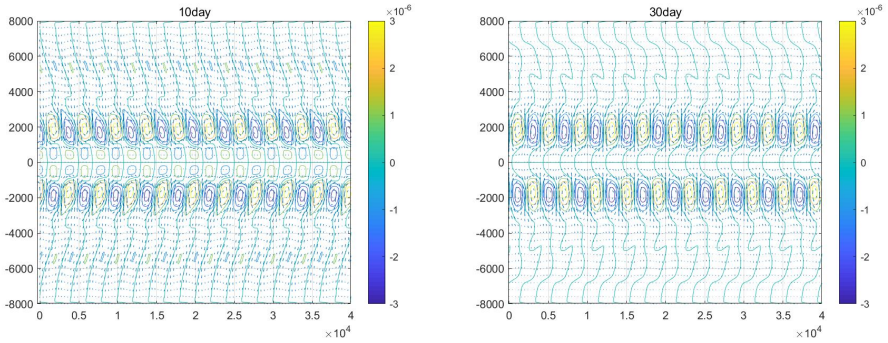

Rossby, wavenumber 8, wavespeed -1.120 m/s

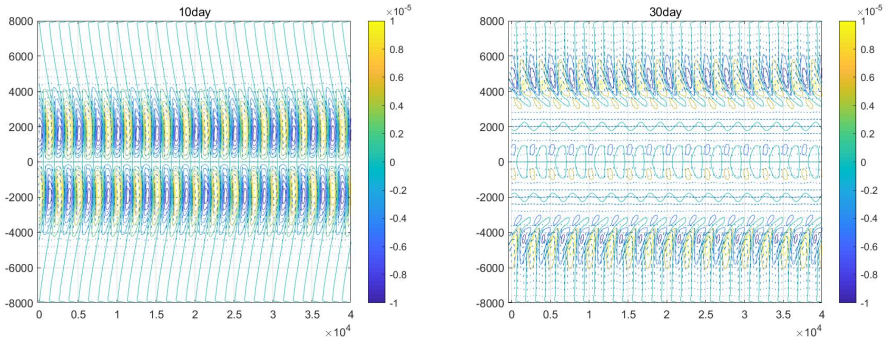

Rossby, wavenumber 8, wavespeed -0.774 m/s

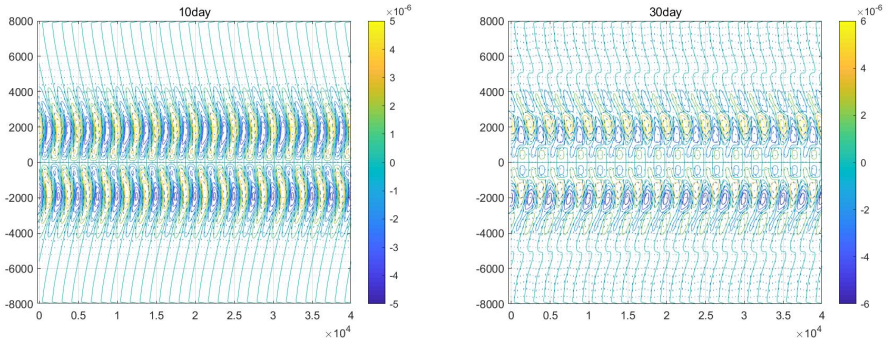

Rossby, wavenumber 8, wavespeed -0.271m/s

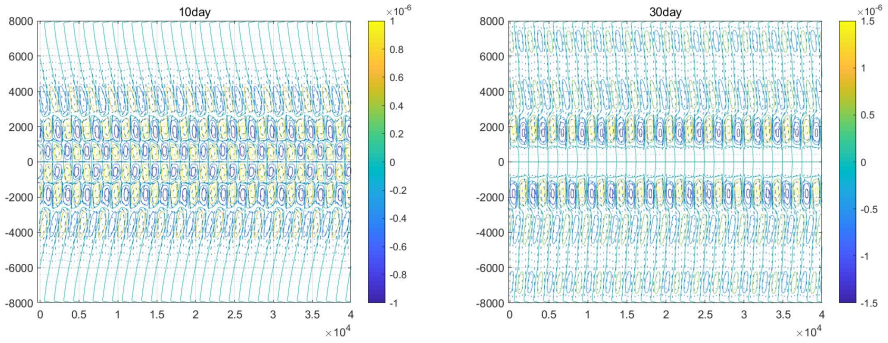

Rossby, wavenumber 10, wavespeed -0.780 m/s

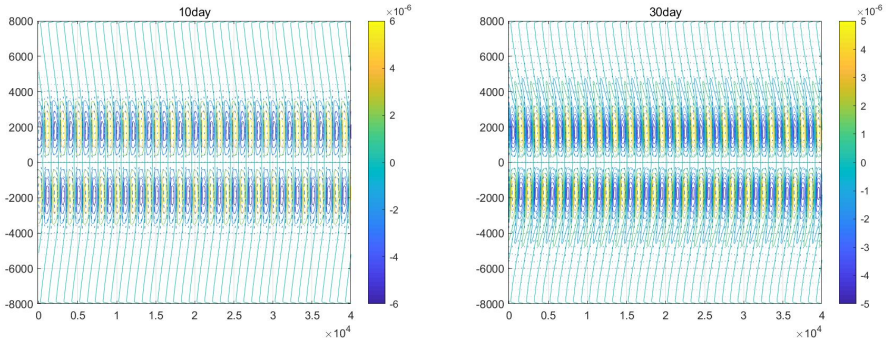

Rossby, wavenumber 10, wavespeed -0.595 m/s

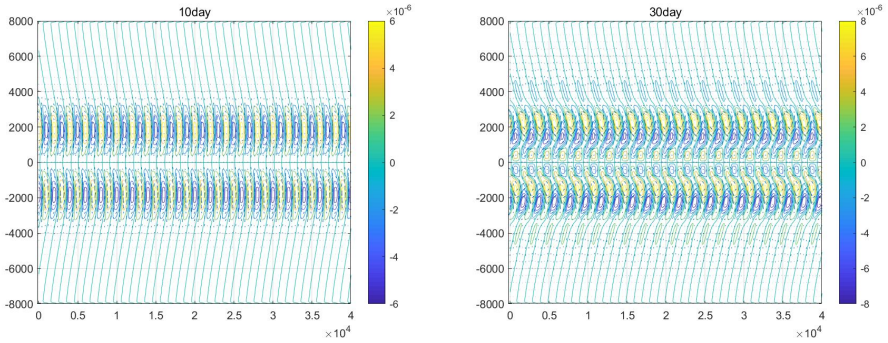

Rossby, wavenumber 10, wavespeed -0.245 m/s

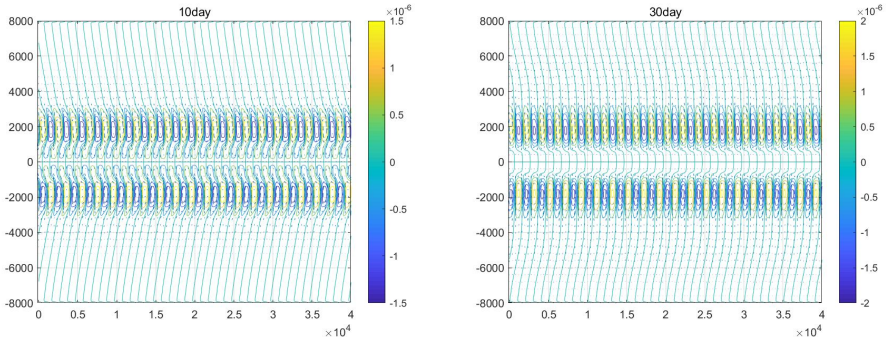

MRG, wavenumber 1, wavespeed 45.481 m/s

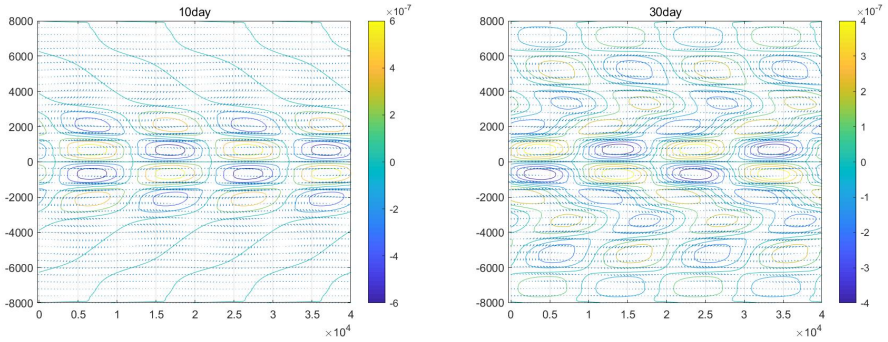

MRG, wavenumber 1, wavespeed 24.142 m/s

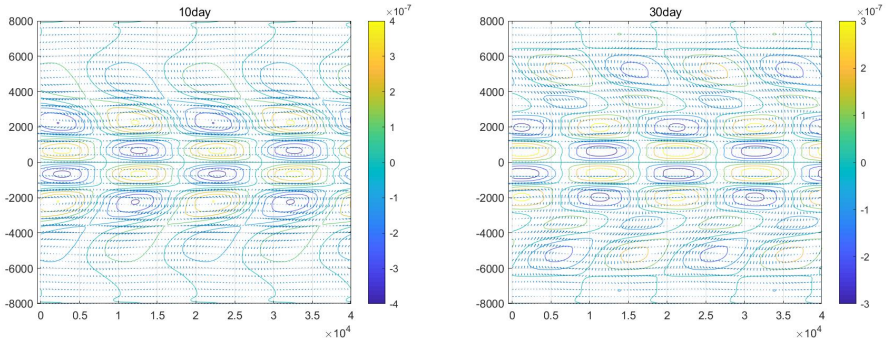

MRG, wavenumber 1, wavespeed 10.127 m/s

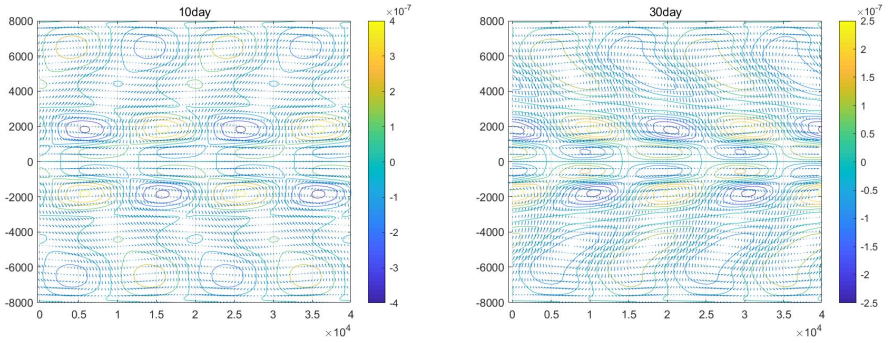

MRG, wavenumber 2, wavespeed 27.571 m/s

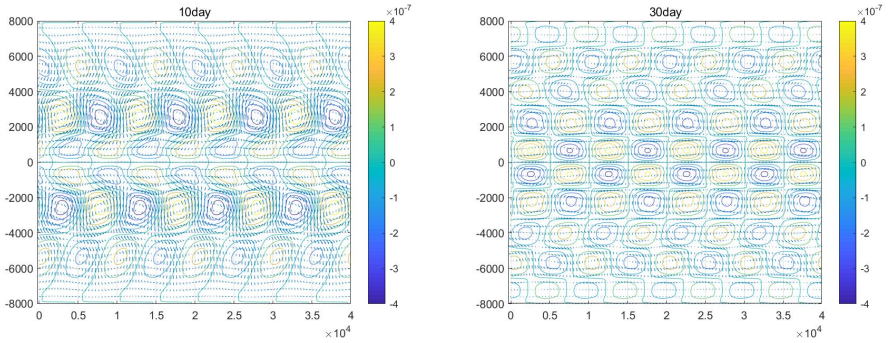

MRG, wavenumber 2, wavespeed 13.535 m/s

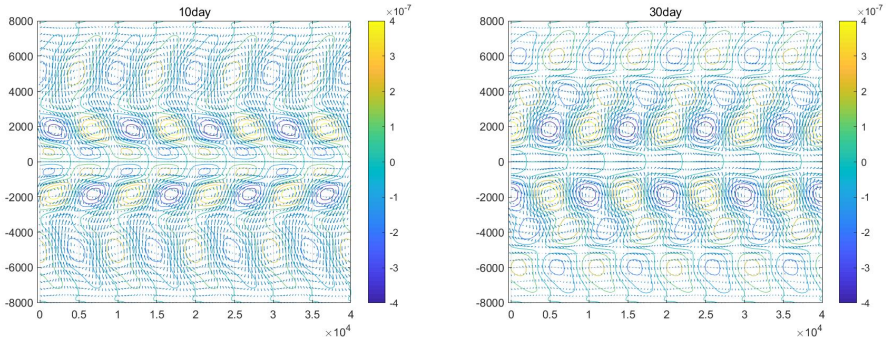

MRG, wavenumber 2, wavespeed 5.333 m/s

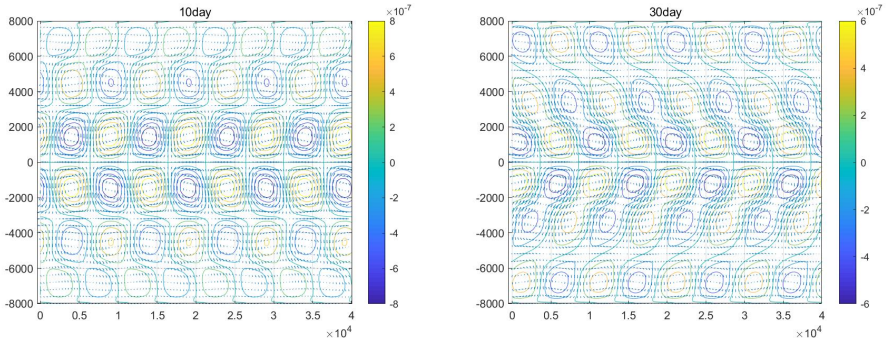

MRG, wavenumber 4, wavespeed 19.454 m/s

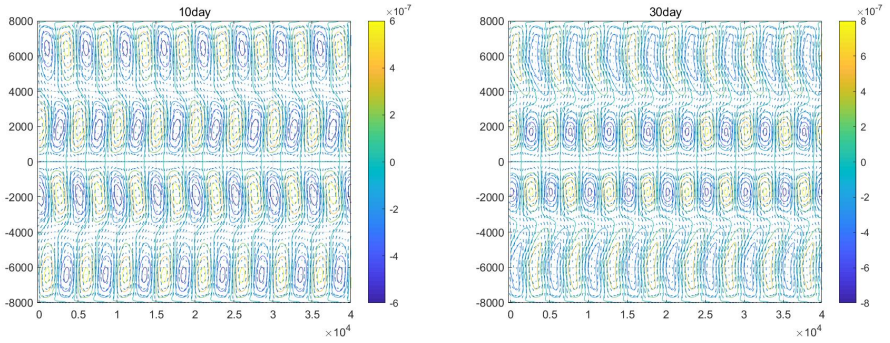

MRG, wavenumber 4, wavespeed 8.427m/s

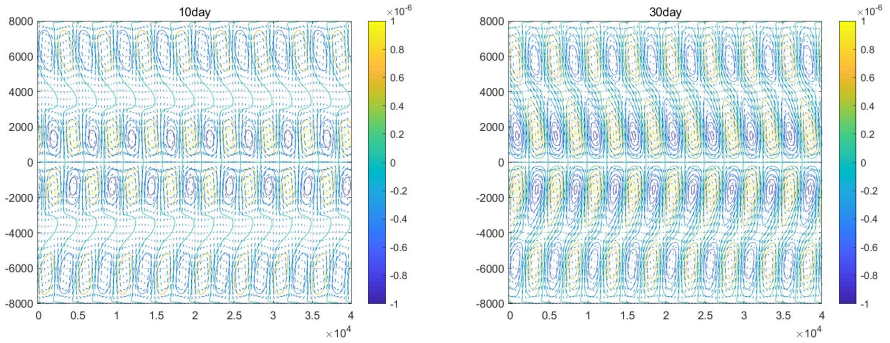

MRG, wavenumber 4, wavespeed 2.955m/s

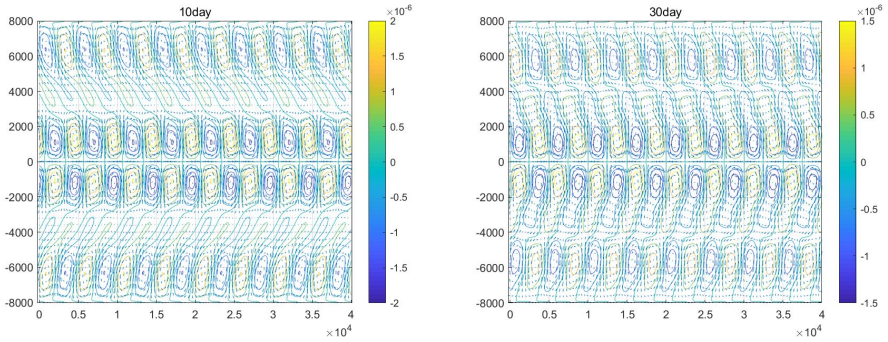

MRG, wavenumber 5, wavespeed 18.069 m/s

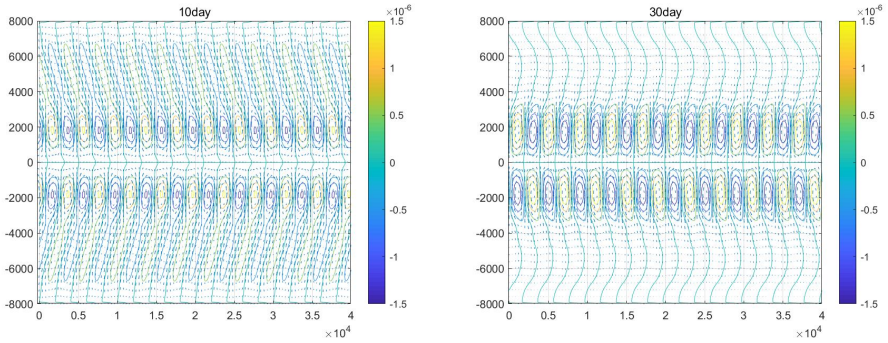

MRG, wavenumber 5, wavespeed 7.473 m/s

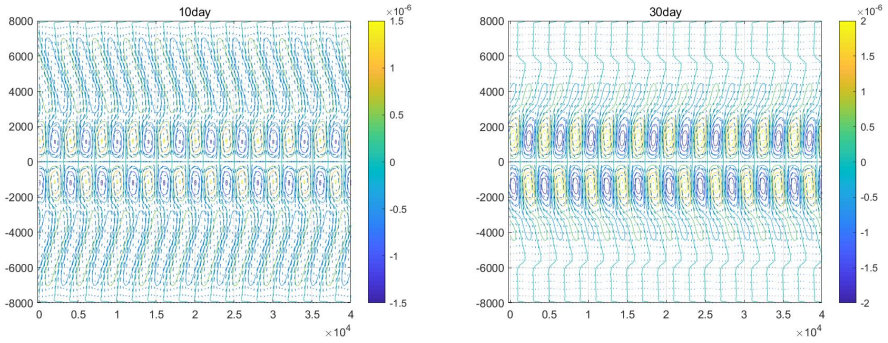

MRG, wavenumber 5, wavespeed 2.487 m/s

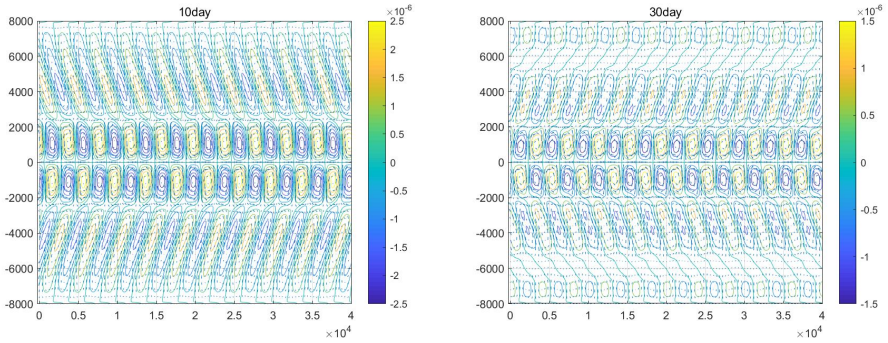

MRG, wavenumber 8, wavespeed 16.327 m/s

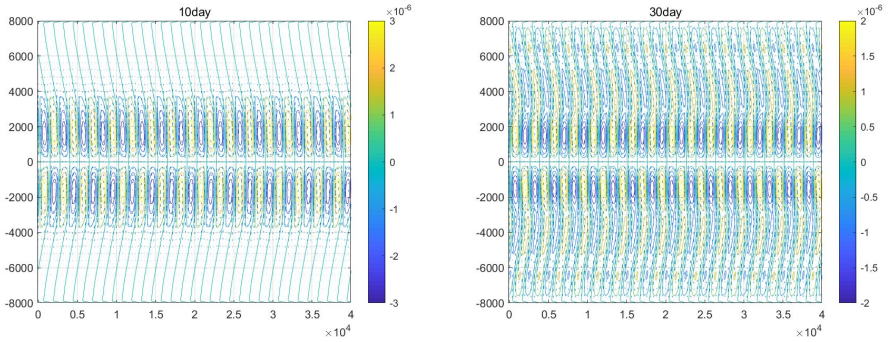

MRG, wavenumber 8, wavespeed 6.170 m/s

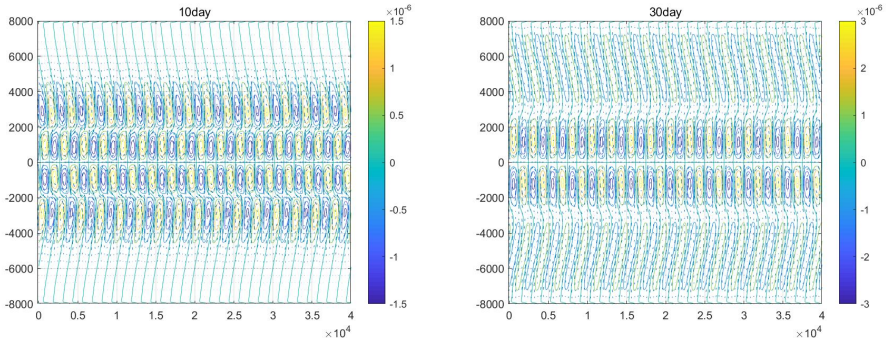

MRG, wavenumber 8, wavespeed 1.802 m/s

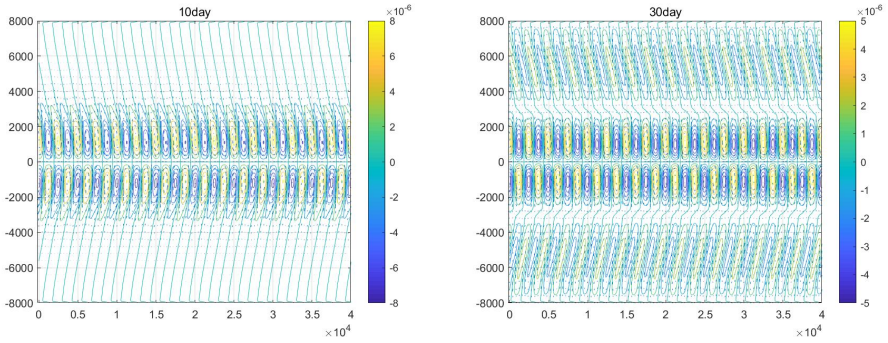

MRG, wavenumber 10, wavespeed 15.873 m/s

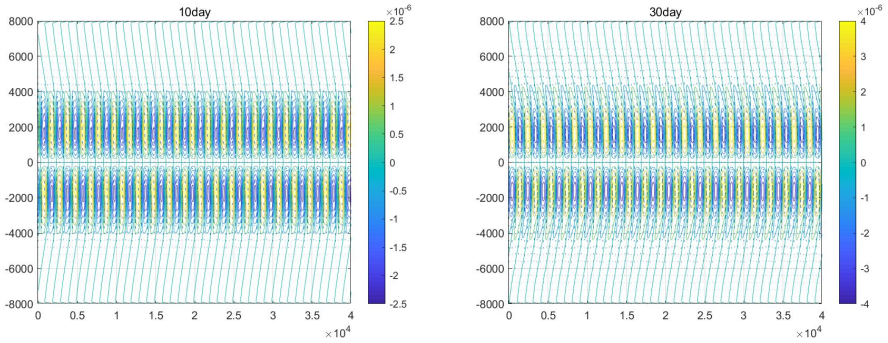

MRG, wavenumber 10, wavespeed 5.797 m/s

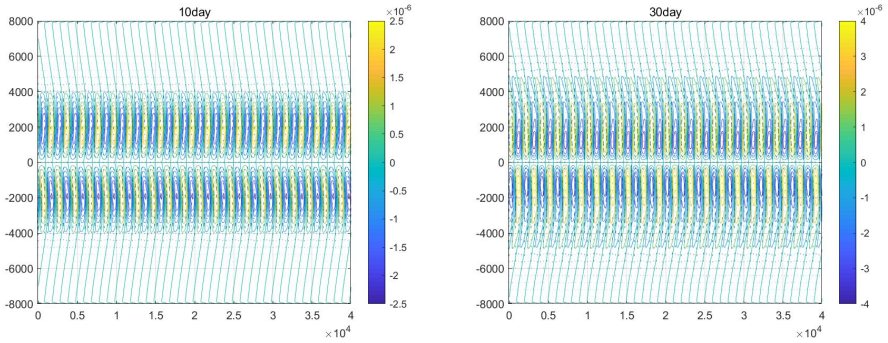

MRG, wavenumber 10, wavespeed 1.584 m/s

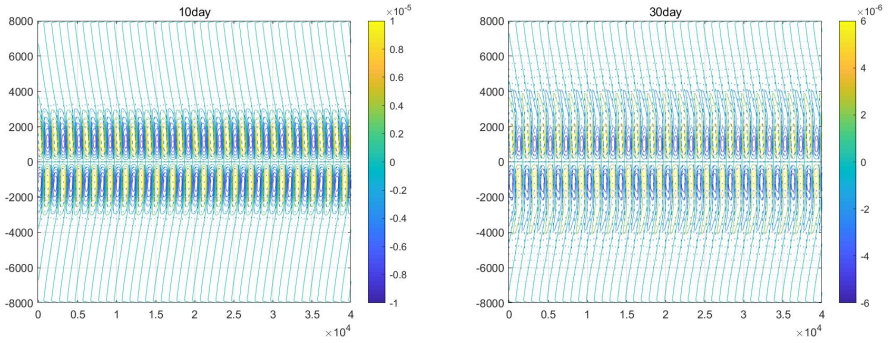

Bibliography

[1] M Awais and S Ibrahim. Nonlinear instability for the boussinesq equations with diabatic forcing. *Nonlinear Analysis*, 166:1–18, 2018.

[2] Lester E Carr III and Russell L Elsberry. Monsoonal interactions leading to sudden tropical cyclone track changes. *Monthly Weather Review*, 123(2):265–290, 1995.

[3] Dongho Chae and Hee-Seok Nam. Local existence and blow-up criterion for the boussinesq equations. *Proceedings of the Royal Society of Edinburgh Section A: Mathematics*, 127(5):935–946, 1997.

[4] Johnny CL Chan and RT Williams. Analytical and numerical studies of the beta-effect in tropical cyclone motion. part i: Zero mean flow. *Journal of the atmospheric sciences*, 44(9):1257–1265, 1987.

[5] James Ferguson, Boualem Khouider, and Maryam Namazi. Two-way interactions between equatorially-trapped waves and the barotropic flow. *Chinese Annals of Mathematics, Series B*, 30(5):539–568, 2009.

[6] Michael Fiorino and Russell L Elsberry. Some aspects of vortex structure related to tropical cyclone motion. *Journal of the atmospheric sciences*, 46(7):975–990, 1989.

[7] Houze Jr and Robert A. Clouds in tropical cyclones. *Monthly Weather Review*, 138(2):293–344, 2010.

[8] Boualem Khouider and Andrew J Majda. A non-oscillatory balanced scheme for an idealized tropical climate model part i: Algorithm and validation. *Theoretical and Computational Fluid Dynamics*, 19(5):331–354, 2005.

[9] Boualem Khouider and Andrew J Majda. A non-oscillatory balanced scheme for an idealized tropical climate model part ii: Nonlinear coupling and moisture effects. *Theoretical and Computational Fluid Dynamics*, 19(5):355–375, 2005.

[10] Boualem Khouider, Andrew J Majda, and Samuel N Stechmann. Climate science in the tropics: waves, vortices and pdes. *Nonlinearity*, 26(1):R1, 2012.

[11] George N Kiladis, Matthew C Wheeler, Patrick T Haertel, Katherine H Straub, and Paul E Roundy. Convectively coupled equatorial waves. *Reviews of Geophysics*, 47(2), 2009.

[12] Doron Levy and Eitan Tadmor. Non-oscillatory central schemes for the incompressible 2-d euler equations. *Mathematical Research Letters*, 4:321–340, 1997.

[13] Xiaofan Li and Bin Wang. Barotropic dynamics of the beta gyres and beta drift. *Journal of the atmospheric sciences*, 51(5):746–756, 1994.

[14] Andrew J Majda, Andrew J Majda, and Andrea L Bertozzi. *Vorticity and incompressible flow*, volume 27. Cambridge university press, 2002.

[15] Carolyn A Reynolds, James D Doyle, and Xiaodong Hong. Examining tropical cyclone–kelvin wave interactions using adjoint diagnostics. *Monthly Weather Review*, 144(11):4421–4439, 2016.

[16] Rebecca J Ross and Yoshio Kurihara. A simplified scheme to simulate asymmetries due to the beta effect in barotropic vortices. *Journal of the atmospheric sciences*, 49(17):1620–1628, 1992.

[17] Daniel P Stern, James R Brisbois, and David S Nolan. An expanded dataset of hurricane eyewall sizes and slopes. *Journal of the Atmospheric Sciences*, 71(7):2747–2762, 2014.

[18] RT Williams and Johnny CL Chan. Numerical studies of the beta effect in tropical cyclone motion. part ii: Zonal mean flow effects. *Journal of the atmospheric sciences*, 51(8):1065–1076, 1994.

[19] Liguang Wu, Huijun Zong, and Jia Liang. Observational analysis of tropical cyclone formation associated with monsoon gyres. *Journal of the Atmospheric Sciences*, 70(4):1023–1034, 2013.

[20] Bin Wang Xiaofan Li. The beta drift of three-dimensional vortices: A numerical study. *Monthly weather review*, 120(4):579–593, 1992.

[21] H Zhao and L Wu. Modulation of convectively coupled equatorial rossby wave on the western north pacific tropical cyclones activity. *International Journal of Climatology*, 38(2):932–948, 2018.

[22] Xiaqiong Zhou and Bin Wang. Transition from an eastern pacific upper-level mixed rossby-gravity wave to a western pacific tropical cyclone. *Geophysical Research Letters*, 34(24), 2007.